REPORT NO. FRA-OR&D-76-270 PB

NONDESTRUCTIVE MEASUREMENT OF LONGITUDINAL RAIL STRESSES

JULY 1976
INTERIM REPORT

Prepared for

U. S. DEPARTMENT OF TRANSPORTATION
FEDERAL RAILROAD ADMINISTRATION
Office of Research and Development
Washington, D.C. 20590

01-Track & Structures

NOTICE

The United States Government does not endorse products or manufacturers. Trade or manufacturers' names appear herein solely because they are considered essential to the subject of this report.

Technical Report Documentation Page

1. Report No.	2. Government Accession No.	3. Recipient's Catalog No.
FRA-OR&D-76-270		

4. Title and Subtitle	5. Report Date
NONDESTRUCTUVE MEASUREMENT OF LONGITUDINAL RAIL STRESSES	June 1975
	6. Performing Organization Code
	8. Performing Organization Report No.
7. Author(s) D. M. Egle and D. E. Bray	
9. Performing Organization Name and Address University of Oklahoma School of Aerospace, Mechanical & Nuclear Engineering 865 Asp Avenue, Room 200 Norman, Oklahoma 73069	10. Work Unit No. (TRAIS) 11. Contract or Grant No. DOT-OS-40091
12. Sponsoring Agency Name and Address Department of Transportation Federal Railroad Administration 2100 Second Street, SW. Washington, D.C. 20590	13. Type of Report and Period Covered Interim Report 6/1/74 - 6/1/75 14. Sponsoring Agency Code
15. Supplementary Notes	

16. Abstract

A study of the effect of applied stress on the wave velocity (acoustoelasticity) of railroad rail steel has shown that a potentially useful technique exists for the nondestructuve measurement of longitudinal stresses. The detection of extreme stress levels would contribute toward increased rail safety by decreasing accidents due to track buckling and weld pull aparts in continuously welded rail. Velocity variations between various new rails and between new and used rails were found to be significant. The overall effect of this is expected to be minimized by either establishing a base line velocity profile for rail or by comparing the velocity change of two waves, each experiencing a different change with applied stress.

17. Key Words	18. Distribution Statement
Rail Stress Measurement, Nondestructive Stress Measurement, Ultrasonic Stress Measurement, Acoustoelasticity, Guided Waves, Rail Material Properties	Document is available to the public through the National Technical Information Service, Springfield, Virginia 22161

19. Security Classif. (of this report)	20. Security Classif. (of this page)	21. No. of Pages	22. Price
UNCLASSIFIED	UNCLASSIFIED	127	

Form DOT F 1700.7 (8-72) Reproduction of completed page authorized

ACKNOWLEDGMENTS

The authors would like to acknowledge the contribution of many individuals who, through discussion, material assistance or otherwise, have contributed to the progress of this research. Mr. W. B. O'Sullivan, Technical Monitor in the Federal Railroad Administration, offered frequent and useful comments on operational and technical matters. Dr. W. J. Harris, Jr., Vice-President, Research and Test Department, Association of American Railroads, also provided valuable technical comments as well as a financial contribution. The Atchison, Topeka and Santa Fe Railway Company showed a continued interest in the work through the contribution of several rail samples and the personal interest of Mr. W. S. Autrey, Chief Engineer-System, Mr. L. D. Vallet of Mr. Autrey's staff and Mr. C. W. Groh, Assistant Division Engineer, Oklahoma City. Others whose contributions have also been of assistance in various ways include Mr. W. H. Chidley, Chairman, Technical Committee on Railway Materials, American Iron and Steel Institute, Mr. Charles O. Frederick, Project Manager (Track), The Railway Technical Centre, British Rail, Dr. Roger Steel, Transportation Systems Center, and Mr. Dan Stone, Research Metallurgist, Research Center, Association of American Railroads. The able assistance of Mr. Mark Bohon, Graduate Student, University of Oklahoma, contributed greatly to the planning and execution of the research.

Table of Contents

LIST OF FIGURES

LIST OF TABLES

NONDESTRUCTIVE MEASUREMENT OF LONGITUDINAL RAIL STRESSES

SUMMARY

Introduction The effect of thermal expansion and contraction on the longitudinal stresses in continuously welded rail is well known in the railroad industry. When the temperature is high and rail expansion has created excessive longitudinal compressive stresses, the track is prone to buckle. Extremely cold temperatures create tensile stresses which may pull welded joints apart. In its report [5] on an accident caused by track buckling, the National Transportation Safety Board (NTSB) stated:

> "The railroad industry needs badly a portable stress measuring device which would give instant readings of the compression or tension in a rail without disturbing it."

It is clear there is a need for a nondestructive technique for the measurement of longitudinal rail stresses. This research project addresses that need.

Problems Studied The major objective of this project was to develop a technique adaptable to the in-situ measurement of longitudinal stresses. The basis of the measurement is the acoustoelastic effect or the stress induced changes in the speed of ultrasonic waves. The initial concept employs guided waves travelling in the longitudinal direction rather than the conventional approach of bulk waves propagating normal to the applied stress. Toward this end, the following specific tasks were initiated.

(1) The effect of an applied uniaxial stress on the propagation of bulk ultrasonic waves in railroad quality steel was measured experimentally. This task was undertaken to determine if differences exist between the acoustoelastic constants of rail steel and other varieties of steel.

(2) The acoustoelastic effect for guided waves was studied experimentally in a bar machined from the head of a 12 lb ASCE rail. This was done to determine if indeed the effect existed (although intuitively it did, previous investigations were limited to surface waves) for guided waves and to evaluate the magnitude of the effect.

(3) An experimental verification of the acoustoelastic effect in a length of model rail was undertaken in order to evaluate the influence of the rail geometry on the proposed technique. A special purpose load frame, with a hydraulic actuator and a strain gaged length of model rail, was constructed for this purpose.

(4) A study of several bulk and guided wave speeds in full size new and used rail sections was undertaken to determine the variations to be expected in the wave propagation characteristics of typical main line rail. Measurements of wave speeds in a variety of short rail sections plus wave speed variations along the length of longer rails were made and summarized statistically. The dependence of Rayleigh wave speed on the depth of penetration (or frequency) was evaluated for a number of new and used rails.

Results Achieved

(1) The magnitude of the acoustoelastic effect for longitudinal waves travelling parallel to the applied stress was found to be nearly twice

as large as that for shear waves travelling perpendicular to the load. The magnitude of the acoustoelastic effect for both perpendicular and parallel polarized shear waves travelling transverse to the applied load was in excellent agreement with other experimental results for steel.

(2) The magnitude of the acoustoelastic effect for guided waves was found to depend significantly on the wave propagation mode. The largest effect was associated with wave modes consisting primarily of longitudinal waves travelling nearly parallel to the applied load with smaller effects for Rayleigh waves and for transverse waves travelling at 45^{o} to the applied load.

(3) The geometry of the model rail curtailed the number of wave modes that could be successfully transmitted but an acoustoelastic effect did exist both in the rail head and web for those modes that could be excited. Further, the magnitude of the effect was found to be dependent on the sign of the applied longitudinal stress.

(4) Velocity differences in the several wave types propagated in new and used unstressed rail indicated that material property variations are a major problem to be overcome in making absolute stress measurements with this technique. The work hardened zone on the rail head affects the propagation velocity to the extent that measurements from this surface do not seem practical. Moreover, there appears to be differences in velocities of new rail and of used rail in the bulk material away from the worked zone indicating a property change with rail service. A large variation in velocities between two new, 11.9 m (39 foot) rail sections was also found. The least variation in velocities were found to occur in the web of control cooled rail making this location the most desirable for performing the stress measurement.

Utilization of Results A device or system for measuring stress levels in continuously welded rail could be utilized by operating railroads and the Office of Safety in the Federal Railroad Administration. The condition of high speed, main line railroad track is of vital concern to both. The portable device proposed herein could be used by track maintenance forces during track installation to obtain proper adjustment of the rail. It could also be used for monitoring track conditions during periods of temperature extremes.

Conclusions The conclusion from this phase of the program is that the acoustoelastic technique is potentially useful for performing nondestructive stress measurements in continuously welded rail. It is felt that with the information developed in the first phase of this study, these measurements can be made at a specific location on a specific rail with a portable unit as proposed herein. Continuous measurement with a test car type installation will require further evaluation.

INTRODUCTION

Purpose The work performed under this contract had a dual objective. One was to study the effect of applied stress on the propagation of ultrasonic pulses in high carbon, railroad quality rail steel. This was accomplished by the experimental measurement of the acoustoelastic effect for bulk waves and guided waves in samples of rail steel. The major objective, however, was to initiate research utilizing ultrasonic pulses that will result in techniques adaptable to the in-situ measurement of longitudinal stresses. It is contemplated that these tests can be performed with both a small portable device and via a test car moving at standard operating speeds. Measurement of these stresses will enable operating railroads to locate highly stressed areas in rail. These highly stressed areas often cause rail and track deformation and are a major cause of derailments.

Background The overriding goal of this phase was to develop a technique for in-situ measurement of rail stresses caused by changes in ambient temperature. The expansion and contraction of materials with temperature change is a well known phenomenon. This is particularly noticeable in railroad rails since they are exposed to the full range of outdoor temperatures, typically 47.7°C to -41.7°C (118°F to -43°F). Actual rail temperature is often much higher than the ambient because of the absorption of radiant heat from the sun [1].

The effect of the rail expansion and contraction is more noticeable in continuous welded rail than in bolted (or jointed) rail. Relative motion within the joints in bolted rail can prevent high stresses from occurring. High maintenance costs and the propensity for fatigue cracks at the joint, plus the occurrence of end batter on the rail have all led to the replacement of this

type of rail with continuous welded rail (CWR). In most cases, these strings of CWR are 439 m (1440 feet) long. They are field welded into various lengths up to 16.1 km (10 miles) long. These rails, while clearly superior to the old jointed rail, do not have the ability to release the expansion and contraction forces through linear movement. Instead, this is accounted for by changes in the internal stresses of the rail. Typical high temperature stresses for properly installed rail have been estimated to be near 82.737 MN/m^2 (12,000 psi) [2].

Normal installation practice usually considers the annual temperature range of the location and the temperature of the rail at the time of installation. An attempt is made to adjust the installed stress level to such that the rail will not exceed acceptable compressive or tensile stresses throughout the annual temperature range. This estimate of installation stress level is, at best, guesswork based on prior experience. During periods of extreme temperatures track personnel must maintain a vigil over the rail in order to detect overstressed conditions. The judgement of overstressed conditions is based on the ability of an individual inspector to detect such a situation.

When the temperature is high and rail expansion has created excessive longitudinal compressive stresses in the rail, it is primed for buckling. Track buckling occurs because rails react to axial loads much like any structural column. A perturbation such as an additional temperature increase or train motion can trigger the lateral buckling. Extreme cold puts tensile stresses in the rail. If the rail stresses are not properly adjusted upon installation, these low temperature tensile stresses can create forces sufficient to pull apart welded joints. A more detailed discussion of this behavior is contained in references 1, 2, 3 and 4.

A well-documented accident that was attributed to track buckling

occurred at Glen Dale, Maryland on 28 June 1969, when the passenger train, the Silver Star, derailed while running at a speed between 134 and 138 km/hr (83 and 85 mph). In this instance 144 of the 541 passengers were treated at area hospitals for injuries. This derailment occurred at 38°C (100°F) temperature on Penn Central track which regularly handled the Metroliners travelling at speeds near 201 km/hr (125 mph). The National Transportation Safety Board (NTSB) investigated the accident and reported " . . . the derailment was caused by lateral movement of the track under the train. The lateral movement was caused by buckling of the track." [5] Other statements from the NTSB report which are relative to the study are as follows:

> "The railroad industry needs badly a portable stress measuring device which would give instant readings of the compression or tension in a rail without disturbing it." In the general conclusion, the NTSB reported, "A more significant conclusion for the long term is that the general state of the art of railroad track design and maintenance is scientifically weak, and that safety relies on judgement of individuals rather than on any firm or logical criteria." In the recommendations, the report states, "The Safety Board recommends that the American Railway Engineering Association and the Association of American Railroads undertake studies to determine more accurately the stresses developed in welded rail track in extremes of temperature and the role of these stresses in hazardous track movements."

It is clear from the above discussion that there is a need for a technique for the nondestructive measurement of longitudinal rail stresses. This report addresses that need.

The problem caused by high stress conditions in rail exists throughout the United States and the rest of the world. It is most acute in areas where daily temperatures have an extreme range. A large seasonal range also creates stress problems. Many desert or arid areas experience large daily

variations in temperature while the northern states have the largest seasonal changes. Obviously, the temperate climates such as in Florida would have the least problem.

Present State of Knowledge Nondestructive measurement of residual stress in structural members is certainly not a new problem. Several techniques have been developed that have been successfully applied by other industries. X-ray diffraction is perhaps the most well known today. Other methods which are emerging from the laboratory to field usage are Barkhausen Noise Analysis and shear wave acoustic birefringence. X-ray diffraction and Barkhausen Noise Analysis [6,7] are both surface effect techniques, that is they are techniques used to measure surface stresses. A fundamental difficulty arises in applying either of these methods to the measurement of rail stresses in that the high loads generated by the contact of wheel and rail severely deform the rail head. The top of the rail head has a surface layer of plastically deformed metal that has properties different from the body of the rail. Estimates of the depths of this zone are from 6.4 to 9.6 mm (1/4 in to 3/8 in) below the surface [8]. Moreover, the sides of the rail heads are distorted by this plastic working giving a generally nonuniform rail geometry. Hence the method chosen for the rail stress measurement must be independent of this plastic working on the head. The reliability of surface effect measurement of body stresses through plastically deformed surfaces has not been established. On the other hand, the acoustic birefringence technique is capable of measuring body stresses and thus, of the three methods, is the one warranting further study.

The technique presented here is the use of guided waves propagating along the length of the rail rather than the usual bulk shear waves propagating across the rail. Guided waves can also be made to penetrate deep into the body of the material. This depth is a function of the ultrasonic pulse frequency

and can be controlled to fit the situation.

A difficulty with applying both the bulk shear wave (acoustic birefringence) and the Barkhausen Noise Analysis techniques is that they require a highly uniform probe contact area. Neither the field side nor the gauge side of the rail are completely desirable for contact because of the rolling deformation and operational difficulties related to switches, crossovers, etc. The shear wave acoustic birefringence technique cannot be used here because two parallel surfaces are required for either pulse echo or through transmission techniques. Besides being distorted from service, the vertical surface of new rail heads are often slightly inclined.

An early paper on the relationship of ultrasonic pulse velocity and attenuation and material strain was presented by Truell in 1959 [10]. This paper discussed in general some of the work in this area by the author and several others. A more definitive paper was presented by Smith in 1963 [11]. A brief discussion of this paper will show the technical rationale behind the current study.

The interference of stress and ultrasonic wave propagation has been designated as the acoustoelastic effect. It is analogous to the photoelastic effect where applied stress has been shown to interfere with light waves so that stress patterns on a material surface can be photographed. The acoustoelastic effect offers the possibility that internal stresses can be observed in a similar manner.

Considering stress conditions alone and discounting other causes of anisotropy, Hughes and Kelly [12] obtained seven equations for acoustic velocities within otherwise isotropic material. Smith has discussed their work and the effect of internal stress. A more general approach by Toupin and

Bernstein [13] produced the same results. A modified form of the equations of Hughes and Kelly, as presented by Smith, are shown as equations 1-7:

$$C_{Lp}^2 = \frac{1}{\rho_o}\left[\lambda + 2\mu - \frac{P}{3K_o} f_1(\lambda,\mu,1,m)\right] \quad (1)$$

$$C_{Tp}^2 = \frac{1}{\rho_o}\left[\mu - \frac{P}{3K_o} f_2(\lambda,\mu,m,n)\right] \quad (2)$$

$$C_{Lx}^2 = \frac{1}{\rho_o}\left[\lambda + 2\mu + \frac{T}{3K_o} f_3(\lambda,\mu,1,m)\right] \quad (3)$$

$$C_{Tx}^2 = \frac{1}{\rho_o}\left[\mu + \frac{T}{3K_o} f_4(\lambda,\mu,1,m)\right] \quad (4)$$

$$C_{Ly}^2 = \frac{1}{\rho_o}\left[\lambda + 2\mu - \frac{T}{3K_o} f_5(\lambda,\mu,1,m)\right] \quad (5)$$

$$C_{Ty}^2 = \frac{1}{\rho_o}\left[\mu + \frac{T}{3K_o} f_6(\lambda,\mu,m,n)\right] \quad (6)$$

$$C_{Tz}^2 = \frac{1}{\rho_o}\left[\mu - \frac{T}{3K_o} f_7(\lambda,\mu,m,n)\right] \quad (7)$$

In these expressions, C is a particular wave velocity where the subscripts L and T represent a longitudinal wave and a transverse wave respectively. The second subscript classifies the type of induced stress. In this p is internal hydrostatic type pressure (similar to residual stress within rolled material) and x,y and z are the axes of applied load. On the right hand side of the equations, ρ_o is the unstressed density, λ and μ are the usual Lamé constants, P is the hydrostatic pressure, T is the uniaxial load, and

K_o is the bulk modulus for an isotropic material in the unstrained state. The terms k, l and m are third order elastic constants discussed by Smith which relate the applied stress to the change in velocity. When there is no internal pressure and no applied load (i.e., P and T equal zero) it is easily seen that the last terms disappear in each case and the general wave equations that are left are those used for longitudinal and transverse waves propagating in unbounded isotropic material, i.e.:

$$C_L^2 = \frac{\lambda + 2\mu}{\rho_o} \tag{8}$$

and

$$C_T^2 = \frac{\mu}{\rho_o} \tag{9}$$

Using an arrangement similar to that shown in Figure 1, Smith described an experimental verification of these relationships. In this set-up, test pieces A and B are identical aluminum bars and the transmitting and receiving transducers are as identical as possible. For shear wave studies, the transducers were fixed to the material so that polarization (i.e., particle motion) was in the y direction and the load was applied to block A in the y and z directions. The transmitting transducers receive the same high frequency pulse. It is passed through the material and received at the other side of the test pieces where it is amplified and displayed by the electronic items. The carrier frequency of the ultrasonic pulses was 5 MHz. Small changes in C_{Ty}, C_{Ly} and C_{Tz} could be detected by comparing the transmission times in blocks A and B. Smith observed that transverse (shear) waves polarized parallel to the direction of applied stress were most affected by the load. These would be waves with a velocity C_{Ty}. When loaded, the velocities of these waves were found to vary from that of other shear waves, designated by velocities C_{Tx} and C_{Tz},

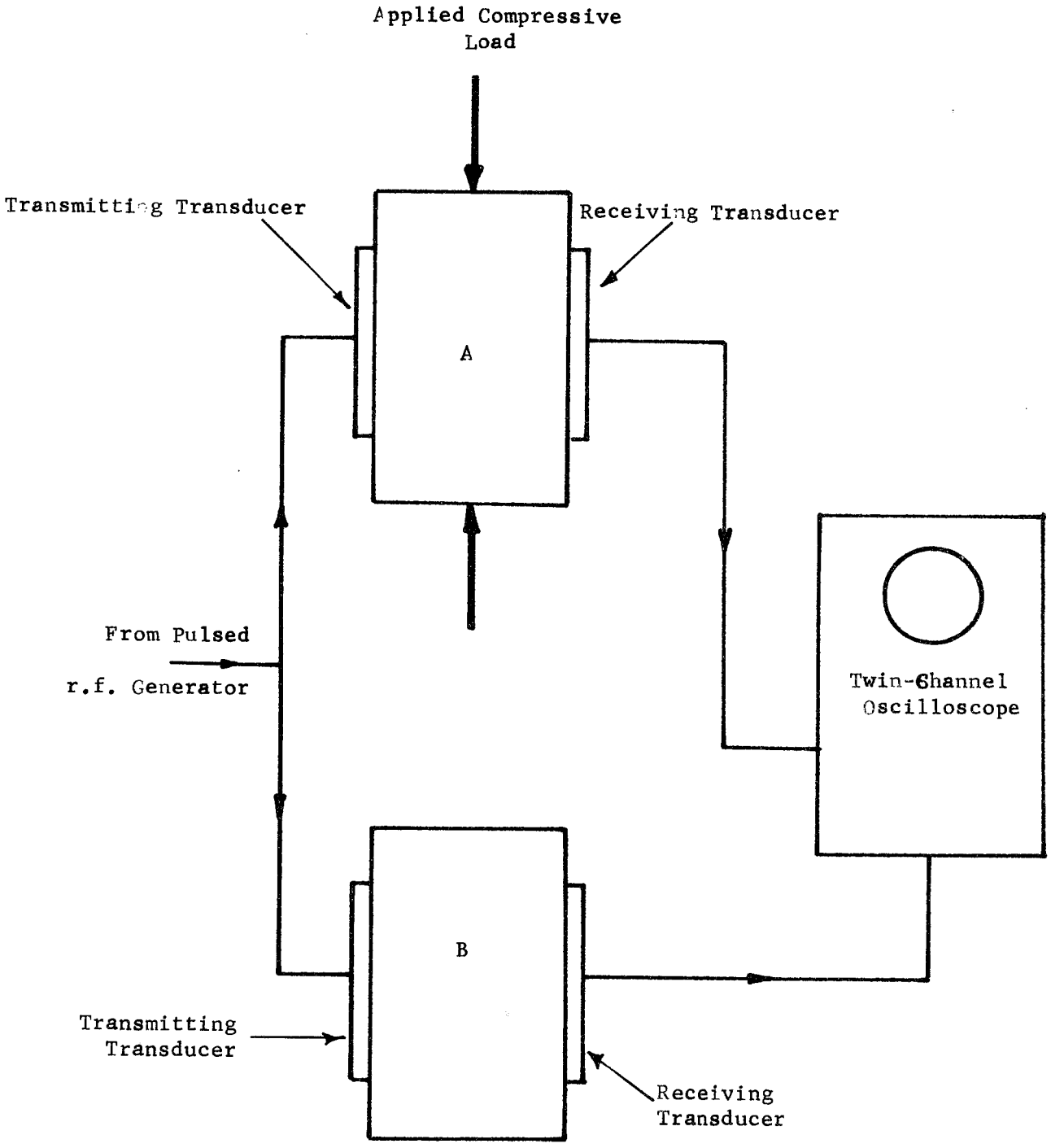

Figure 1 Arrangement for Measuring Differential Velocity Shifts in Transit Times of Ultrasonic Pulses.

respectively. This is different from the isotropic case where all shear waves have the same velocity. Smith also discussed work showing that applied stress affects the phase of an ultrasonic pulse to the extent that decay within the material is no longer exponential. As he states, a transverse wave travelling within a stressed medium will break up into two components, i.e., one with particle motion parallel to the applied stress and one with particle motion normal to the direction of applied stress. As the two components progress through the material, the stress effect upon the wave with particle motion parallel to the stress causes a phase shift.

Kammer and Vigness [14] discuss the results of some attempts to apply the acoustoelastic effect for stress measurement in several materials, including steel. This work, performed in 1964, reported mixed results. Their primary concern about the usefulness of the technique was the time base accuracy required to measure the very small velocity changes. In this experiment a travel time change near 6.0 nsec per inch of travel was observed for 1020 steel with 137.895 MN/m^2 (20,000 psi) tensile stress applied. They postulated that other anisotropic conditions, such as grain orientation and residual magnetism were having an appreciable effect on their results.

Surface waves were used for experimental stress measurement work by McKannan of NASA [15]. Although aluminum was used as the test material, they were able to measure velocity changes to 0.1 nsec, indicating some sophistication in the measurement of these small changes. Alers also reported the measurement of small changes in ultrasonic velocity [16]. This work discusses the effect of magnetic fields, dislocations, superconductivity and static stress. Some procedures for determining the higher order elastic constants were also discussed. Both McKannan's and Alers' work were presented in 1966.

In another paper, Breazeale gives a very thorough theoretical and

experimental analysis related to the higher order elastic constants [17]. Noronha, Chapman and Wert discuss their work in the application of ultrasound to residual stress measurement [18]. Becker has also discussed the application of surface waves to residual stress measurement [20].

Hsu [21] presented experimental data on the stress-induced changes in wave speed for aluminum and steel and showed that the acoustoelastic effect could be used for relative stress measurement under controlled conditions. Clotfelter and Risch [22] presented experimental results showing that residual stress measurements in railroad wheels and rail are possible. They limited their investigation to bulk waves travelling transverse to the major stress direction and to surface waves. Martin [23,24] has reported on a surface wave technique for measuring residual stresses in several aluminum alloys. A number of techniques for accurately measuring wave speeds are discussed in reference 25.

ACOUSTOELASTIC CONSTANTS FOR RAIL STEEL

The stress induced changes in wave speed were measured in two test specimens machined from rail steel. One was a bar of dimensions 25 x 66 x 607 mm (1 x 2.58 x 23.9 in) taken from the head of a 115 lb rail (specimen 8, table VI). The other, which had dimensions 14.8 x 67.3 x 425 mm (0.58 x 2.65 x 16.7 in) was cut from the web of the same rail. A photo of one of the specimens and the apparatus used for these measurements is shown in Figure 2. The specimens were loaded in tension with a conventional 2.67×10^5 N (60000 lb) testing machine.

The acoustoelastic constants were determined for shear waves propagating transverse to the applied load with both parallel and perpendicular polarizations and for longitudinal waves propagating in the direction of the applied load. The shear waves were generated and received by an identical pair of 5 MHz damped shear wave transducers (Panametrics VIP 5/.25) coupled to the specimen with a viscous resin (Dow V-9) and held in place with a spring loaded holder. The longitudinal waves were generated and detected with the transducers mounted on 28° Plexiglas wedges clamped to the specimen surface. The source transducer was a 25.4 mm square piezoelectric plate 1.27 mm thick, with a nominal resonant frequency of 1.6 MHz. A 5 MHz damped longitudinal wave transducer (Panametrics VIP 5/.5) was used as the receiver.

Several techniques for measuring the time of wave travel were compared for consistency. The "sing-around" technique [25], although allowing a continuous measurement of velocity as a function of load, yielded inconsistent wave speed measurements at low stresses because of

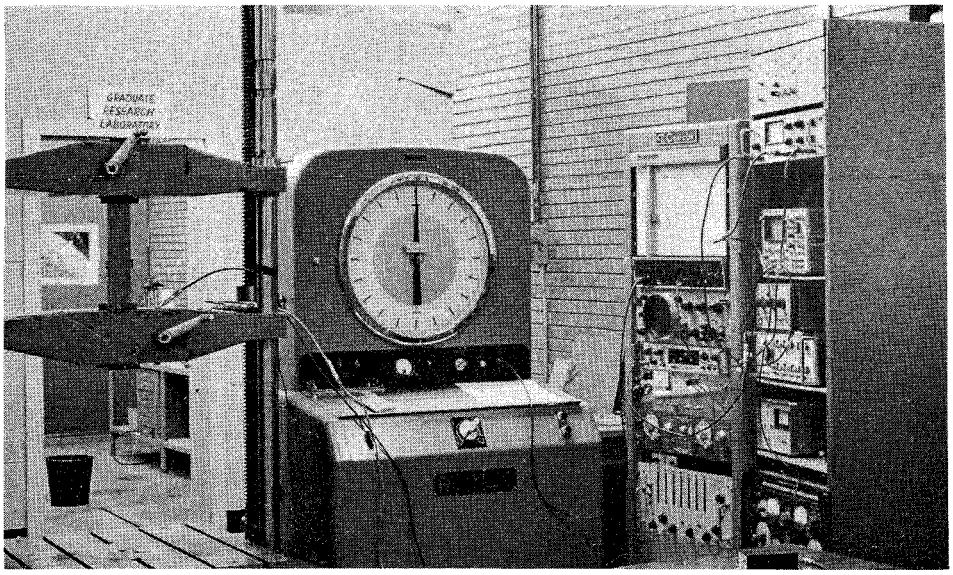

Figure 2a Instrumentation for Acoustoelastic Constant Measurement.

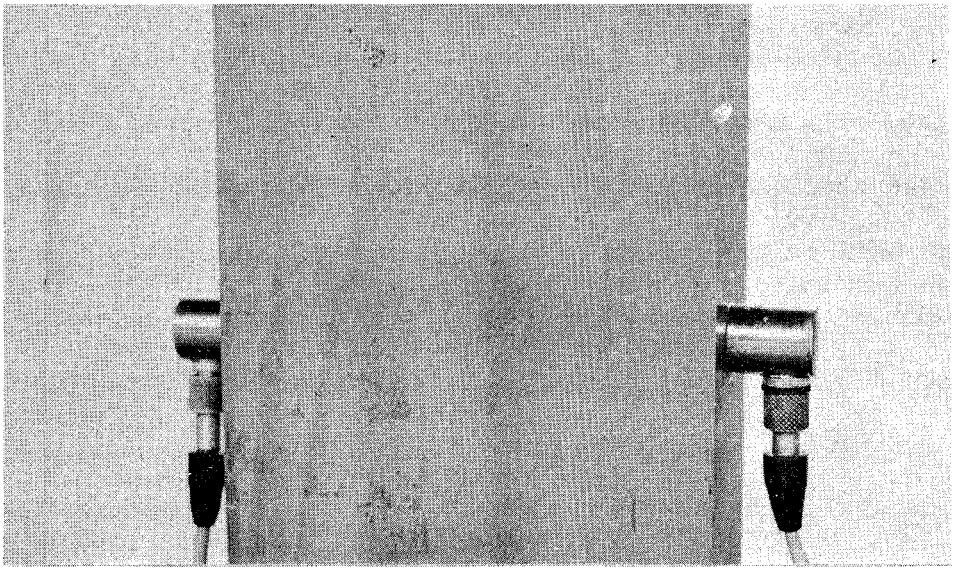

Figure 2b Specimen Machined from Rail and Shear Wave Transducers.

slight changes in received wave-form believed due to an increase in material damping with load. The wave-form changes are manifested as apparent changes in wave speed which cannot be separated from the actual changes. A resonant frequency technique, which utilized the phase difference between the generated and received signals for detecting resonance, while very sensitive to wave speed changes, yielded inconsistent changes in wave speed at low stress levels making results obtained with this method questionable.

The most consistent data was yielded by a pulse overlay technique; a modification of the pulse-echo-overlap method used by Hsu [21]. A schematic showing the instrumentation for this measuring technique is shown in Figure 3. A stable precision oscillator triggered a gated wave generator which produced ten cycles of a 3 MHz simple harmonic signal. This signal along with the amplified received signal were superimposed on the oscilloscope display by adjusting the oscillator period to coincide with the wave travel time across the specimen. The oscillator frequency was determined to within 1 part in 10^5 with the digital counter. The wave speed is the product of this frequency and the actual path length. The overall accuracy of the technique was estimated to be 4 parts in 10^5.

The actual path length was slightly different from the initial length due to the specimen strain. The effect of specimen strain may be incorporated in the measured date by noting that since

$$C = FL$$

where C - wave speed

F - measured pulse repetition frequency

L - actual path length

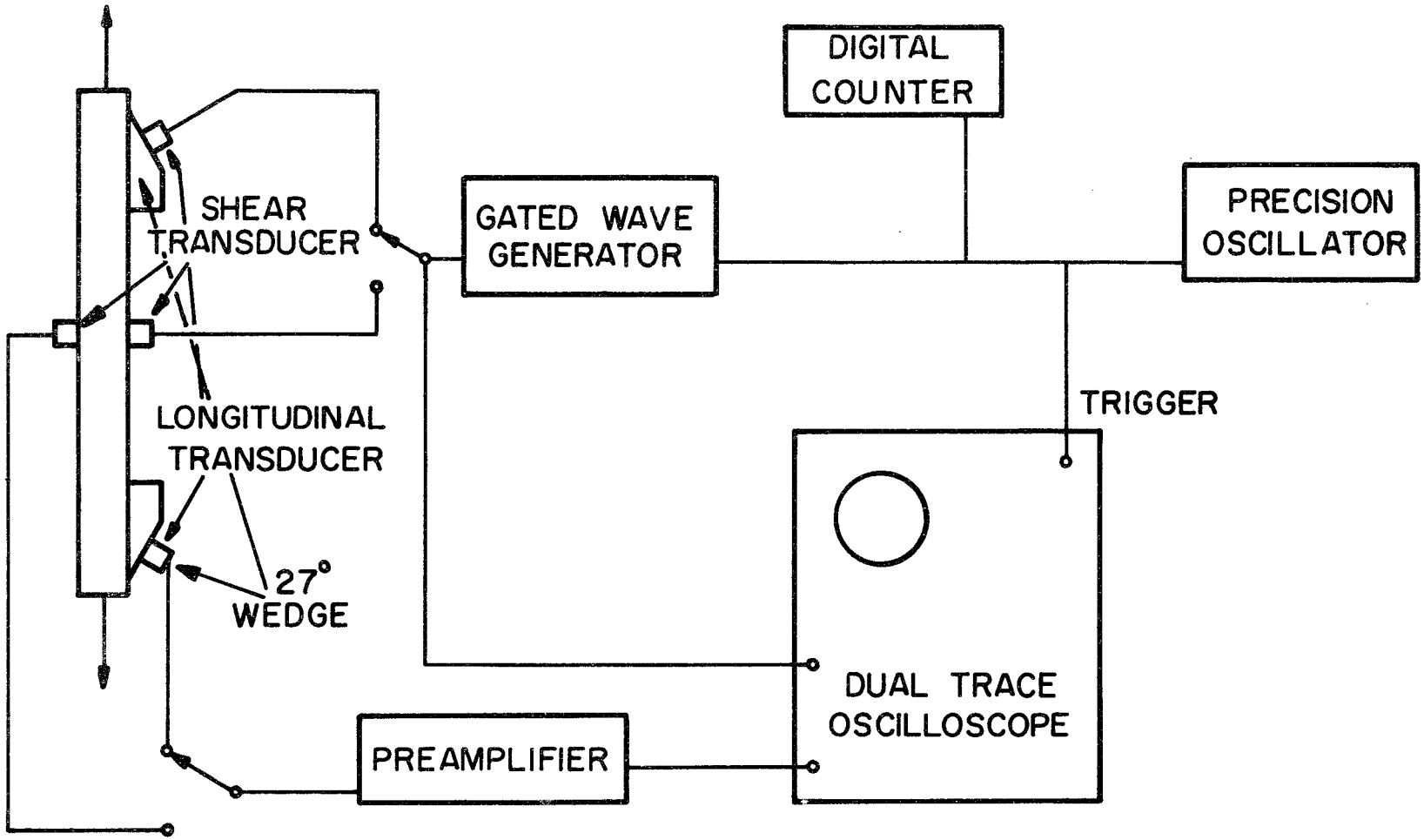

Figure 3 Schematic of Pulse Overlay Technique for Wave Speed Measurements.

then

$$\frac{\Delta C}{C_o} \approx \frac{\Delta F}{F_o} + \frac{\Delta L}{L_o} \quad . \tag{10}$$

Here the subscript o indicates that the quantity is evaluated at zero stress. For a path length transverse to the applied load

$$\frac{\Delta L}{L_o} = -\nu \frac{\sigma}{E} \tag{11}$$

where

σ - axial stress

ν - Poisson's ratio

E - elastic modulus

If the path length is parallel to the applied load, then

$$\frac{\Delta L}{L_o} = \frac{\sigma}{E} \tag{12}$$

Hence the relative change in wave speed may be calculated using equations (10) and (11) or (12) as appropriate.

The results of the wave speed measurements for the two rail specimens are shown in Figure 4. The data points shown are averages of two or more measurements. The largest deviation of my particular measurement from the average was about $\pm$ 0.5 x 10^{-4} while the more typical deviation was $\pm$0.2 x 10^{-4}. As expected from previous work, the variation in wave speed is linear with stress. The shear wave speed changes for perpendicular polarization are small compared to the larger changes for parallel polarization. The speed change for longitudinal waves is 60% larger than the shear wave speed change.

A comparison of acoustoelastic constants for steel taken from

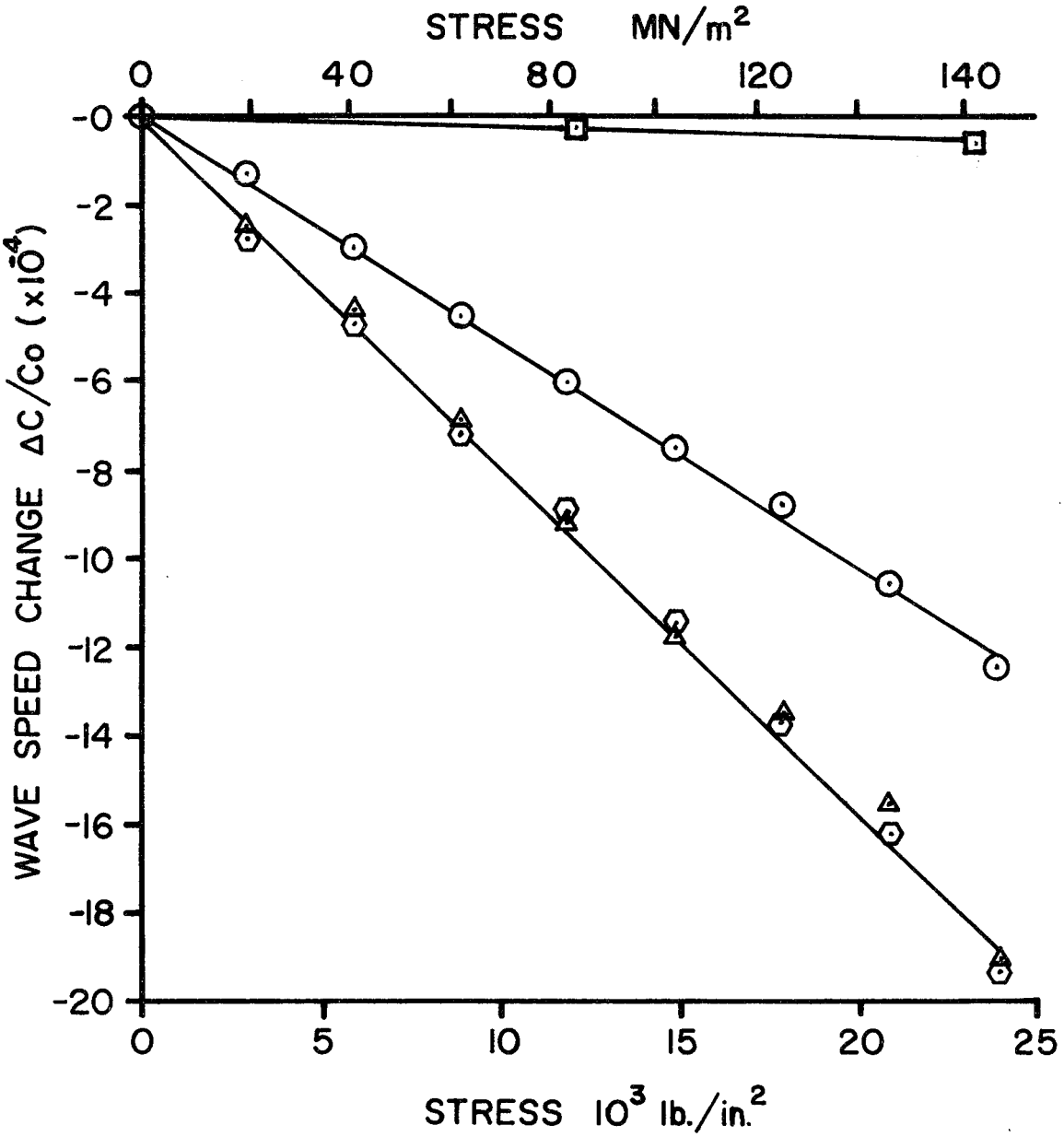

Legend

- ○ Shear Wave Propagating Transverse to and Polarized Parallel to Load.
- □ Shear Wave Propagating Transverse to and Polarized Perpendicular to Load.
- △ Longitudinal Wave Propagating Parallel to Load (Specimen from rail head).
- ⬡ Longitudinal Wave Propagating Parallel to Load (Specimen from rail web).

Figure 4 Stress Induced Wave Speed Changes for Rail Steel.

several sources is shown in Table I. The constants are given as the relative change in wave speed per unit strain $\Delta(C/C_o)/\Delta\epsilon$ which is determined by multiplying the slope in Figure 4 by the elastic modulus. The data taken from references 9 and 22 were corrected for strain as discussed above. The data from reference 21 had apparently been corrected. The agreement between the various sources is remarkably good especially considering the difficulty of the measurement. It should be noted that although several specimens were evaluated in reference 21, sufficient raw data was given for only one specimen and that one happened to have the lowest acoustoelastic constants of the group.

Wave Type	$\frac{\Delta(C/C_o)}{\Delta\epsilon}$ 1	2	3	4
a	-2.40	____	____	____
b	-1.55	-1.6	-1.58	-1.44
c	-0.09	0	0.05	0.05

a longitudinal wave propagating parallel to applied load

b shear wave propagating transverse to load and polarized parallel to load.

c shear wave propagating transverse to load and polarized perpendicular to load.

1 present data

2 data from reference 21, Figure 3

3 data from reference 9, Table 3

4 data from reference 22, Table 7

TABLE I Comparison of Acoustoelastic Constants for Steel from Several Sources.

ACOUSOELASTIC EFFECT FOR GUIDED WAVES

Description of Apparatus A series of experiments were conducted to determine the changes in wave speed due to applied stress for guided waves propagated in a steel bar. The specimen tested was a rectangular parallelpiped of cross-section 7.42 x 22.9 mm (.29 x .90 in) and length 600 mm (23.6 in). The bar was machined from the head of a length of 12 lb ASCE rail. The bar was loaded axially in tension using a 2.67×10^5 N (60 kip) Riehle hydraulic test machine. The maximum load applied was 2.67×10^4 N (6 kips) which corresponds to an axial stress of 157.2 MN/m^2 (22780 psi).

A schematic diagram of the apparatus used in the test is shown in figure 5. The bar was excited by a longitudinal piezoelectric transducer coupled to the bar with a variable-angle Plexiglas wedge. This transducer was driven directly from an oscillator gated by a variable width, variable repetition rate pulse generator. The signal from the receiving transducer and wedge, identical to the transmitting set, was amplified 60 db and displayed on a scope along with the input signal to the transmitter.

The experiment consisted of measuring the change in arrival time of the received signal relative to the transmitted signal as the load changed from zero to 2.67×10^4 N (6 kips). This was done by using the time delay feature of the dual time base scope which allows a small portion of the received pulse to be displayed at an expanded sweep rate. Having established a reference with the bar under zero stress, the load was increased and the time delay of the received pulse measured directly from the expanded display. Accuracy of the time delay measurements is estimated to be $\pm$ 5 ns.

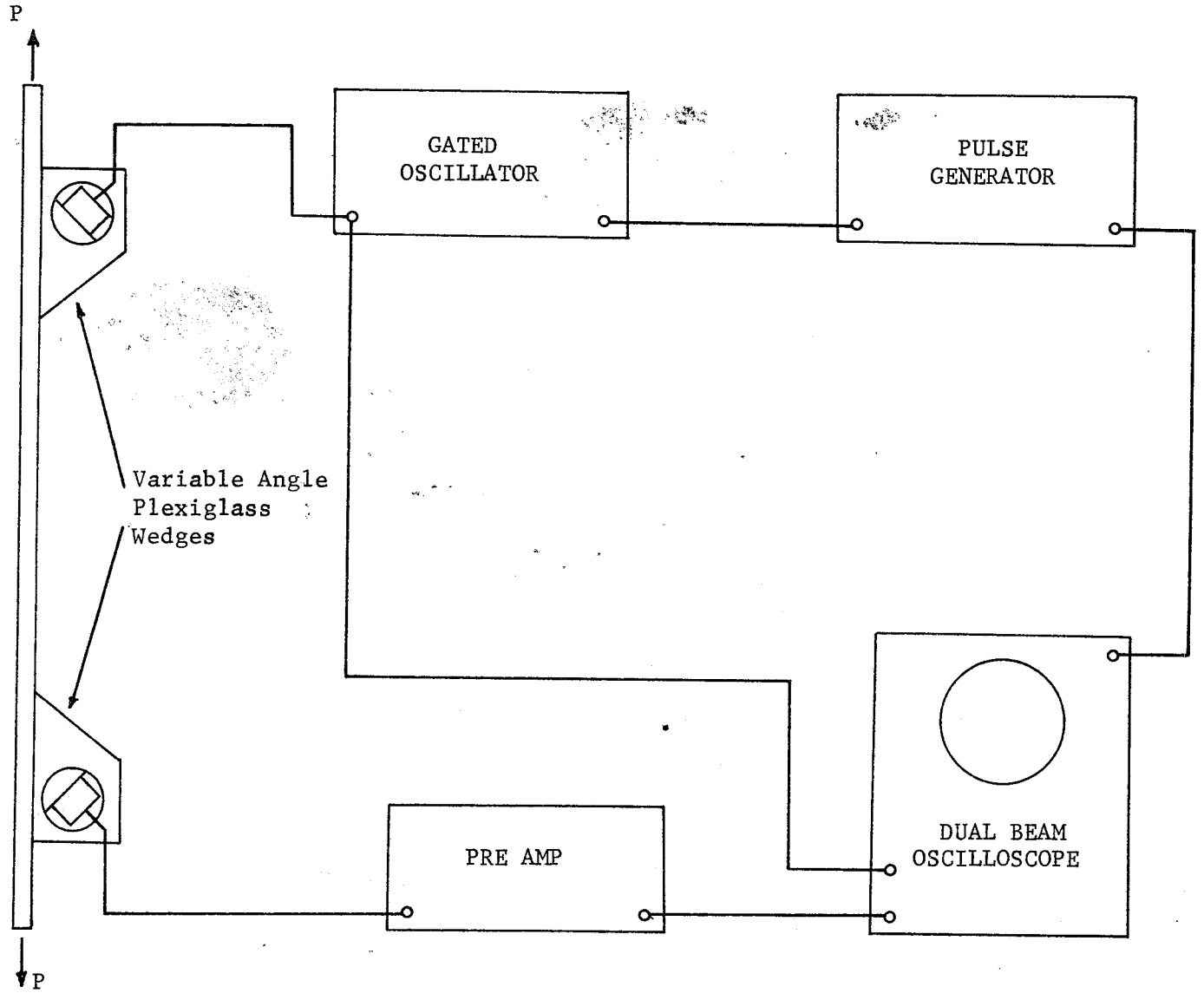

Figure 5 Apparatus for the Measurement of the Acoustoelastic Effect on Guided Waves.

Received Wave Identification A diagram of the method used to excite waves in the bar is shown in figure 6. The initial longitudinal wave propagates toward the bar at angle α_P to the normal. At the interface between the wedge and the steel bar the wave divides into a longitudinal and a transverse component, travelling at angles α_L and α_T, respectively. Because wave propagation in the bar is dispersive, the pulse shape is not generally maintained as the wave travels through the bar and may separate into more than one disturbance. The velocities at which these disturbances travel are a function of the frequency of the initial wave and the angle α_P (or alternatively, α_L or α_T). For purposes of identifying the received disturbances the classical wave solution for an infinite homogeneous, isotropic plate (Lamb waves) has been useful. Figure 7 is a plot of the phase velocity as a function of frequency, according to the Lamb wave solution, for a plate having the following properties:

thickness	= 7.42 mm (0.292 in)
density	= 7800 kg/m^3 (0.730 x 10^{-3} lb-sec^2/in^4)
Young's modulus	= 21.64 x 10^{10} N/m^2 (31.4 x 10^6 lb/in^2)
Poisson's ratio	= 0.2767
dilatational wave speed	= 5933 m/s (233600 in/sec)
distortional wave speed	= 3297 m/s (129800 in/sec)

Young's modulus and Poisson'a ratio were determined from the measured dilatational and distortional wave speeds and the density as given above.

The group velocity for the same solution is shown in Figure 8. the A(antisymmetric) or S(symmetric) in Figure 8 refer to the antisymmetry or symmetry of the plate displacements about the middle plane of the plate. The subscripts are used to order the various possible wave modes. It is

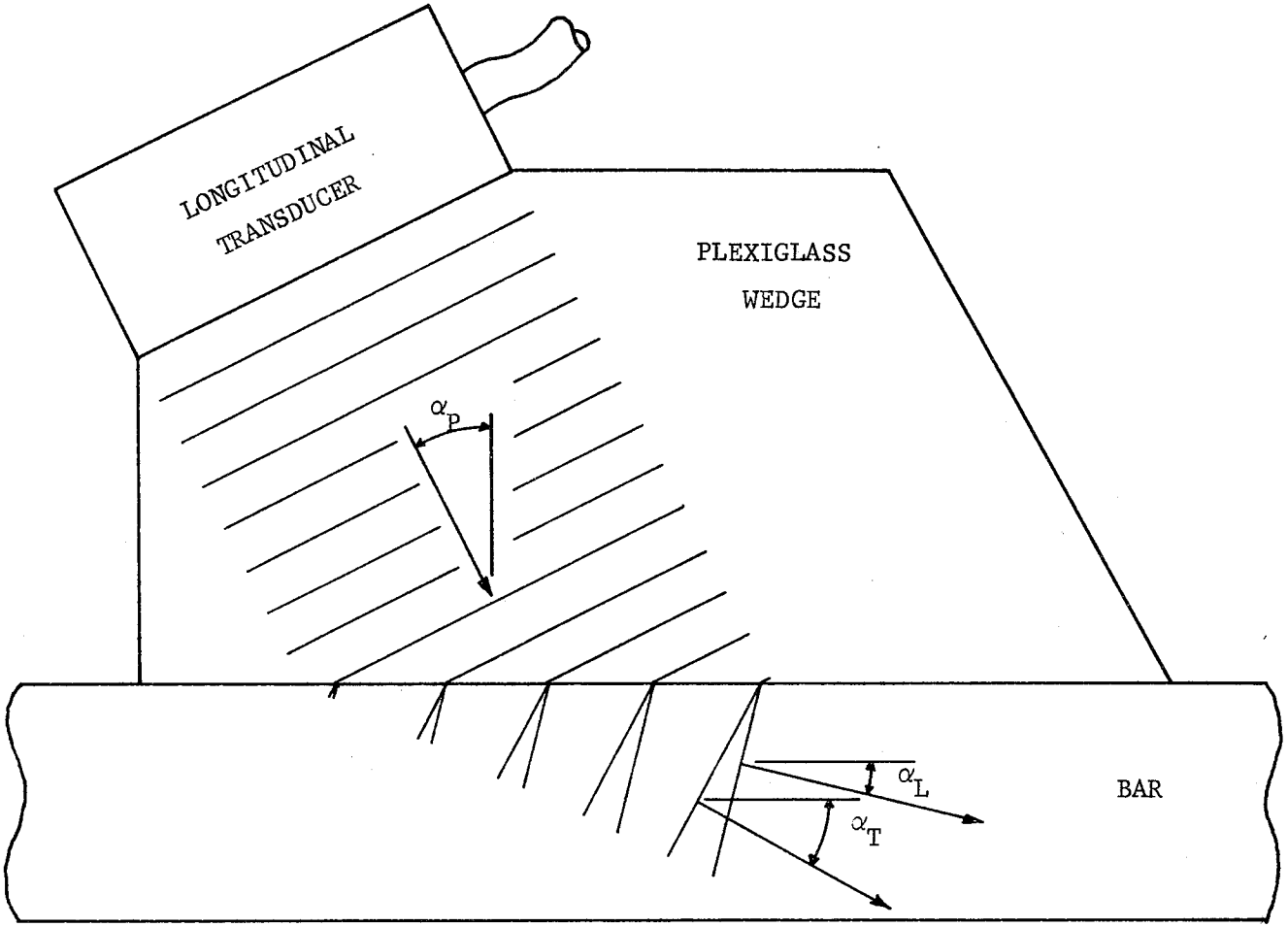

Figure 6 Method Used to Excite Waves in Bar.

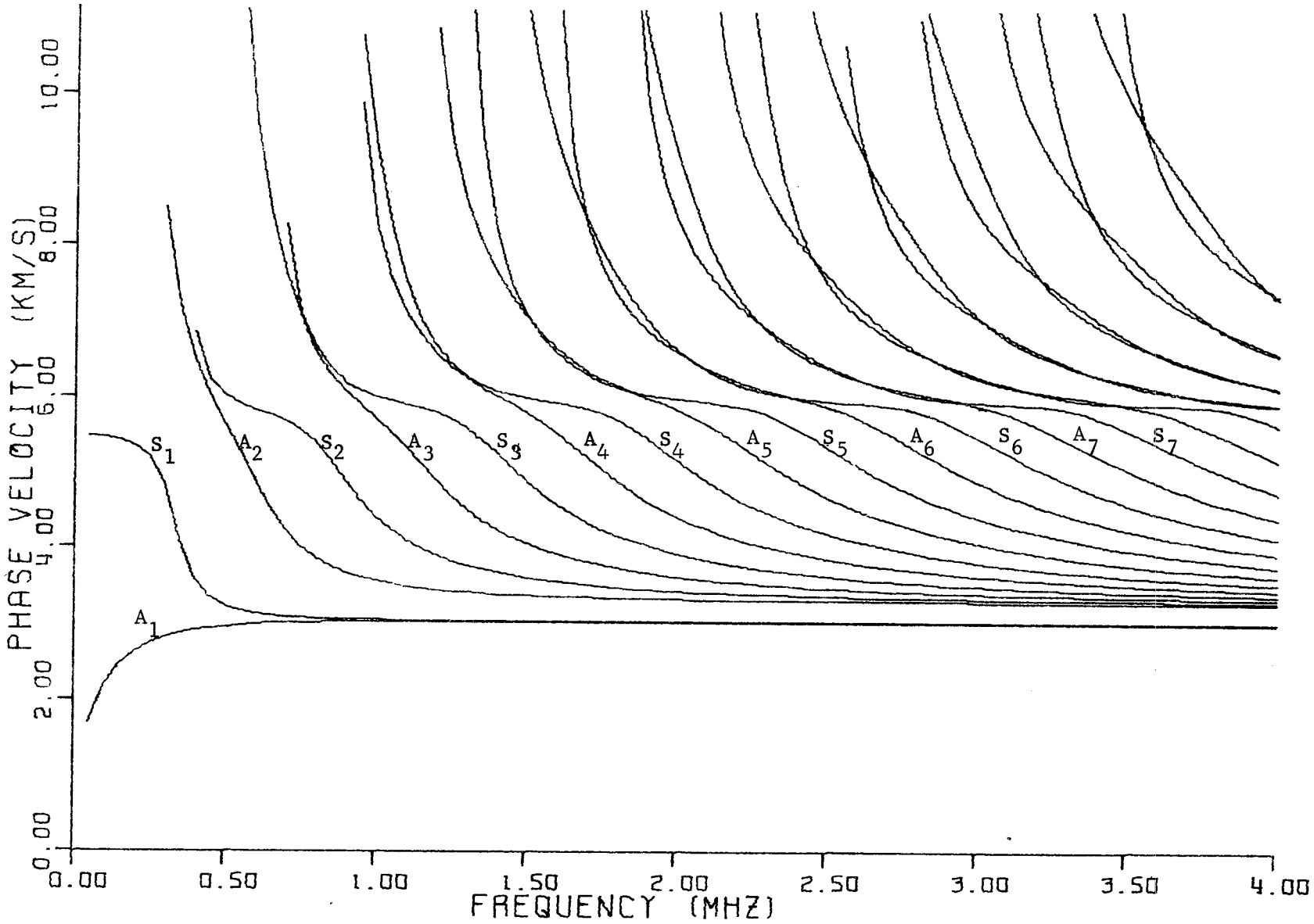

Figure 7 Phase Velocities for Lamb Waves in a Steel Plate of Thickness 7.42 mm.

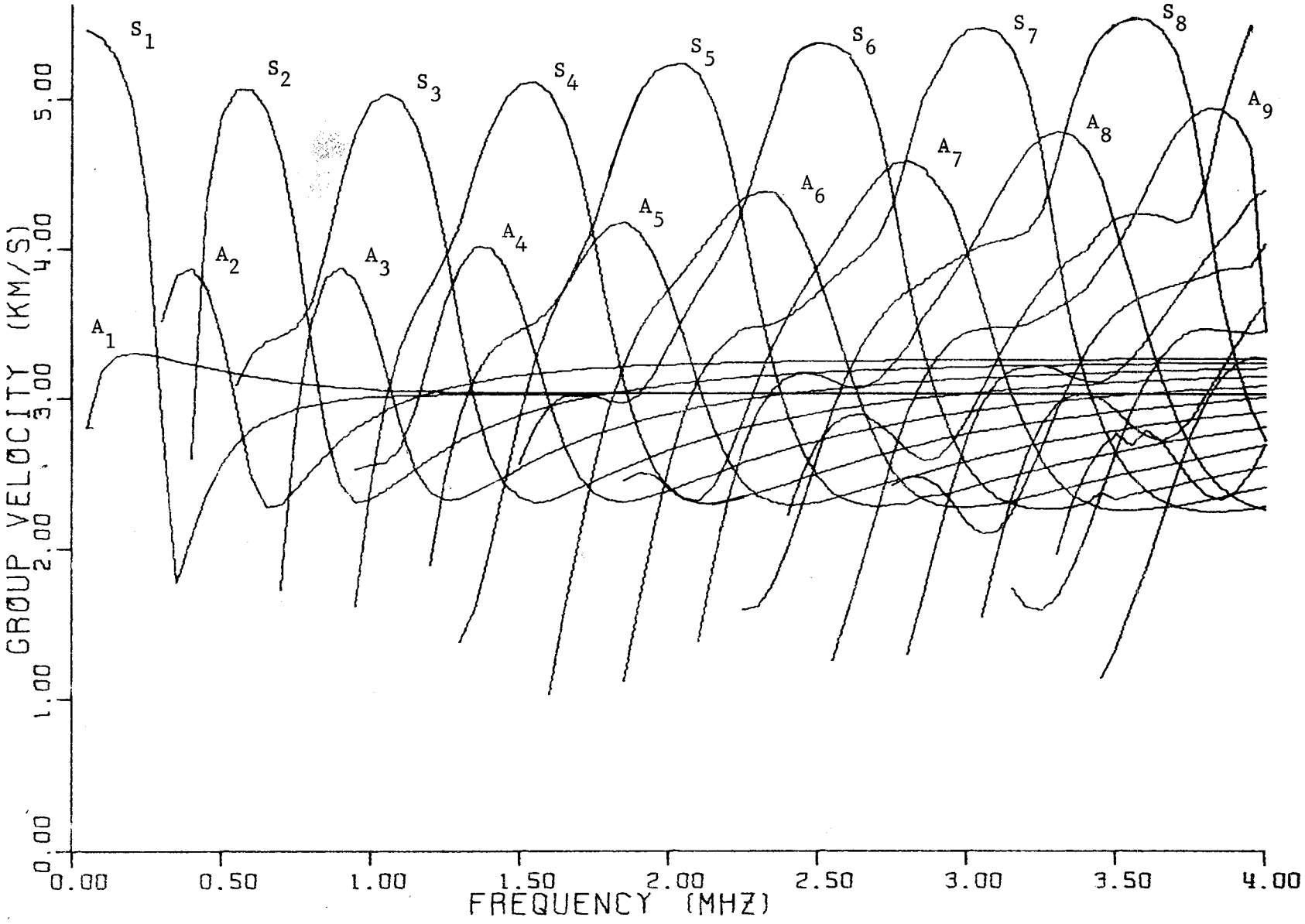

Figure 8 Group Velocities for Lamb Waves in a Steel Plate of Thickness 7.42 mm.

known that the frequency of the largest propagated disturbances will be near those frequences of zero slope of the group velocity curve. Energy put into the plate at other frequencies disperses resulting in a rapid reduction in peak amplitude. Hence the signal received should only have components associated with the frequencies and group velocities of those points in Figure 8 having zero slope. Further, each wave mode is associated with particular values of α_L and α_T (or alternatively α_P) for a given frequency. These values of α_P are shown in Figure 9.

Using Figures 8 and 9, the frequency and incident angle, α_P, needed to excite a particular mode may be determined. For example, the group velocity maximum (C_g = 4.1 km/s) for mode A_2 requires a frequency near 0.44 MHz (from Figure 8) and an incident angle of 25.9 degrees (from Figure 9). Thus an excitation pulse of 0.44 MHz at an angle of 25.9 degrees should results in a recognizable disturbance arriving at the receiver at a time corresponding to a speed of 4.1 km/s. There may of course be other disturbances arriving at different times. For this example, the modes A_1, A_2 and possibly S_3 may contribute to the received signal.

The association of an incident angle, a frequency and a particular region of zero slope on the group velocity plot has simplified the identification of the various components of the received signal in these experiments. Interestingly, in spite of the fact that the width/thickness ratio of the bar is only slightly greater than 3, the Lamb wave analysis shows reasonable agreement with the experimental values of group velocity and frequency.

Tables II, III and IV show data taken from the calculations leading to Figures 7, 8, and 9, for regions of zero group velocity vs. frequency slope. The first three columns identify the mode, frequency and group

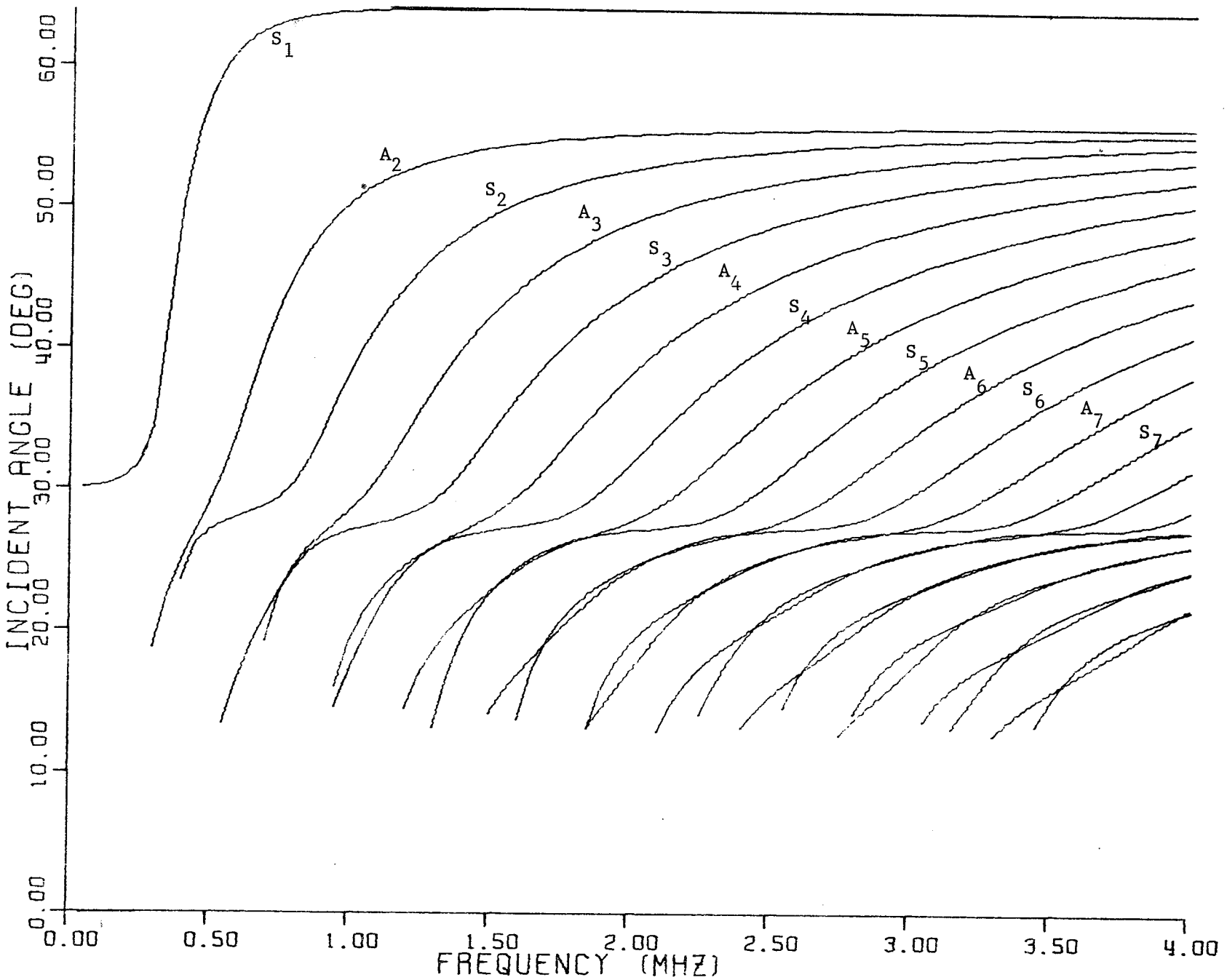

Figure 9 Incident Angle, α_p, in Plexiglas Wedge Needed to Excite Lamb Waves in a Steel Plate of Thickness 7.42 mm.

MODE	FREQ MHz	C_g km/s	Long Trans.	α_L deg	α_P deg
A_2	0.44	4.13	2.08	19.1°	25.9
S_2	0.56	5.09	2.38	0	27.8
A_3	0.88	3.89	2.28	15.5	26.5
S_3	1.04	5.05	2.53	5.7	27.4
A_4	1.36	4.01	2.22	13.6	26.7
S_4	1.52	5.14	2.98	7.7	27.3
A_5	1.80	4.17	2.15	15.5	26.5
S_5	2.04	5.26	3.45	6.8	27.3
A_6	2.32	4.40	2.32	13.	26.8
S_6	2.52	5.33	4.26	7.0	27.3
A_7	2.80	4.61	2.58	12.6	26.8
S_7	3.04	5.49	4.98	6.2	27.4
A_8	3.32	4.80	2.88	11.2	27.0
S_8	3.52	5.60	5.79	6.0	27.4
A_9	3.80	4.97	3.30	10.8	27.0
S_9	3.96	5.48	5.78	6.2	27.4

TABLE II Characteristics of Disturbances Propagated in a 7.42 mm Plate for Incident Angles Near 27°.

MODE	FREQ MHz	C_g km/s	Long. / Trans.	α_T deg	α_P deg
S_1	0.32	2.16	.048	43.9	36.8
A_2	0.68	2.28	.033	40.3	39.4
S_2	1.00	2.34	.009	41.6	38.5
A_3	1.28	2.33	.002	44.0	36.8
S_3	1.56	2.33	.0004	45.4	35.7
A_4	1.84	2.32	.0009	46.4	35.0
S_4	2.16	2.31	.0002	46.1	35.3
A_5	2.40	2.30	.0006	47.7	34.0
S_5	2.68	2.29	.0004	48.2	33.7
A_6	2.96	2.29	.0003	48.5	33.4
S_6	3.24	2.27	.0002	48.8	33.2
A_7	3.52	2.27	.0001	49.1	33.0
S_7	3.84	2.26	.00003	48.7	33.3
A_8	4.00	2.27	.0002	50.7	31.8

TABLE III Characteristics of Disturbances Propagated in 7.42 mm Plate for Incident Angles near 35°.

MODE	FREQ MHz	C_g km/s	Long. / Trans.	α_S deg	α_P deg
A_1	>1.0	3.05	10^{-6}	—	64.3
S_1	>1.0	3.05	10^{-6}	—	64.3
A_2	>1.5	3.29	10^{-10}	3.7	56.1
S_2	>2.5	3.26	10^{-10}	7.4	55.6
A_3	>3.0	3.23	10^{-9}	11.1	54.7

TABLE IV Characteristics of Disturbances Propagated in a 7.42 mm Plate for Incident Angles Near 55^{o} and 65^{o}.

velocity of the expected disturbance. Column four indicates the ratio of the displacements of the longitudinal to transverse components of the motion. The angle of the predominant wave type is listed in column five. The last column lists the wedge angle needed to excite the wave.

Note that all of the maxima of the group velocity curves for the higher order modes are excited near 27^{o} and that these disturbances are largely longitudinal waves. Also all of the minima (except A_1) are excited near 35^{o} and these disturbances are primarily shear waves. The modes shown in Table IV are relatively dispersion free because of the wide frequency ranges having constant group velocity. The S_1 and A_1 modes in Table IV are surface waves and the remainder are shear waves travelling parallel to the plate surface.

Results of Acoustoelastic Measurements A summary of the data taken in the acoustoelastic experiment is shown in Table V. Columns 1 and 2 define the input signal and column 3 gives the wedge angle. The travel distance, column 4, is the separation between the centers of the transmitted and received ultrasonic beams at the Plexiglas-steel interface. The travel time, column 5, has been adjusted for the delay in the Plexiglas wedges. Column 6, the group velocity, is assigned as described above. The time delay of the received disturbance due to the application of a 2.67×10^{4} N (6 kips) load is shown in column 8. Column 9 is the relative time delay, column 8 divided by column 5, and column 10 is the relative time delay per unit axial strain. The last column shows the relative change in wave speed per unit strain computed from:

$$\frac{\Delta c}{\epsilon c} = 1 - \frac{\Delta t}{\epsilon t} \qquad (13)$$

1	2	3	4	5	6	7	8	9	10	11
INPUT Freq. MHz	Duration μs	α_p deg	Travel Dist. mm	Travel Time μs	C_g km/s	Mode	Δt @ 6 kips ns	$\frac{\Delta t}{t}$ $\times 10^{-4}$	$\frac{\Delta t}{\epsilon t}$	$\frac{\Delta \epsilon}{\epsilon c}$
0.5	40	68	218	71	3.1	A_1	65	9.2	1.27	-0.27
1.0	40	68	218	71	3.1	A_1	65	9.2	1.27	-0.27
1.5	40	68	218	71	3.1	A_1	65	9.2	1.27	-0.27
0.5	40	58	243	76	3.2		55	7.2	0.99	+0.01
1.1	40	58	243	78	3.1	A_1	65	8.3	1.14	-0.14
2.0	40	58	243	71	3.4	A_2	70	9.9	1.36	-0.36
3.1	40	58	243	71	3.4	A_2	70	9.9	1.36	-0.36
0.6	40	35	270	121	2.2	A_2	70	5.8	0.80	+0.20
1.0	40	35	270	123	2.2	S_2	70	5.7	0.79	+0.21
1.2	40	35	270	115	2.4	A_3	70	6.1	0.84	+0.16
1.4	40	35	270	117	2.3	S_3	80	6.8	0.94	+0.06
1.9	40	35	270	115	2.4	A_4	80	7.0	0.96	+0.04
2.7	40	35	270	115	2.4	S_5	75	6.5	0.90	+0.10
0.5	11	25	278	77	3.6	A_2	100	13.0	1.79	-0.79
0.75	40	25	278	89	3.1		100	11.2	1.54	-0.54
0.85	11	25	278	73	3.8	A_3	100	13.7	1.89	-0.89
1.3	40	25	278	93	3.0		100	10.8	1.49	-0.49
1.4	8	25	278	57	4.9	S_4	110	19.3	2.66	-1.66
1.8	10	25	278	55	5.0	S_5	110	20.0	2.75	-1.75
2.0	10	25	278	67	4.2	A_6	105	15.7	2.16	-1.16
2.3	10	25	278	53	5.3	S_6	110	20.1	2.77	-1.77
2.6	5	25	278	73	3.8	S_8	110	15.1	2.08	-1.08
3.0	5	25	278	73	3.8	S_8	105	14.4	1.98	-0.98

TABLE V Acoustoelastic Data for a 7.42 mm x 22.9 mm x 600 mm Rail Specimen Subjected to an Axial Stress.

where

c - wave speed

ϵ - applied axial strain

t - wave travel time

The first term in equation (13) arises from the correction for increasing path length due to axial deformation of the bar.

The data in Table V show two interesting features. First the delay time, Δt, for the different modes are approximately constant for the same excitation angles. This is especially interesting for the modes excited at 25^{o} since the group velocities vary from 3.0 to 5.3 km/s. Secondly, the relative change in wave speed per unit strain shown varies from + 0.21 to -1.77 and several modes show a very small acoustoelastic effect. This latter feature suggests one technique for an absolute stress measurement.

If, as the data implies, the speed of one or more disturbances is relatively independent of applied stress, these speeds may be used to determine the properties of the rail, assuming the rail is homogenous and isotropic. That information should allow the determination of the zero stress wave speed of other disturbances which do exhibit an acoustoelastic effect. Hence the difference between the actual speed of a stress sensitive disturbance should relate to the stress in the rail.

ACOUSTOELASTIC EFFECT IN MODEL RAIL

Load Frame for Model Rail Experiments A photograph of a load frame designed to provide a tensile or compressive longitudinal force of up to 207 MN/m^2 (30,000 psi) to a 12 lb ASCE model rail is shown in Fig. 10a. The cross-members to which the rail is anchored are not fastened to the frame but rest on wooden slides that permit free longitudinal and vertical motion. The cross-members provide lateral restraint similar to that encountered in actual track. The structure at the right of the frame is a transducer support which can be used for maintaining the transducer spacing and position relative to the rail.

The axial force was applied to the rail through a 4 in. hydraulic cylinder shown in the foreground of Figure 10a. This force was measured by means of a strain gage transducer located on the cylinder rod. A schematic of the load measuring bridge is shown in Figure 11.

Stress Distribution in Model Rail Eighteen electrical resistance type strain gages were bonded to the model rail at a cross-section equidistant from the ends to allow monitoring a typical stress distribution during the tests. A photo of the gages is shown in Figure 10b and gage placement is given in Figure 12. The gages were bonded to the rail with a cyano-acrylate contact adhesive after mechanical and chemical cleaning and coated with a air drying polyurethane for protection. In addition, four gages were bonded at each of the remaining quarter points of the rail for determining approximate stress distributions at these locations. A schematic of the strain gage switching circuits and instrumentation is given in Figure 13.

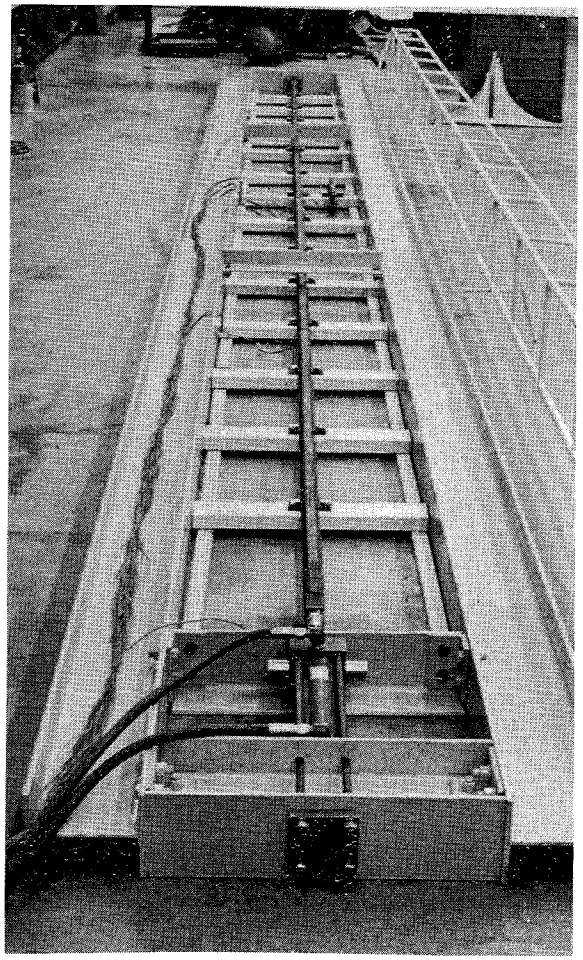

Figure 10a

Load Frame for Model Rail

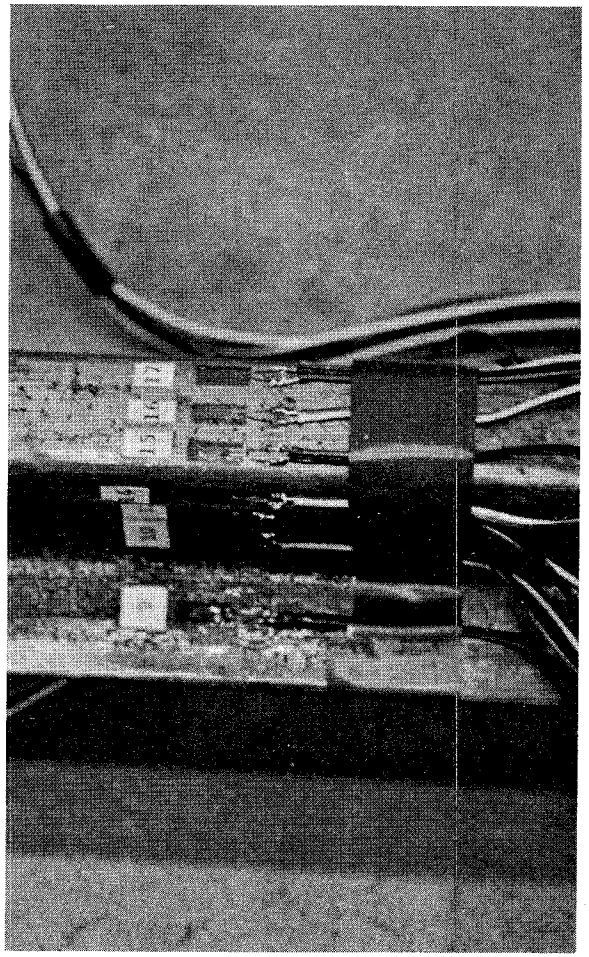

Figure 10b

Strain Gages for Stress

Distribution Measurements

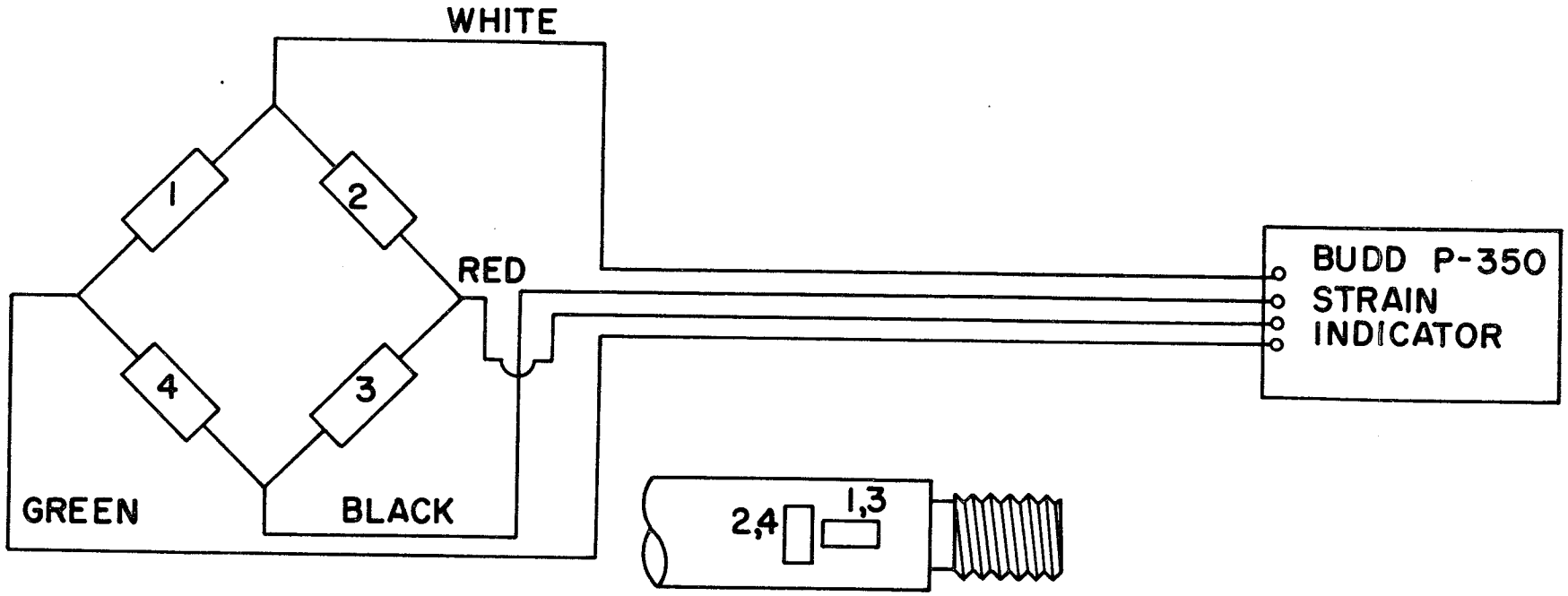

FIGURE 11 Strain Gage Bridge for Measuring Axial Force on Model Rail.

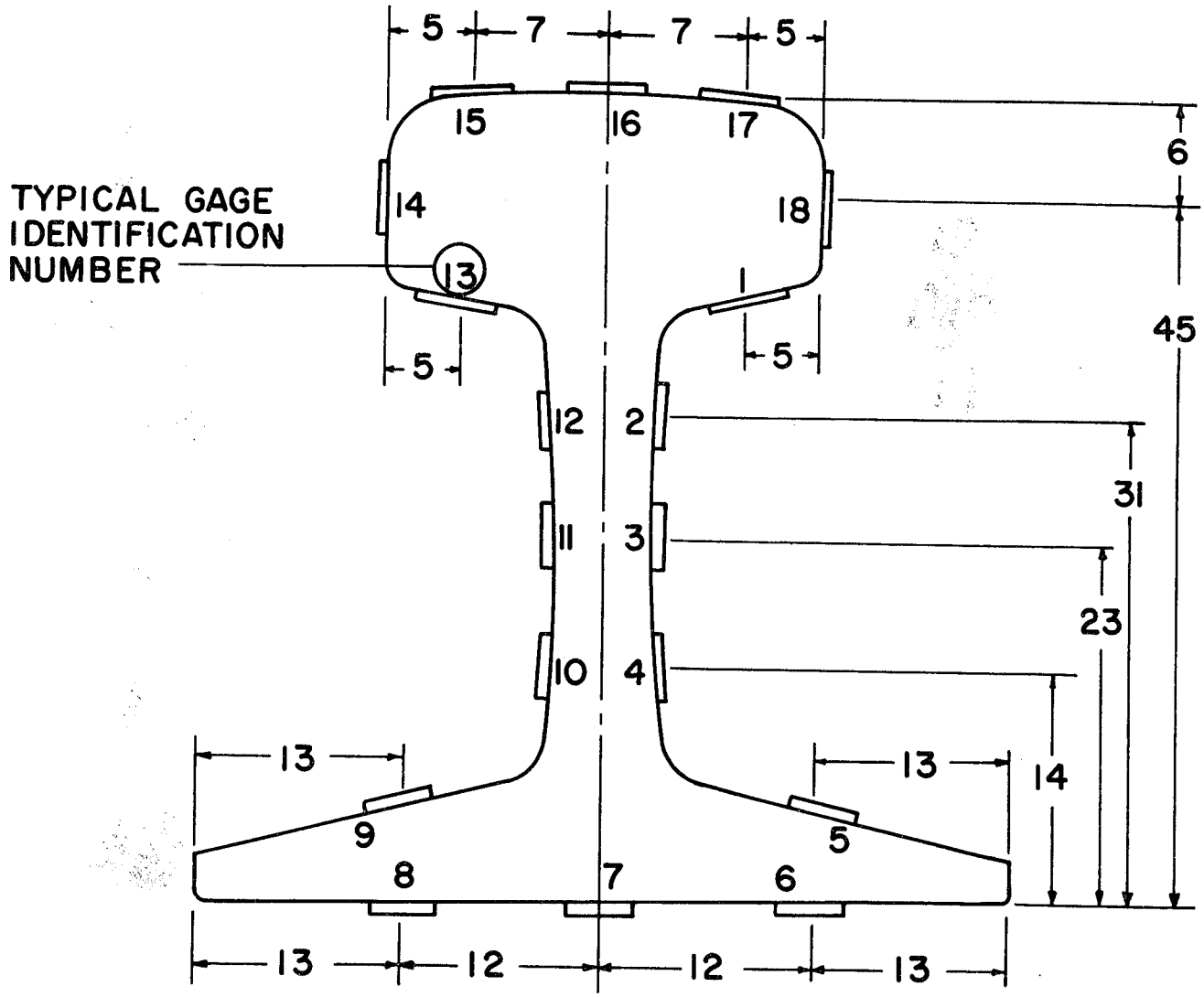

ALL DIMENSIONS IN MILLIMETERS

GAGES 1-18 MICRO-MEASUREMENTS TYPE EA-06-125BT-120

FIGURE 12 Strain Gage Placement for Stress Distribution Measurement.

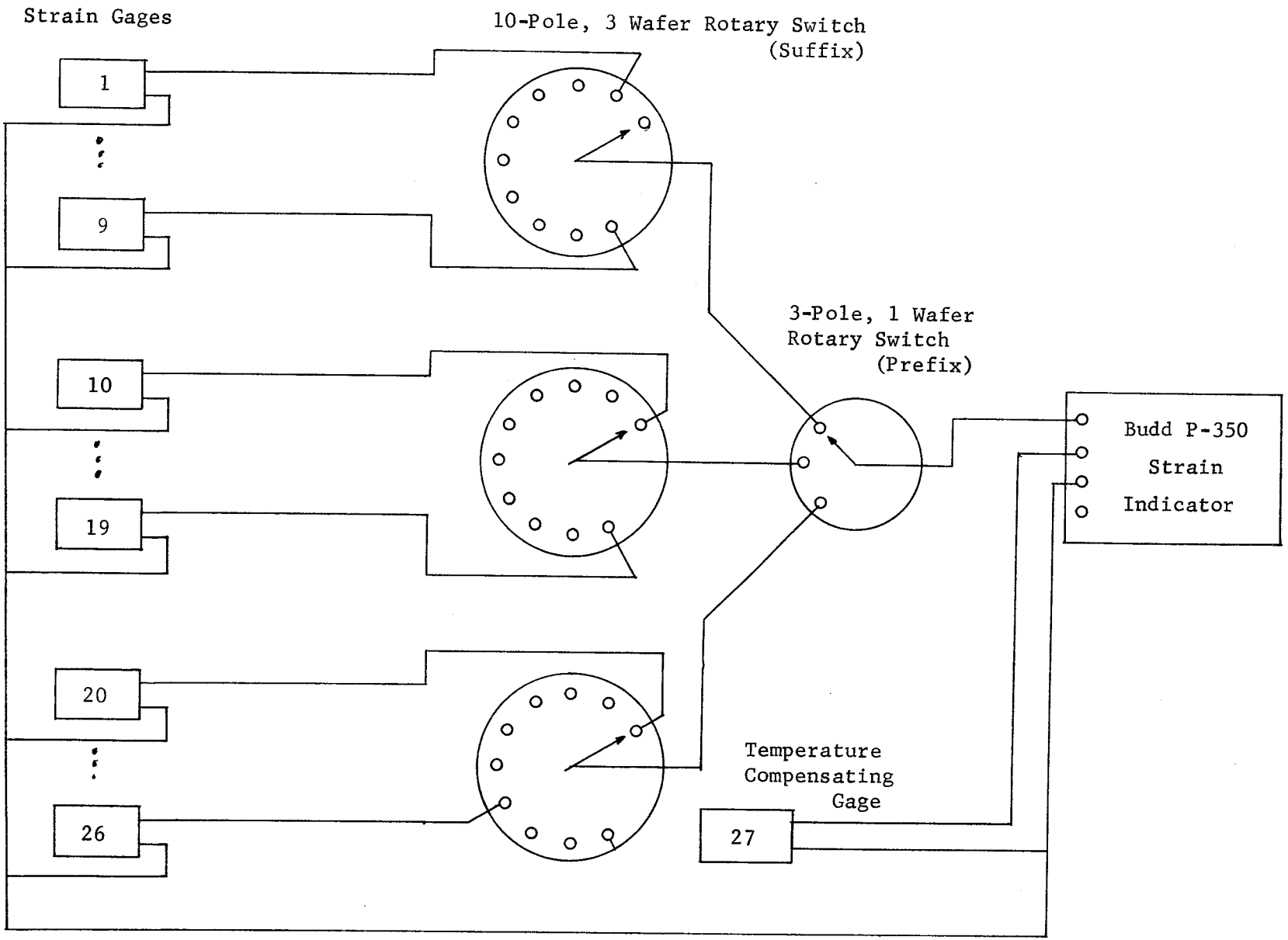

FIGURE 13 Schematic for Strain Gage Selector.

A typical variation of strain as a function of applied tensile load is shown in Figure 14. The data from the two gages 14 and 18, which are located on the lateral extremes of the rail head, see Figure 12, show that there is a flexural strain present in addition to the uniform extension in the rail. This is perhaps more evident from the stress distributions shown in Figure 15, which have been calculated from the strain measurements at a tensile load of 89 x 10^3 N(20 x 10^3 lb) corresponding to an average extensional stress of 124 x 10^6 N/m^2 (18 x 10^3 psi). The obvious flexure about the vertical axis is a result of initial curvature in the rail. Estimates show that an initial eccentricity of 0.1 mm is sufficient cause for the flexural stresses shown in Figure 15.

The stress distribution at the middle of the model rail for an applied compressive load of 67 x 10^3 N(15 x 10^3 lb) or stress of 97.7 MN/m^2 (12.7 x 10^3 psi) is shown in Figure 16. The flexural component here is larger than that encountered under tensile loading because the rail tends to buckle laterally at this load being restrained only by the cross-members to which it is attached.

These flexural stresses about a vertical axis have little effect on the wave speeds because the rail curvature tends to alternate over the total length, reducing the average flexural stress. However variations about a horizontal axis which are not seen in Figure 16, but become apparent when the applied load is near the buckling force, do affect the wave speeds.

Results of Acoustoelastic Measurements The changes in wave speed due to longitudinal stress on the 12 lb ASCE rail were determined with the instrumentation described previously and sketched in Figure 5. Results for

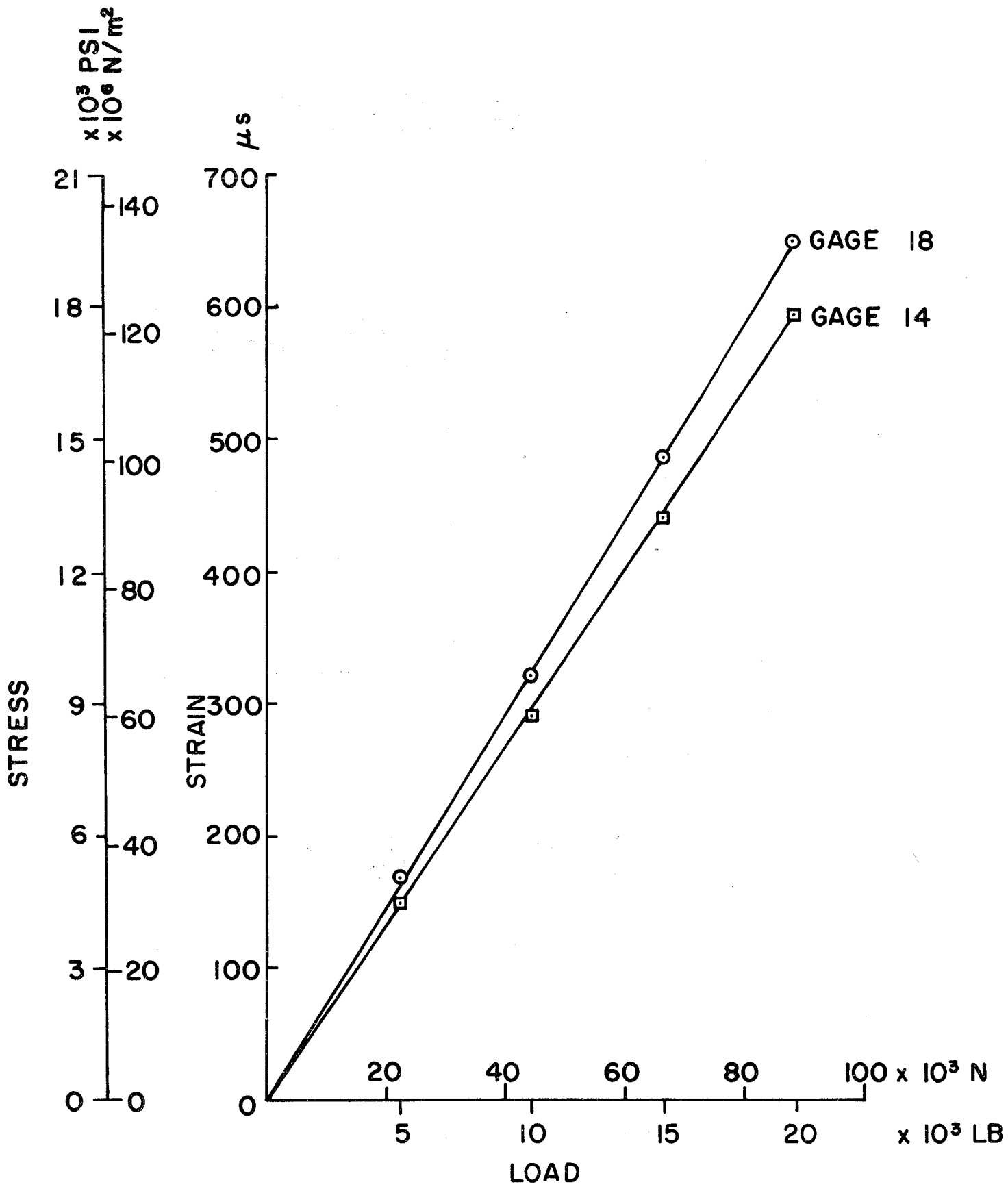

FIGURE 14 Typical Strain (Stress) Data as a Function of Applied Tensile Load.

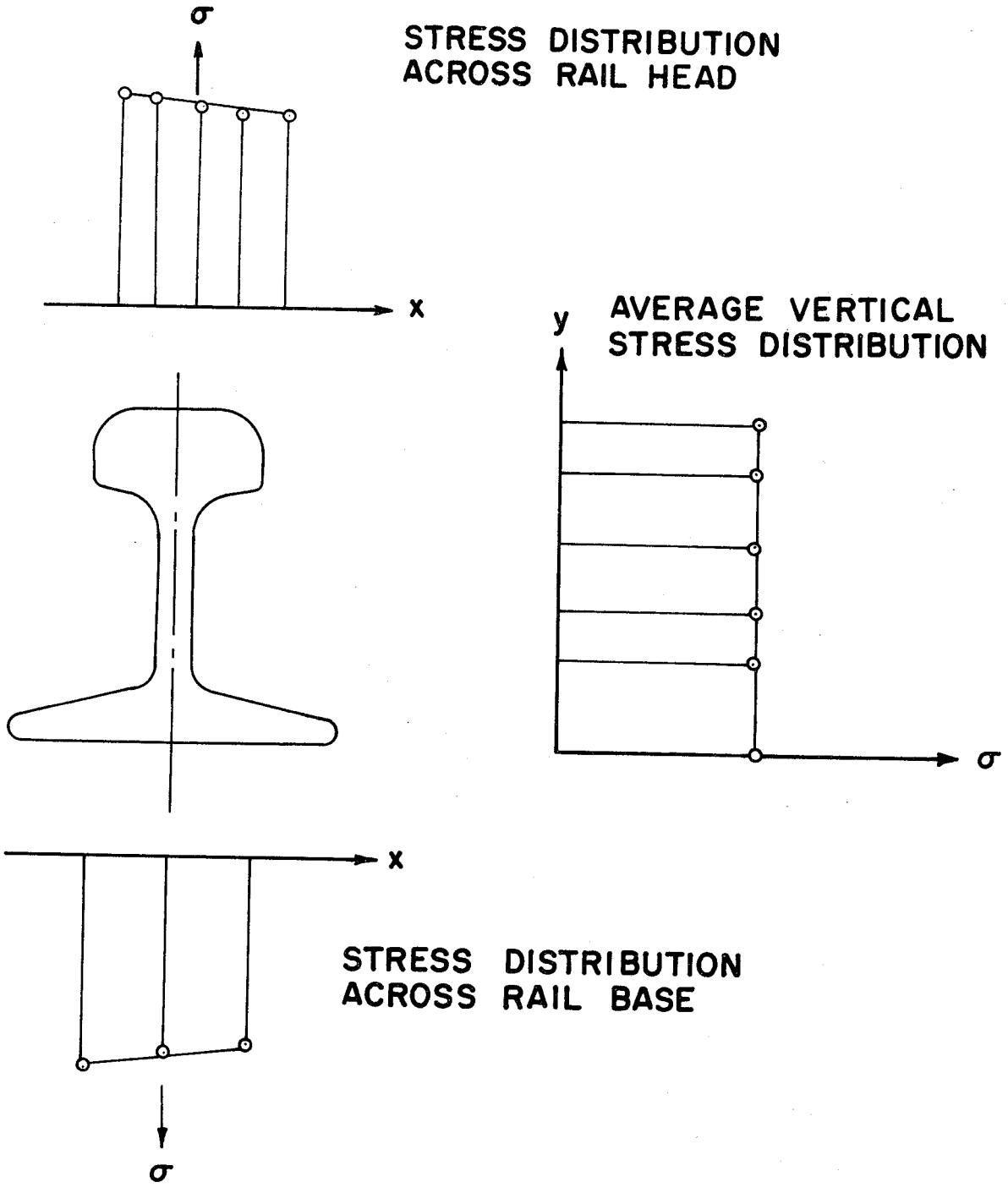

FIGURE 15 Stress Distribution for Tensile Load.

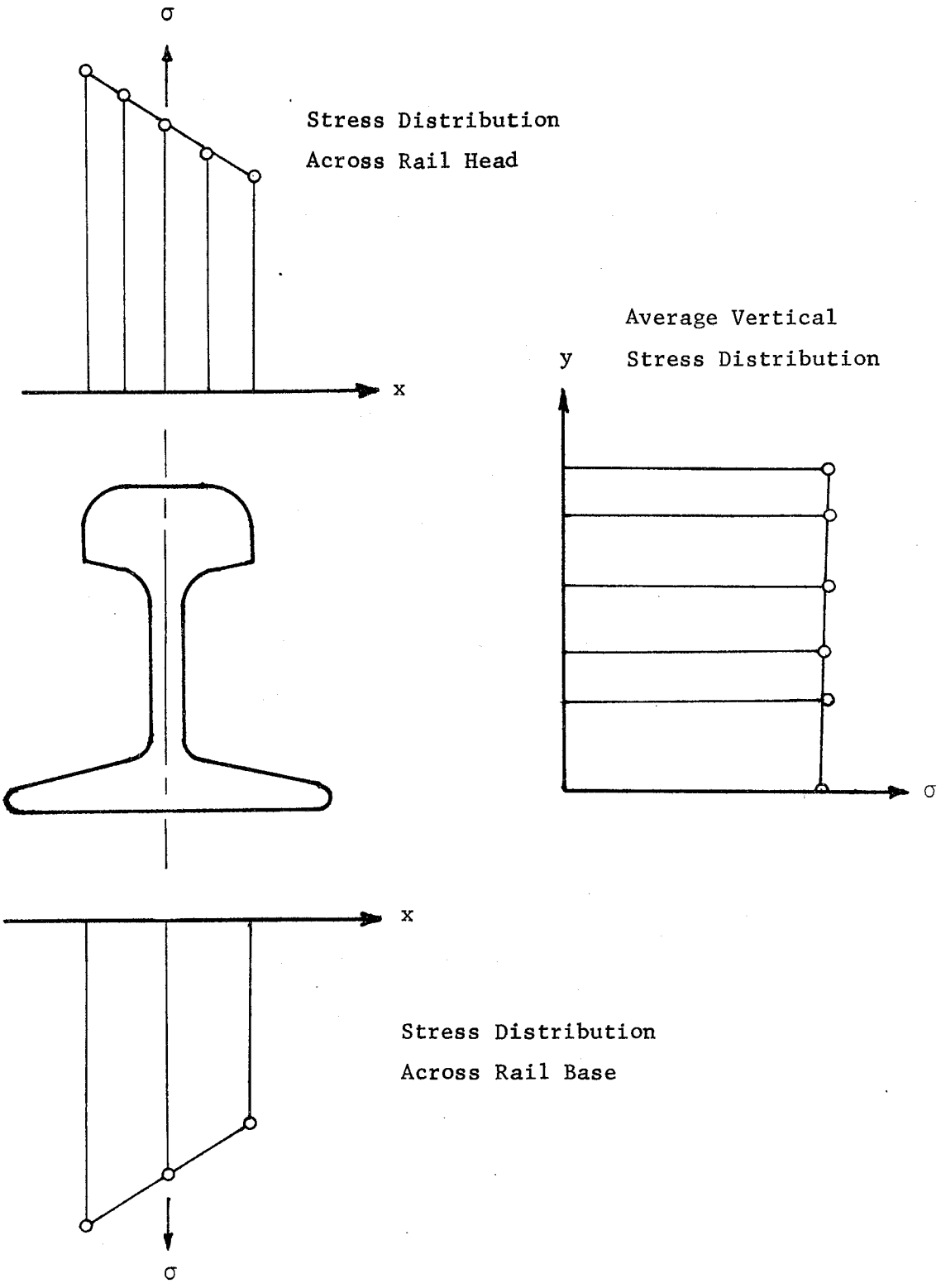

FIGURE 16 Stress Distribution for Compressive Load.

waves in the rail head are shown in Figure 17 and those for waves in the rail web are shown in Figure 18. The relative delay, $\Delta t/t$, has been corrected for the change in path length caused by the transdueers being clamped to the rail. The correction is given by:

$$\frac{\Delta t}{t} = \left(\frac{\Delta t}{t}\right)_u - \epsilon \qquad (14)$$

where $\left(\frac{\Delta t}{t}\right)_u$ is the uncorrected relative delay

and ϵ is the longitudinal strain.

In Figure 17 the two wave modes for which results are shown correspond to the A_1 and S_1 modes in Figure 8. The wave modes in Figure 18 are more difficult to identify positively. The fastest mode (C_g = 3.74 km/s) is closest to the maximum of A_2 in Figure 8 while the slowest (C_g = 2.12 km/s) probably corresponds to the minimum of A_2. The other mode (C_g = 2.51 km/s) has not yet been identified.

The most interesting aspect of the data shown in Figure 17 and 18 is the difference in slope between the delays caused by tensile and compressive stresses. The cause of this difference of slope is not known to us but is suspected to be a consequence of the fact that these waves, travelling in directions other than the longitudinal direction, are subjected to shear as well as normal stresses. It is speculated that wave speed changes due to applied shear stresses are proportional to the magnitude of the shear stress but not influenced by its sign. Since the wave in the rail is influenced by both normal and shear stresses, when the external force is reversed that part of the delay due to normal stresses changes sign while the delay due to shear stress does not. The net effect is a different wave speed change for reversed longitudinal stresses.

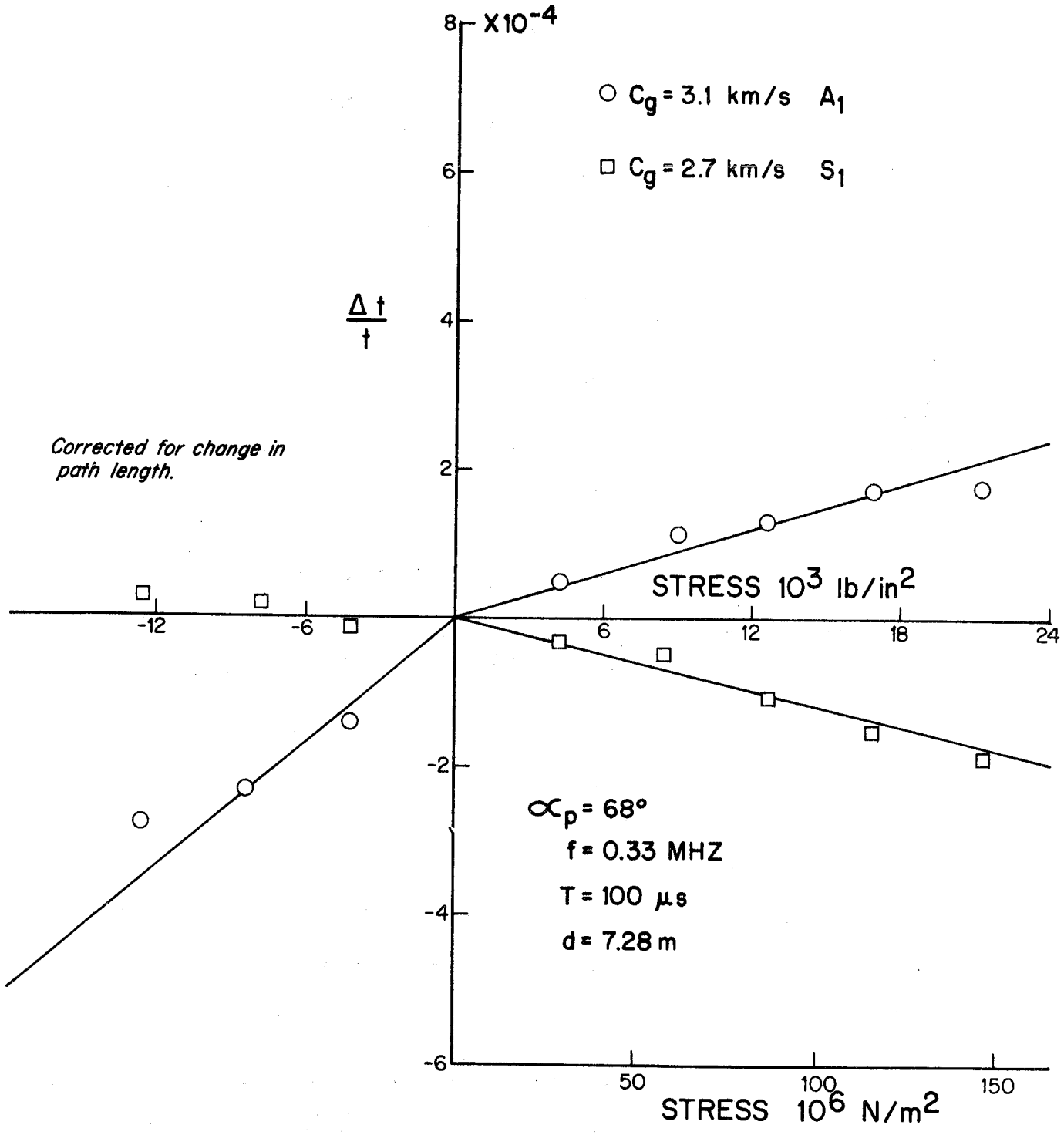

Figure 17 Relative Delay As a Function of Longitudinal Stress for Guided Waves in the Head of a 12 lb ASCE Rail.

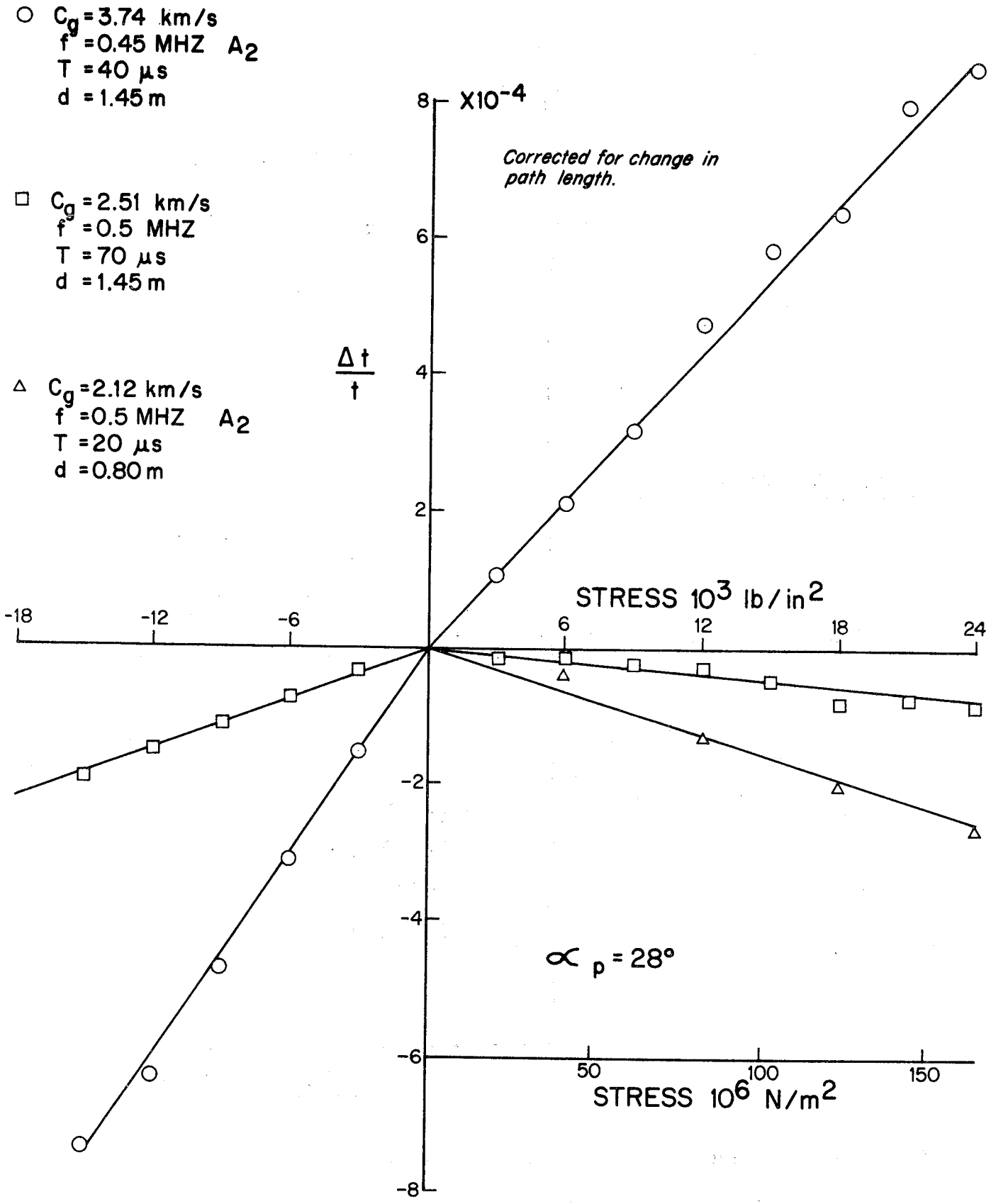

Figure 18 Relative Delay As a Function of Longitudinal Stress for Guided Waves in the Web of a 12 lb ASCE Rail.

WAVE PROPAGATION CHARACTERISTICS OF FULL SIZE RAIL

Introduction In order to anticipate the variations to be expected in the wave propagation characteristics of typical main line rail, a collection of several sections of full size, new and used rail was assembled. These rails, listed in Table VI,are, in most cases, short pieces less than a meter in length. Railroad company records showed that rails number 7, 11 and 12 had seen an estimated 293.6 $(10)^9$ kg (323.6 Million Gross Tons) of service. The history of other used samples is unknown. Rails numbered 13 and 14 are new rail measuring 11.9 meters (39 feet) long. Both bulk and guided waves were propagated along the head and web of these rails.

Apparatus and Test Procedure The basic apparatus used for obtaining wave velocities in full size rail is shown in the photograph in Figure 19 and the schematic is shown in Figure 20. The pulse excitation circuit consisted of a modified Sperry UR Reflectoscope, a separate probe tuning box and the transducer. A variety of source transducers were used. The primary design was a square piezoelectric plate mounted on a plastic surface wave wedge as shown in Figure 21. The piezoelectric plate was "air backed", i.e., it was not mounted with a highly damped backing material as is often the case. This achieves a longer ringing time which is desirable in this situation. Peak tuning is achieved by using either an appropriate internal tuning coil of the Reflectoscope or a separate external coil. The receiving circuit in most cases consisted of a Panametrics V109 transducer mounted on a Plexiglas wedge. This is a highly damped transducer which has a very broad frequency response. When required, a pre-amplifier was used on the

RAIL NO.	DESCRIPTION	LENGTH		SOURCE
		m	ft	
1	136 lb AREA - New	0.851	2.79	ATSF
2	112 lb AREA - Used (112-28 RE 1940 OH ILLINOIS)	0.851	2.79	ATSF
3	70 lb ASCE - Used (L.S. Co.,Buffalo, 700 11, 1907)	0.851	2.79	Univ. of Okla.
4	70 lb ASCE - Used (L.S. Co., Buffalo, 700 11, 1907)	0.625	2.05	Univ. of Okla.
5	12 lb ASCE - New			L.B. Foster Co.
6	110 lb AREA - Used (Colorado g C)	0.893	2.93	L.B. Foster Co.
7	119 lb AREA - Used (Inland, 1956 C, CH 17249)	0.863	2.83	ATSF
8	115 lb - New (Tennessee, 1969 11525 RE-CC)	0.866	2.84	L.B. Foster Co.
9	110 lb AREA - Used (N OH 1930 BREA)	0.902	2.96	L.B. Foster Co.
10	110 lb AREA - Used (OH Tennessee)	0.867	2.91	L.B. Foster Co.
11	119 lb AREA - Used (Inland, 1956 11937 CC)	0.856	2.81	ATSF
12	119 lb AREA - Used (Inland, 1956)	0.625	2.15	ATSF
13	119 lb AREA - New (1190 CC CF & I 1974 1111 CH 26700 D 15)	11.9	39	ATSF
14	119 lb AREA - New (1190 CC CF & I 1974 1111 CH 26700 E 14)	11.9	39	ATSF

TABLE VI Rail Samples on Hand.

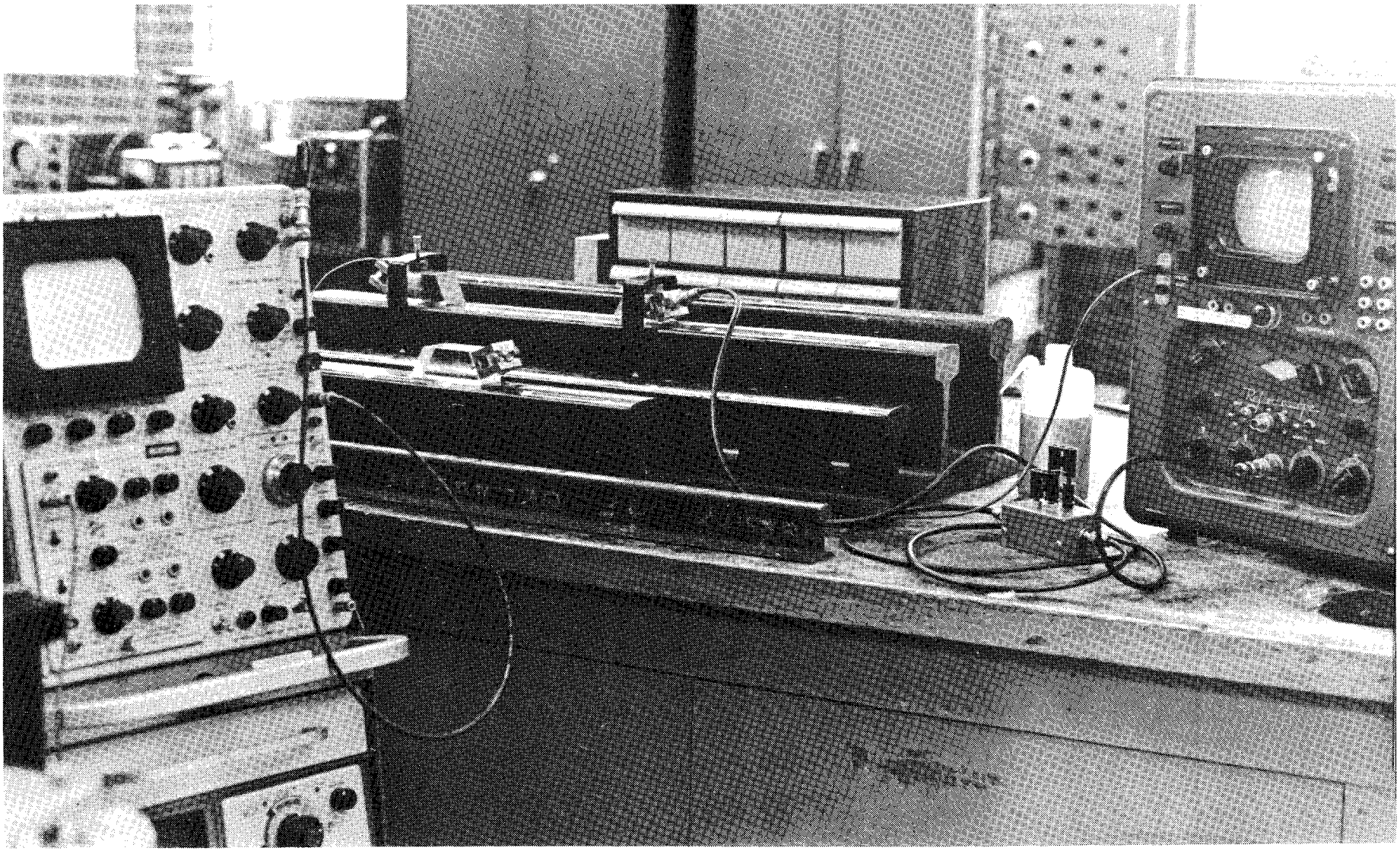

Figure 19 Apparatus for Wave Velocity Measurements on Full Size Rail.

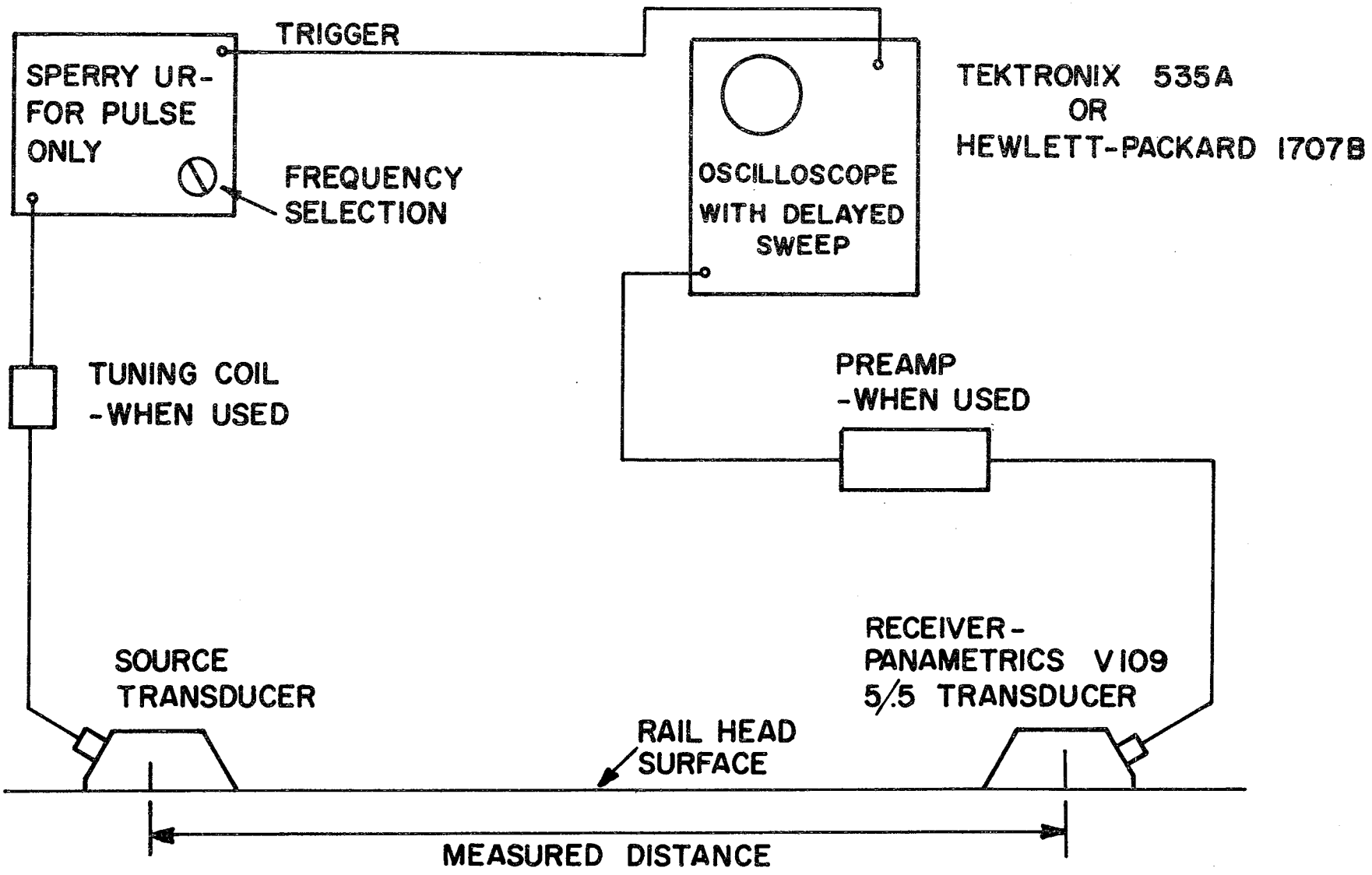

Figure 20 Schematic of Apparatus Used on Full Size Rail.

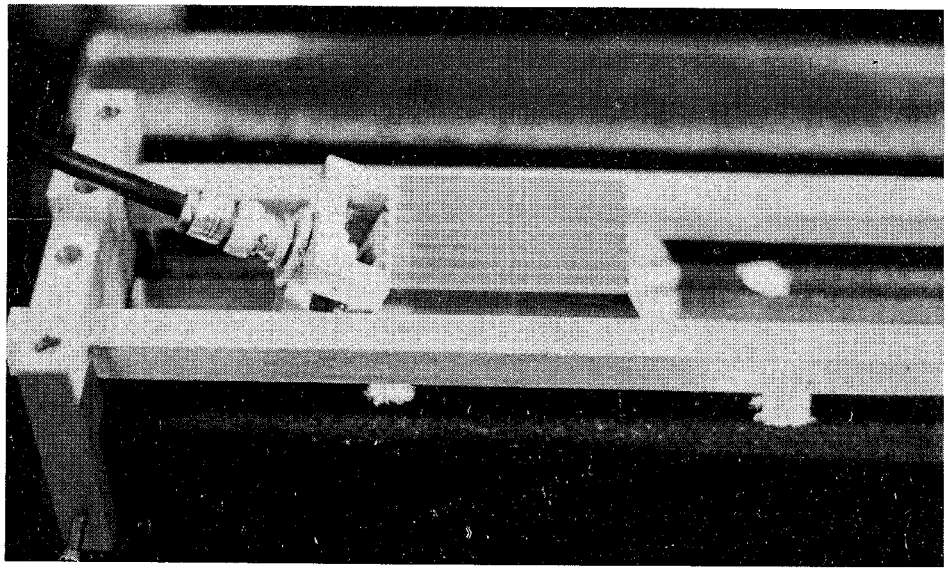

Figure 21

Probe and Guide Arrangement

for Surface Wave Measurements.

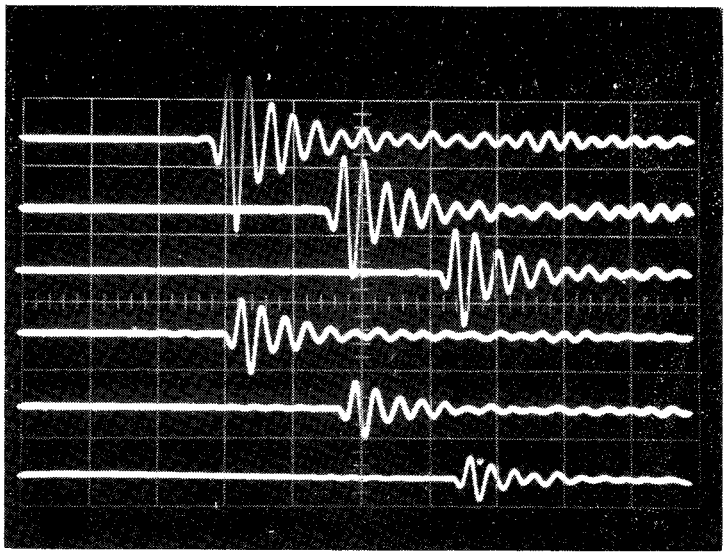

Figure 22

Pulse Arrivals at Six Locations on Rail

(Freq. 0.6 MHz).

received signal. The signal was displayed on either a Tektronix Type 535A or a Hewlitt-Packard 1707B oscilloscope. The oscilloscope trace was triggered by the source pulse of the Reflectoscope.

Wave transmissions times were usually obtained by keeping the receiving transducer at a fixed location and situating the source transducer at six locations along the rail. These locations were 600 mm, 500 mm, 400 mm, 300 mm, 200 mm, and 100 mm from the receiver. An aluminum distance and alignment frame was constructed with the 100 mm increments inscribed thereon. This is partially shown also in Figure 21. A set of velocities were then obtained by dividing the difference in transmission times to the receiving transducer for all possible locations of the source probe by the appropriate distance. In the case of six data points there are fifteen (N(N-1)/2) possible points of velocity data. The final velocity used is an average of these velocities. In a few instances, pulse echoes from the rail end were received by the same transducer instead of using the separate receiving transducer.

The method for obtaining successive arrival times was to locate the same peak in each observed arrival at the center line of the screen and to read the time change from the delay time multiplier on the oscilloscope. Very consistent results were obtained in this way. Figure 22 shows the successive arrivals of the 0.6 MHz pulse propagating on the head of the 136 lb new rail (No. 1). The traces from the lower to the upper are from the 600, 500, 400, 300, 200 and 100 mm locations, respectively.

Wave Velocities in Short Rail Samples The velocities of the several wave types measured are listed in Table VII and a statistical summary of the results is shown in Table VIII. Figure 23 shows a graphical summary of the velocities. The bulk dilatational and shear wave velocities were measured

RAIL	CONTROL COOLED	BULK DILATA-TIONAL	BULK SHEAR	P WAVE (HEAD)	P WAVE (WEB)	S WAVE (HEAD)	RAYLEIGH WAVE (HEAD)	RAYLEIGH WAVE (WEB)
1	Yes	5879	3205	5878	5945	3361(56°)	2985(66°)	2975
2	Note 1	5854	3212	5868	5929	3224(56°)	2985(65°)	2983
6	Note 2	5854	3177	5851	5903	3243(57°)	2941(66°)	2959
7	Yes	5868	3195	5872	5941	3120(59°)	2984(68°)	2973
8	Yes	5875	3202	5880	5945	3375(55°)	2955(65°)	2974
9	No	5866	3208	----	5938	----	----	2982
10	Note 2	5843	3205	5853	5917	3217(59°)	2912(66°)	2980
11	Yes	5855	3195	5890	5927	3013(60°)	2912(69°)	2977
13	Yes	----	----	5874*	----	----	2982*	----
14	Yes	----	----	5931*	----	----	2997*	----
NOMINAL WAVE LENGTH (mm)		2.6	2.0	4.7	3.0	2.4	2.2	1.49

* Date collected at different time than other data in group. This data not included in general discussion in this section.

Note 1 Incomplete information available on this rail. Rail No. 2 may have been control cooled and is included in the control cooled group.

Note 2 Rails number 6 and 10 most likely were not control cooled and are not included in the control cooled data group.

TABLE VII Wave Velocities in Rail (meters/second)

GROUP	BULK DILATIONAL (HEAD)	BULK SHEAR (HEAD)	P WAVE (HEAD)	P WAVE (WEB)	S WAVE (HEAD)	RAYLEIGH WAVE (HEAD)	RAYLEIGH WAVE (WEB)
ALL							
Average (m/s)	5862	3200	5870	5931	3217	2939	2975
% Variation +	0.29	0.38	0.34	0.24	4.9	1.6	0.25
% Variation -	0.32	0.71	0.33	0.46	6.4	1.9	0.55
CONTROL COOLED							
Average (m/s)	5866	3201	5878	5937	3212	2944	2976
% Variation +	0.22	0.32	0.21	0.13	5.1	1.4	0.22
% Variation -	0.21	0.21	0.16	0.17	6.2	2.0	0.11
NEW							
Average (m/s)	5877	3203	5879	5945	3368	2970	2974.5
% Variation +	0.03	0.05	0.02	0	0.21	0.51	0.016
% Variation -	0.03	0.05	0.02	0	0.21	0.50	0.01
USED							
Average (m/s)	5857	3197	5867	5926	3161	2926	2976
% Variation +	0.19	0.16	0.40	0.26	2.6	2.0	0.25
% Variation -	0.23	0.62	1.43	0.38	4.7	1.4	0.56
USED-CONTROL COOLED							
Average (m/s)	5859	3201	5877	5933	3117	2926	2978
% Variation +	0.15	0.35	0.23	0.15	3.4	2.0	0.18
% Variation -	0.08	0.18	0.15	0.09	3.3	1.4	0.16

TABLE VIII Statistical Summary of Wave Velocities

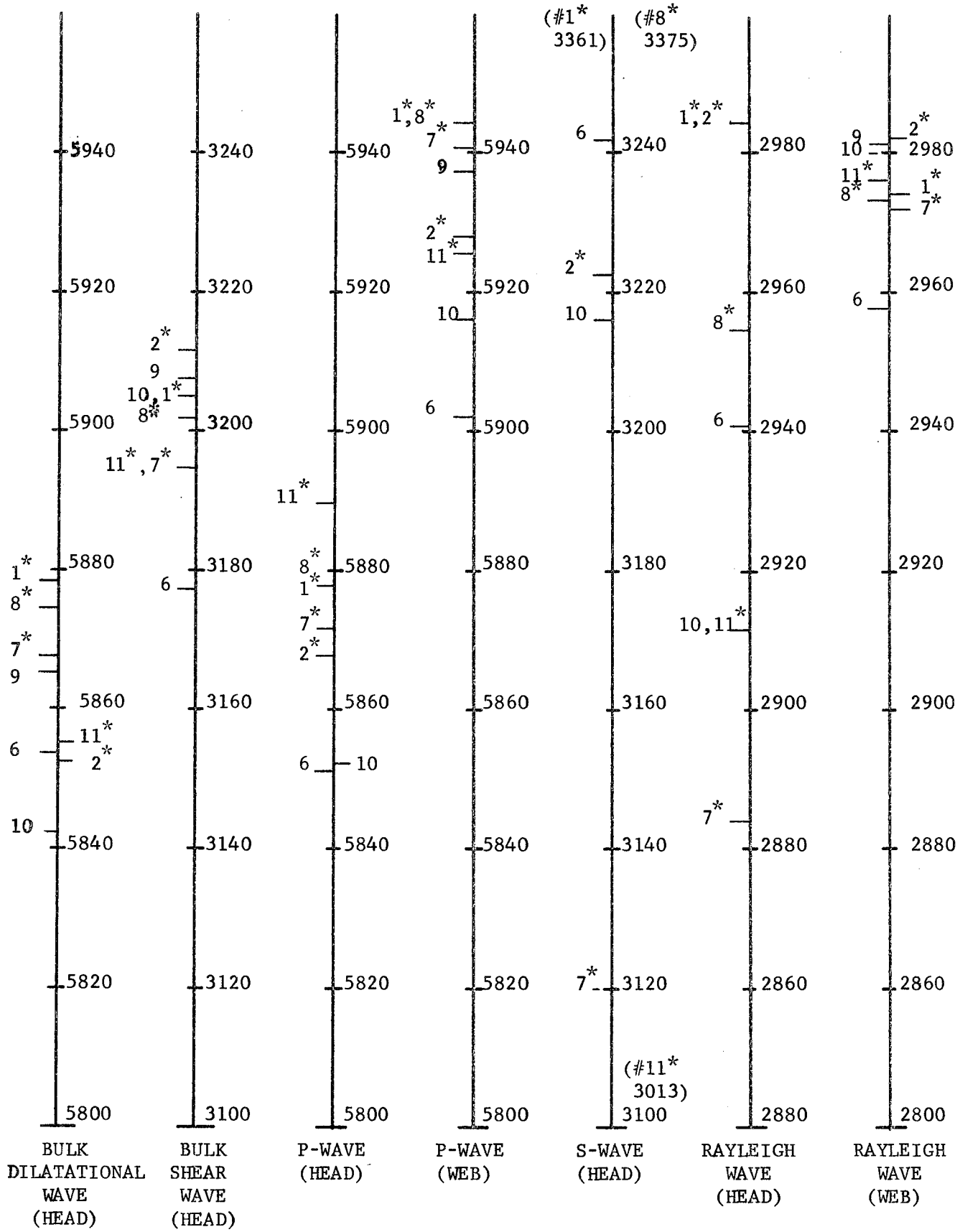

* Indicates control cooled rail

FIGURE 23 Wave Velocities (m/s) in Short Rail Samples.

using end mounted transducers situated near the middle of the rail head cross section. For the dilatational waves, a 2.25 MHz transducer was pulsed by a high voltage spike delivered by a Sperry UR Reflectoscope and the echoes were displayed on a Hewlitt-Packard 1707B Oscilloscope. Arrival times were obtained from the latter. These velocities show a variation of +0.29% and -0.32% for all rail. The dilatational velocities of the new rail (numbers 1 and 8) are distinctly greater than those of the used rail. Also, the velocity variation for control cooled rail (numbers 1, 2, 7, 8 and 11) is +0.22% and -0.21%*. A very similar variation is shown for used rail (+0.19% and -0.23%). The bulk shear wave velocities were obtained at a frequency of 1.6 MHz with a similar equipment arrangement. These values for all rail vary by +0.38% and -0.71%. All except the velocity of rail number 6 fall in a fairly close group with no distinction between new and used rail. Here, the control cooled group shows variations of +0.32% and -0.21%, considerably less than any group other than new rail.

A dilatational wave travelling along the length of the rail and near to the surface of the rail head could be excited by using a wedge oriented at 28^{o} to the vertical. This is commonly referred to as the first critical angle and the wave is often called a critically refracted P-wave [26]. Figure 24a shows the propagation path of this wave. The velocities at 1.25 MHz are also listed in Table VII and shown in Figure 23. Very good agreement between the previously obtained bulk dilational wave velocities and the P-wave velocities in the head is seen for all control cooled rail except for number 11. These P-wave velocities in the head vary by +0.34% and -0.33% for all rail and by +0.21% and -0.16% for control cooled rail. The large variation shown for used rail (+0.4% and -1.43%)

---

* See Appendix A for a discussion on rail manufacturing practices.

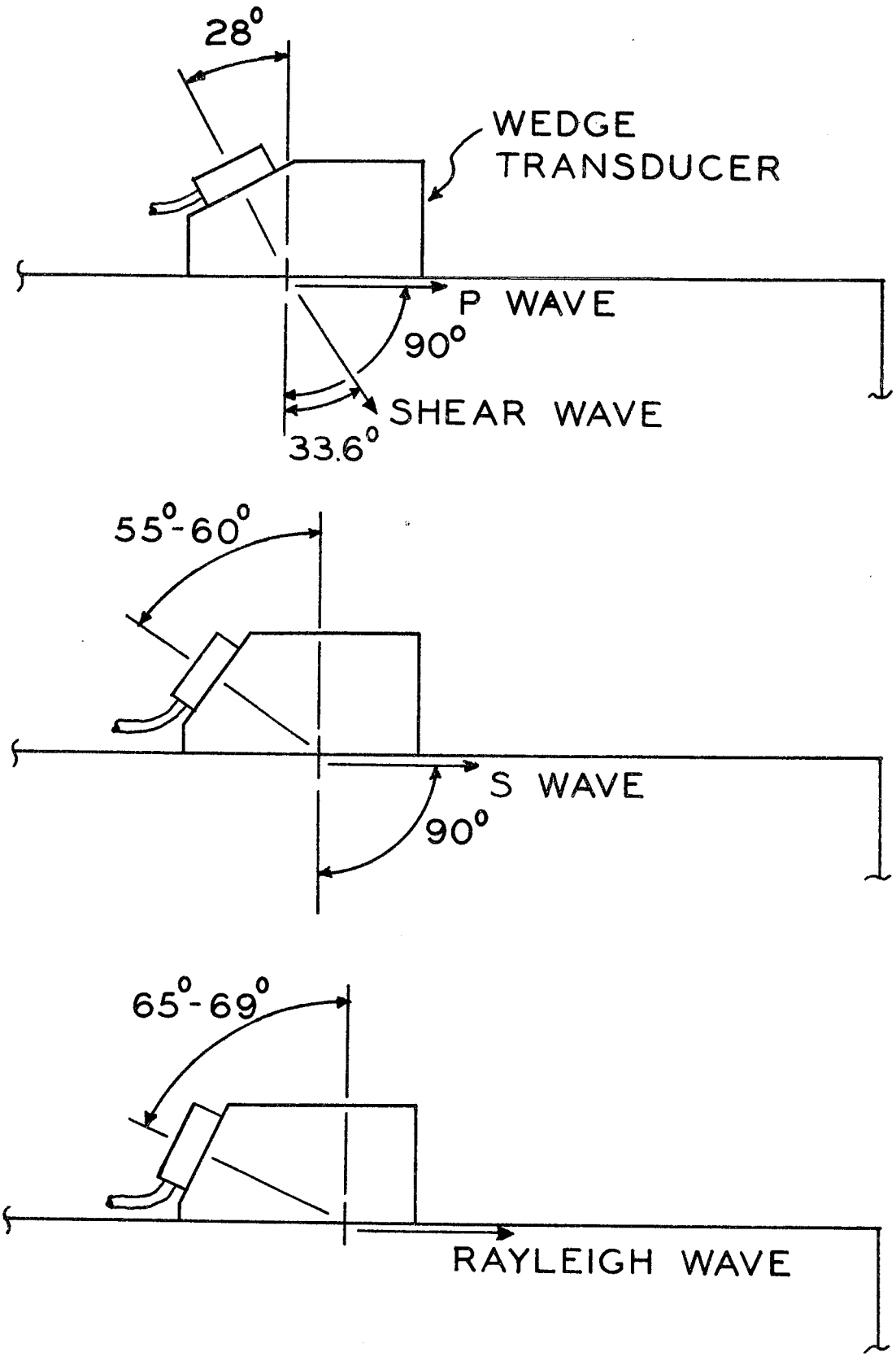

FIGURE 24 a P-Wave Propagation in Rail Heads.
b S-Wave Propagation in Rail Heads.
c Rayleigh Wave Propagation in Rail Heads.

is most likely caused by the presence of the noncontrol cooled rail and not by any change in the mechanical properties as a result of rail service. The control cooled group is dominated by used rail but shows a much lower variation.

At the second critical angle, (55^{o} - 60^{o} to the vertical, Figure 24b), a critically refracted S-wave could be excited in the head. Like the P-wave, this travels along the length of the rail just below the surface. These velocities are also listed in Table VII, summarized in Table VIII and shown in Figure 23. The excitation frequency was 1.33 MHz. Considerable scatter appears for these velocities for all categories except new rail. This could indicate some relationship to rail service as will be discussed later. There is apparent correlation with the bulk shear wave velocities only for used rails 2 and 10. Control cooled rails 1 and 8 possess very high S-wave velocities while numbers 7 and 11 show very low velocities. Listed in parentheses with the wave velocity in Table VII is the wedge angle that produced the pulse of greatest amplitude. The used rail separate themselves from the new rail by virtue of the greater excitation angle for the former. The lower excitation angle of used rail number 2 may be explainable by the fact that a thin layer was removed from the top of the rail early in the program in order to facilitate probe contact. This was also necessary for the two new rail which also are seen to have a lower excitation angle. However, by observing that the S-wave velocities for rails 1 and 8 are greater than for used rail and noting that from Snell's law the excitation angle is inversely proportional to the wave speed in the test material, the angle relationship obtained is clearly what would be expected.

The observed Rayleigh wave critical angle for the head is also listed in Table VII with the accompanying wave speed for an excitation frequency of 1.33 MHz. This data is also summarized in Table VIII and Figure 23. In this case, the most heavily worked rail, numbers 7 and 11, have greater excitation angles but the other angles are near those of the new rail. The Rayleigh wave velocities show a variation of +1.6% and -1.9% for all rail. All other groups, except for new rail, show similar variations. The new rail have distinctly greater velocities.

Surface wave and P-wave velocities were obtained along the web of the short pieces of rail at a position very near to the neutral axis. These velocities were obtained in the manner used in most of the other measurements. The aluminum alignment and distance frame was layed on the web and the contact side of both the sending and receiving transducers was heavily coated with a very viscous couplant in order to obtain good probe contact with the slightly concave shape of the rail web. Arrivals were obtained at successive 100 mm locations.

Instrumentation again consisted of the Sperry UR Reflectoscope as the excitation source and arrivals were displayed on the Hewlitt-Packard 1707B oscilloscope. A 2 MHz pulse was generated at the source probe for the surface wave and received with a Panametrics V109 probe. No external amplifier was used. The 2 MHz pulse had a wave length of 1.49 mm which is at least one-tenth the thickness of the typical rail web. For the P-wave the excitation frequency was also 2 MHz, yielding a wave length of approximately 3 mm, or about one-fifth of the typical web thickness.

Quite good uniformity was achieved in these wave velocities as shown in Table VII and summarized in Table VIII and Figure 23. When all rail samples are considered, there are variations of +0.25% and -0.55% for

the surface waves. Comparable variations for P-waves were +0.24% and -0.46%, respectively. Considering only control cooled rail, however, variations of 0.22% and -0.11% were found for surface waves and +0.13% and -0.17% for P-waves. Rail number 11 shows the largest deviation from the mean velocity for P-waves. This is consistent with the distribution of dilatational wave velocities in the head where the velocity of rail 11 was also lower than that of the other control cooled rail. It should be noted here that the inclusion of rail number 2 in the control cooled group is somewhat questionable. Without rail 2, the surface wave variations on the web are +0.076% and -0.059%. Similarly, for P-waves, the variations are +0.09% and -0.21%.

Even though there are only two new short pieces of rail included in this investigation, the fact they came from different rail plants and were rolled in different years yet showed excellent agreement in most velocity categories indicates good uniformity in basic rail manufacture. The larger variations in the head as compared to the web are most likely a result of either cooling or straightening. More discussion on rail manufacture is contained in Appendix A.

An unexpected, although quite interesting, result of this work was the observation of an individual wave whose characteristics are determined by the cold worked zone on the top of the rail. The behavior of this wave is such that for high frequencies in used rail it appears quite distinctly ahead of the expected surface wave. At high frequencies in new rail and at lower frequencies for all rail it is hardly noticeable, if at all. Figures 25a and 25b show the high frequency (1.5 MHz) appearance of the large surface wave for used rail (No. 7). The arrivals shown are for the six locations along the rail length as previously described.

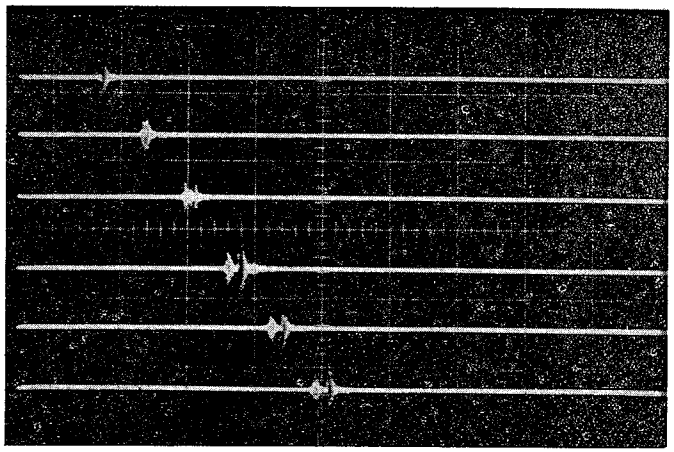

FIGURE 25a
Rail No. 7 119 lb USED
Freq. 1.5 MHz
Time Base 50 μs/cm

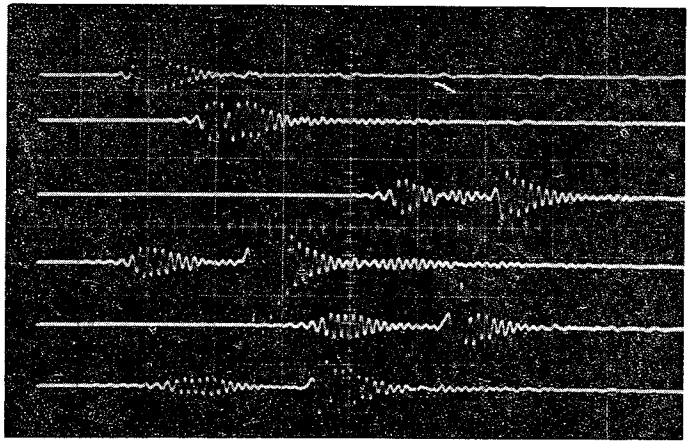

FIGURE 25b
Rail No. 7 119 lb. USED
Freq. 1.5 MHz
Time Base 5 μs/cm

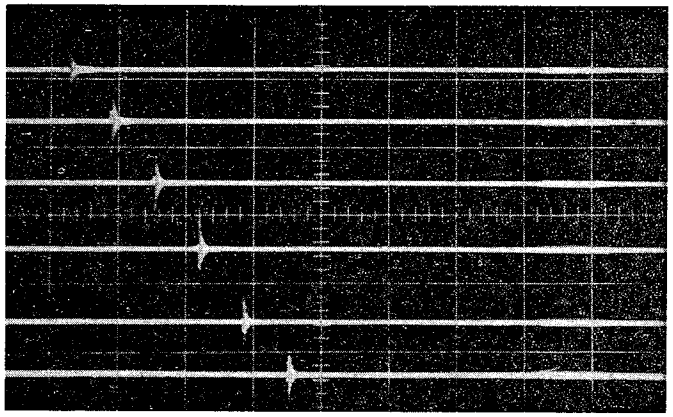

FIGURE 25c
Rail No. 8 115 lb NEW
Freq. 1.5 MHz
Time Base 50 μs/cm

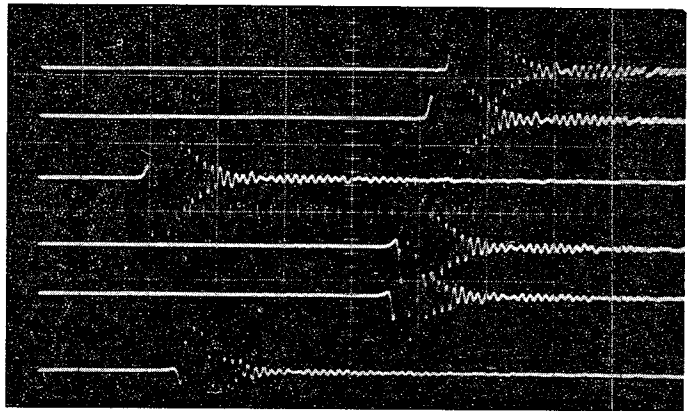

FIGURE 25d
Rail No. 8 115 lb NEW
Freq. 1.5 MHz
Time Base 5 μs/cm

Arriving at approximately ten microseconds before the surface wave is the smaller wave determined by the cold worked area of the head. The complete absence of this wave in the same arrivals in new rail (No. 8) can be seen in Figures 25c and 25d. Figures 25b and 25d are expanded displays of the pulse arrivals in Figures 25a and 25c, respectively.

Figures 26a, 26b, 26c and 26d are oscillograms corresponding to Figures 25a, 25b, 25c and 25d, respectively, but for a lower frequency (0.5 MHz). The very weak arrival of the wave from the cold worked area of rail No. 7 can be seen in Figure 26b. Of course, there is no arrival of this wave from the new rail for this low frequency.

In all cases the surface wave arrival is easily distinguished by its greater amplitude. Pulse dispersion creates the arrivals appearing after the surface wave seen in the figures just discussed. The top of the head of rail 7 is shown in Figure 27. Shelling marks are shown along the lower edge of the rail.

An in-depth study of these cold worked area waves is beyond the scope of the present investigation*. The reason for the current interest is so that the overall effect on stress measurements can be established. The nondestructive detection of severely worked areas, however, is a distinct possibility as is a correlation with impending shelling.

Frequency Dependence of Rayleigh Wave Velocities in Short Rail Samples

The Rayleigh wave velocity has been shown to be a function of both material hardness and residual stress in the material [27]. Rayleigh wave velocities as a function of wave length for several rails in this study are shown in Figure 28. Wave length is inversely proportional to the pulse frequency. Some trends are shown within a few of the rail samples. Rail

* See Appendices B and C for more discussion of the cold worked areas.

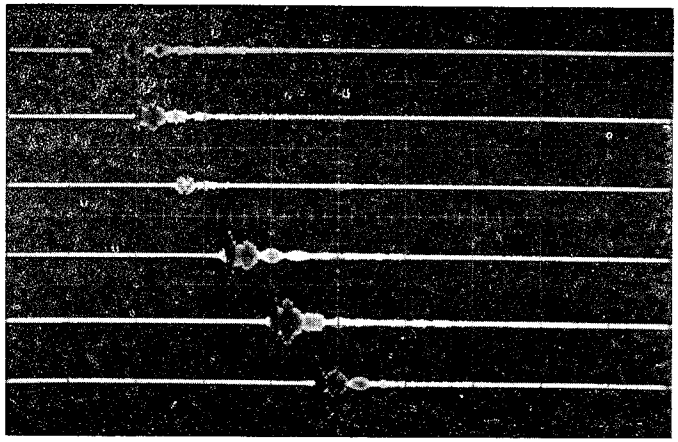

FIGURE 26a
Rail No. 7 119 lb USED
Freq. 0.5 MHz
Time Base 50 μs/cm

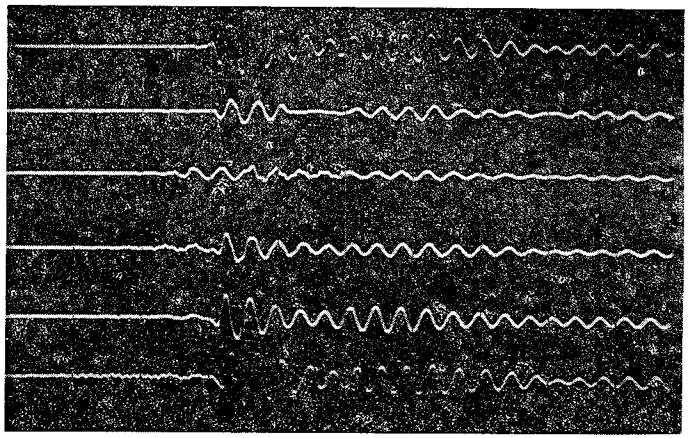

FIGURE 26b
Rail No. 7 119 lb. USED
Freq. 0.5 MHz
Time Base 5 μs/cm

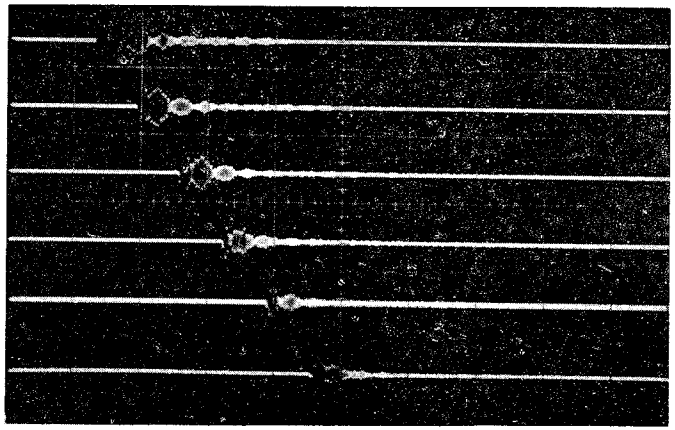

FIGURE 26c
Rail No. 8 115 lb NEW
Freq. 0.5 MHz
Time Base 50 μs/cm

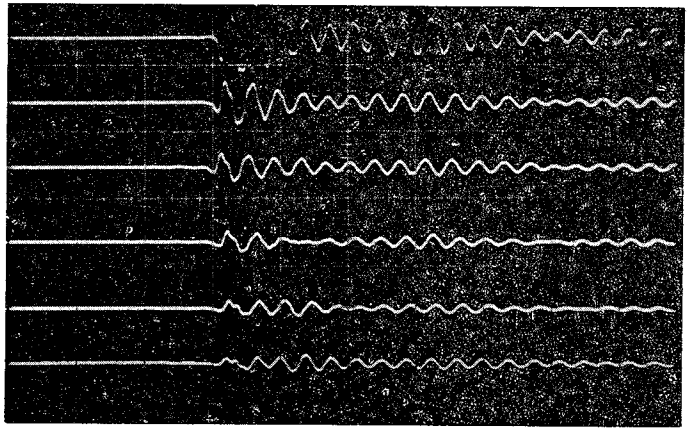

FIGURE 26d
Rail No. 8 115 lb. NEW
Freq. 0.5 MHz
Time Base 5 μs/cm

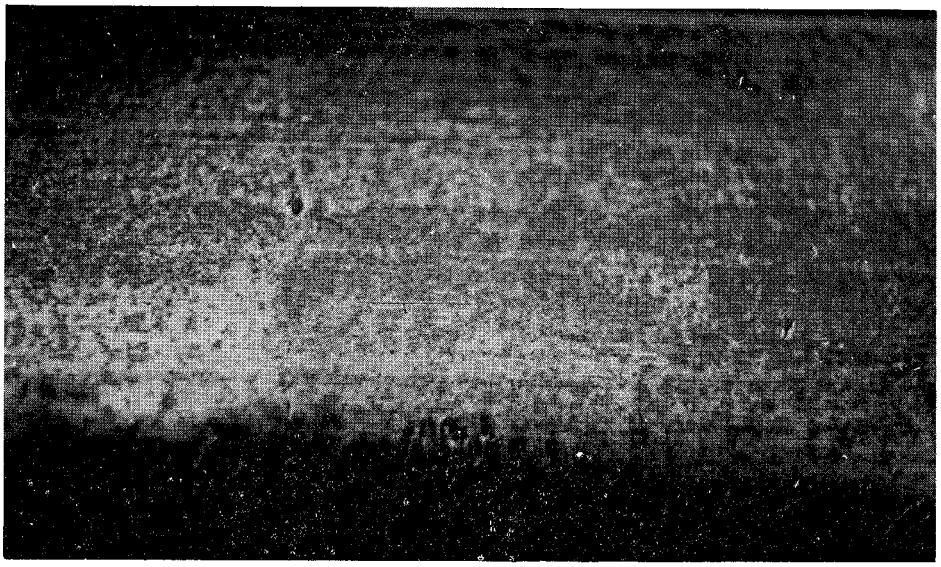

Figure 27

Shelling on Rail Number 7.

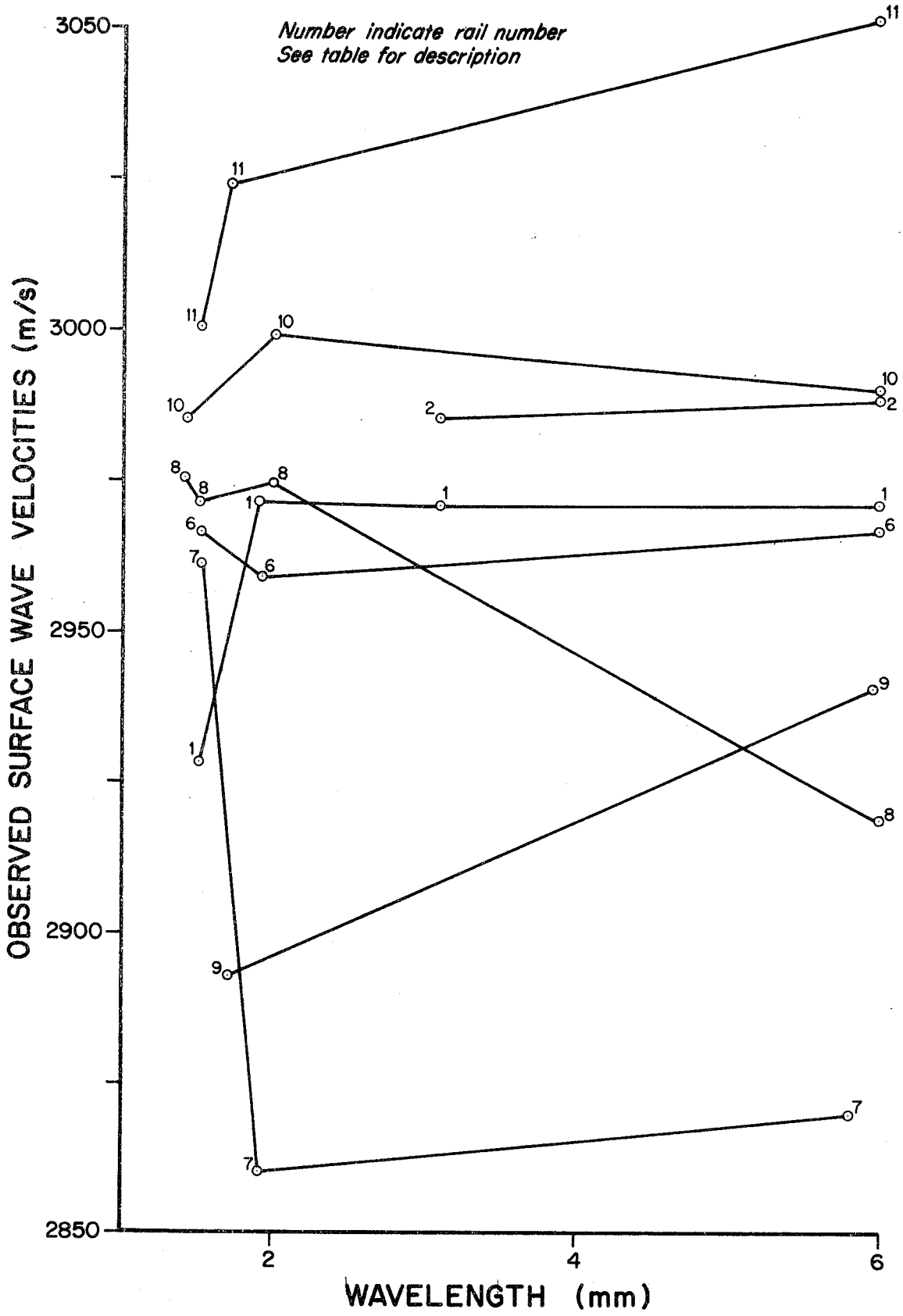

Figure 28 Surface Wave Velocity vs. Wave Length for Short Samples of Full Size Rail.

number 1 shows virtually no change with increasing wave length after 2mm. Rails number 2, 6 and10 show slight changes. Numbers 9 and 11 show large increases with greater wavelength. And, rails number 7 and 8 show rather large changes. Most likely these fluctuations are due to changes in residual stress due to the manufacturing process and to the cold working on the surface due to wheel loads. Variations in residual stresses due to manufacture are discussed in Appendix A.

Rayleigh waves velocities at frequencies lower than 0.5 MHz (approximately equal to a 6 mm wave length) were difficult to determine because of pulse dispersion. At that frequency and below, the wave length is approaching a significant fraction of the head depth and other guided modes are excited.

Rockwell "C" hardness data were taken on the cross-sections of all of the rail samples. The results from rail numbers 7 and 8 are shown in Figures 29 and 30, respectively. This data was required in order to evaluate any correlation of wave speed, depth of penetration (i.e., wave length as a function of frequency) and hardness. Tittman and Thompson have reported a correlation in a case hardened material sample [27]. The change in hardness values they encountered (range of 20 to 50 Rockwell "C") was considerably greater than the values obtained from the rail samples. The range of hardness in the rail is not expected to affect the velocity. The lower graphs in Figures 29 and 30 are a plot of the average hardness seen in the midsection of the rail. The reader should note that higher hardness values are at the lower end of the scale in the bottom graph.

Wave Velocity Variations in New, Full Length Rail The velocity variations previously noted in the short sections of rail encouraged an interest in

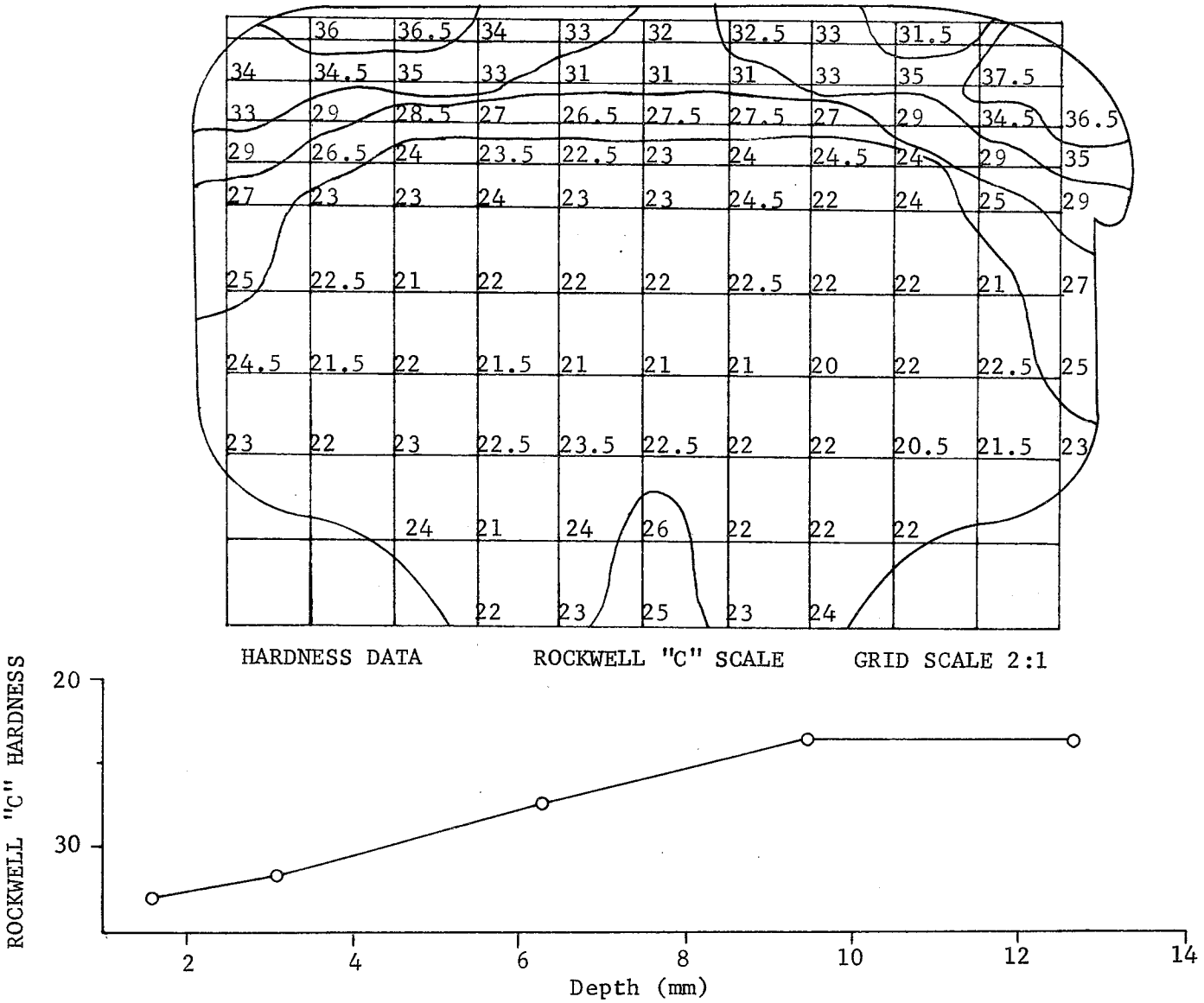

FIGURE 29 Rockwell "C" Hardness Contours in Rail No. 7.

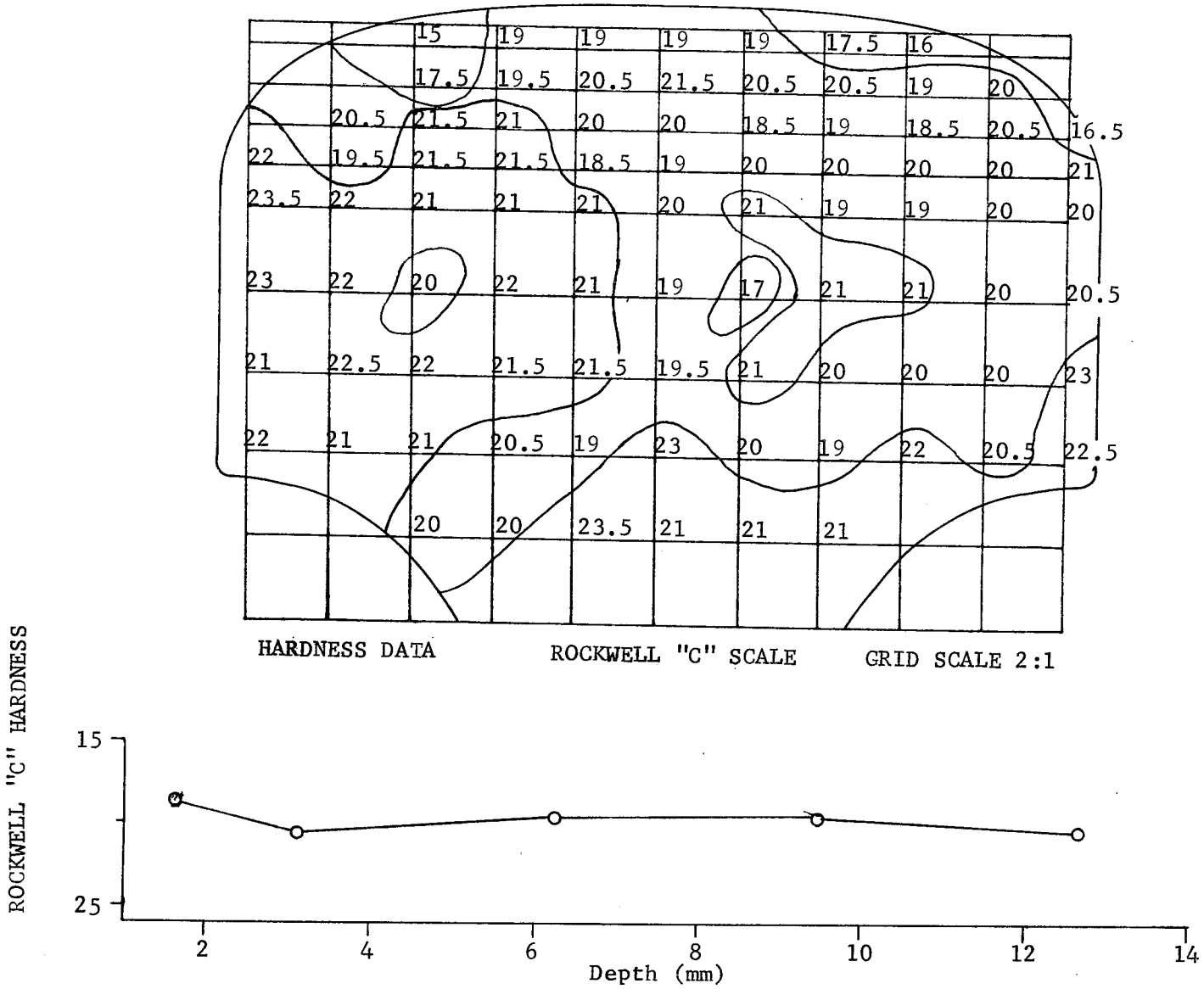

FIGURE 30 Rockwell "C" Hardness Contours in Rail No. 8.

the velocity profiles along longer lengths of rail. In order to investigate this, surface and P-type waves were excited in the heads of two new 11.9 m (39 foot) sections of main line rail. These are rail numbers 13 and 14 as listed in Table VI.

The method used for obtaining the velocity profiles was similar to that previously described for the short sections. There were differences in that the aluminum alignment and distance frame was moved along the rail at 600 mm intervals and successive arrival times were recorded by moving the probes at 300 mm intervals.

Distance measurements were estimated to be accurate to within 0.5 mm or 0.166% over the 300 mm range. Most likely greater accuracy was achieved in practice. Arrival times were read on the Tektronix 535A oscilloscope through the use of the delay time multiplier. Subsequent to taking the data, the oscilloscope was compared to time marks from a Tektronix 184 Time Mark Generator. This is a crystal controlled, temperature stabilized instrument providing accuracy greater than 0.001%. Surface and P-wave arrival times taken from the oscilloscope were corrected according to the comparison with the time mark generator so that time error was effectively negligible in comparison to the distance error. Reading accuracy from the oscilloscope was at least within 0.1%.

Surface waves were excited at a wedge angle of 65^{o} and a frequency of 2.5 MHz, utilizing the high voltage spike from the modified Sperry UR Reflectoscope. An air backed 25.4 mm (1 in.) square piezoelectric plate was used at the transducer. This was fitted with a suitable tuning coil. P-waves were generated with a Panametrics V-109 probe mounted at a wedge angle of 28^{o} and also excited by the Sperry Reflectoscope. Pulse frequency in this case was 1.9 MHz. Received waves were picked up by a similar Panametrics V-109 probe mounted on a wedge identical to that of the source.

The velocity profiles obtained for these two new rails are shown in Figures 31 and 32. Surface wave velocities along the top of rail number 13 are seen to follow a reasonably even distribution about the mean velocity of 2982 m/s. The variation is +0.45% and -0.32% and there does not appear to be any significant slope of the line along the rail length. The P-wave velocities, on the other hand, appear to rise to a maximum at a point about 2.5 meters from the rail end and then to decrease gradually until reaching a minimum nearly 2.5 meters from the opposite end. A much wider range of values is seen for the P-wave data as compared to the surface wave data. Scatter for P-wave is +0.58% and -0.79% about the mean velocity of 5874 m/s.

Rail number 14 shows a velocity profile distinctly different from that of rail number 13. In the case of rail number 14, the surface wave data shows large fluctuations up to approximately 4 meters at which point the velocity change begins to show a slight increase along the length. This regular pattern is interrupted at about 8 meters from the end when more fluctuations begin. These fluctuations continue until the rail end but they are not nearly as large as those seen on the opposite end. There is a definite trend toward higher velocities along the rail length. This is more pronounced after the approximate 4 meter location. The surface wave velocities vary by +1.8% and -1.4% about the mean velocity of 2998 m/sec. P-wave velocities from this rail show a decidedly similar variation. From a lower, slightly fluctuating range near the left end, they increase and become more uniform toward the middle. Greater fluctuation also occurs near the right end of this rail. A fluctuation range of +0.52% and -0.69% from the mean velocity of 5932 m/s is shown for this rail.

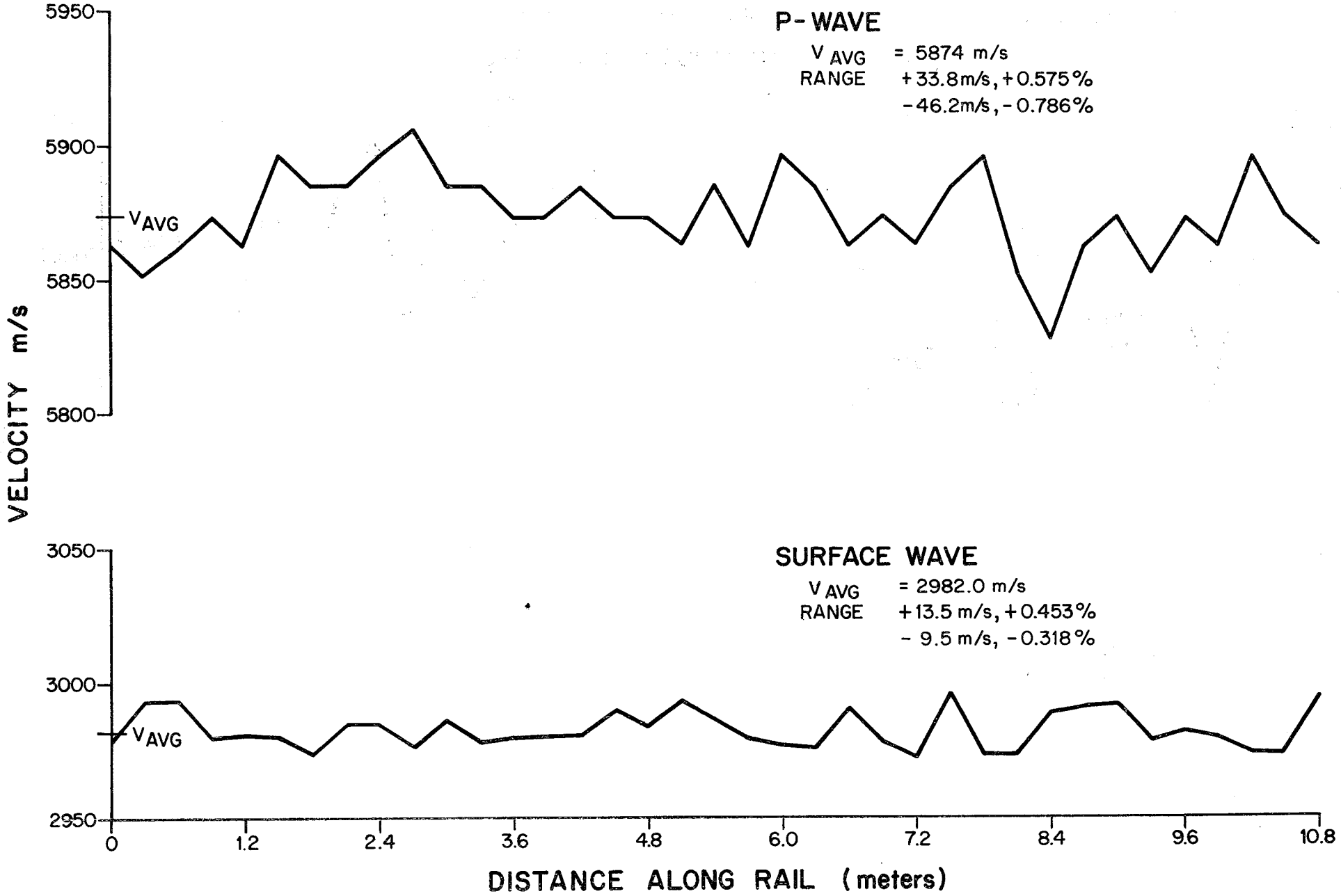

Figure 31 Surface and P-wave Velocities Along the Length of New 119 lb, 39 foot Long Rail (Rail No. 13).

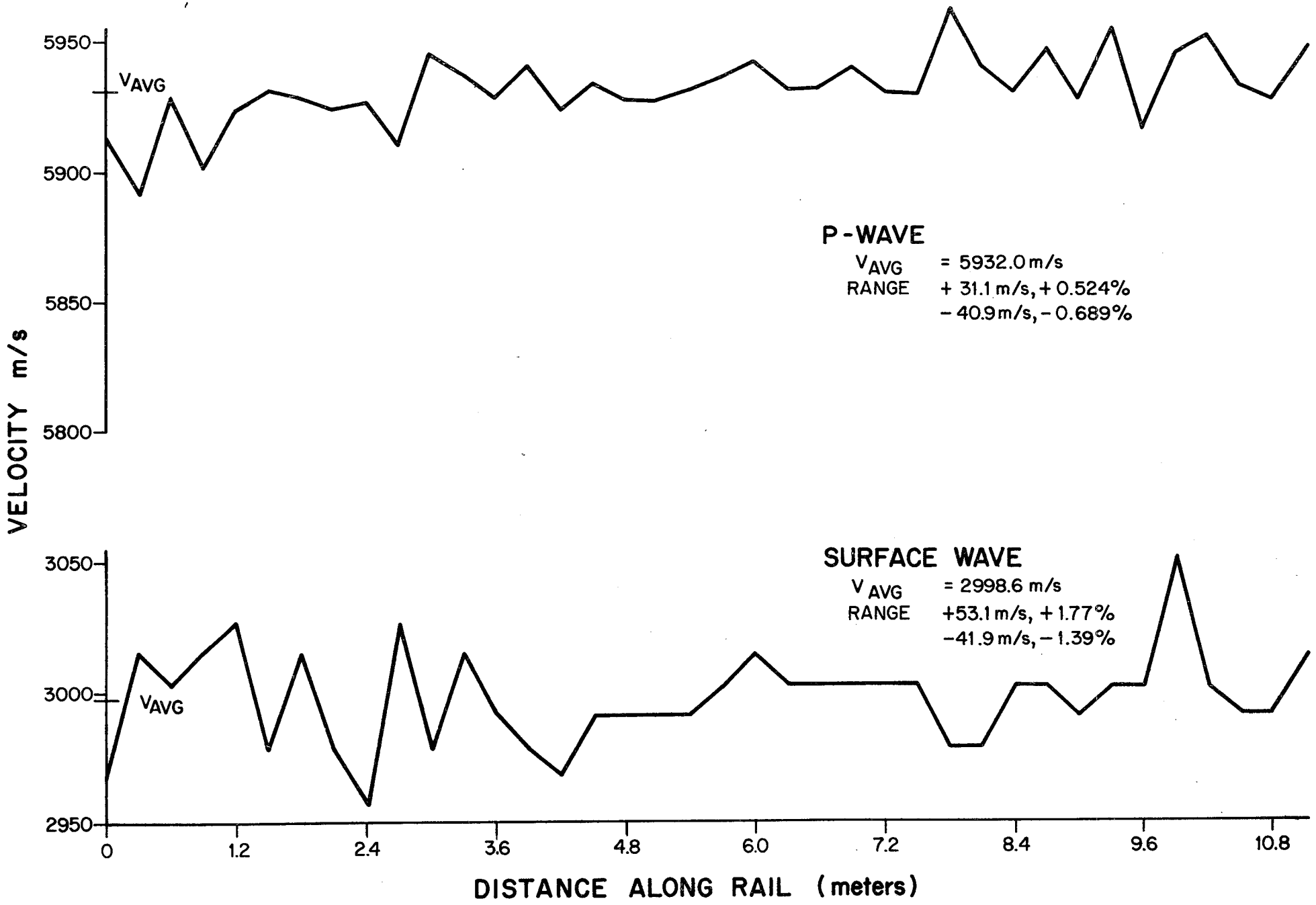

Figure 32 Surface and P-wave Velocities Along the Length of New 119 lb, 39 foot Long Rail (Rail No. 14).

Both the surface and the P-wave velocities are higher for rail 14 as compared to 13. The surface wave average velocity on rail 14 is approximately 0.52% higher than for rail 13. Similarly, the average P-wave velocity for rail 14 is 0.98% higher than for rail 13.

There are undoubtedly physical explanations for these velocity differences such as very small changes in material hardness and internal stress as a result of the manufacturing process. There are possibly other causes of the observed behavior. An investigation of these, however, is beyond the scope of the present effort.

The practical result of the investigation of the velocity variations within long rail lengths is to show the residual variations that might be seen by a travelling test car fitted for ultrasonic stress measurement. As seen here, the velocity changes indicated by a sample of just two rails are significant when compared to the change expected due to variations in applied longitudinal stress.

PROPOSED PORTABLE STRESS MEASUREMENT SYSTEM

Proposed Hardware The results obtained in the laboratory must be converted to practical hardware in order for actual stress measurements to be made. The two requirements for accurate stress measurement are accurate travel path control and accurate travel time determination. Travel path control can be maintained through probe assembly design while travel time determination must be accomplished through design of the electronic instrumentation.

A suggested probe design is shown in Figure 33. The proposed probe essentially consists of a one piece frame machined from steel. The sending and receiving transducer assemblies would be fixed at each end so that the alignment marks on the frame and on the transducer wedges are correctly matched. Probe spacing would be such that a 300 mm (11.81 in.) path length could be maintained. This choice is based on laboratory experience as described in this report. It is possible that a thermal heating circuit should be incorporated into the frame to minimize length changes resulting from ambient temperature variations. This heating circuit would also maintain the plastic wedges at a uniform temperature.

The transducer assemblies would be of conventional design with the wedge angle and excitation frequency optimized for the rail steel and the particular wave mode(s) desired. The contact portion of the wedge would be fitted to the curvature of the rail web. A thermistor could be incorporated in the wedge to measure rail temperatures.

Uniform contact of the probe assembly and the rail would be maintained through the use of a C-clamp apparatus as shown in Figure 34. By using a viscous couplant, no special cleaning of the rail web would be required. In most cases a rag or a wire brush would suffice.

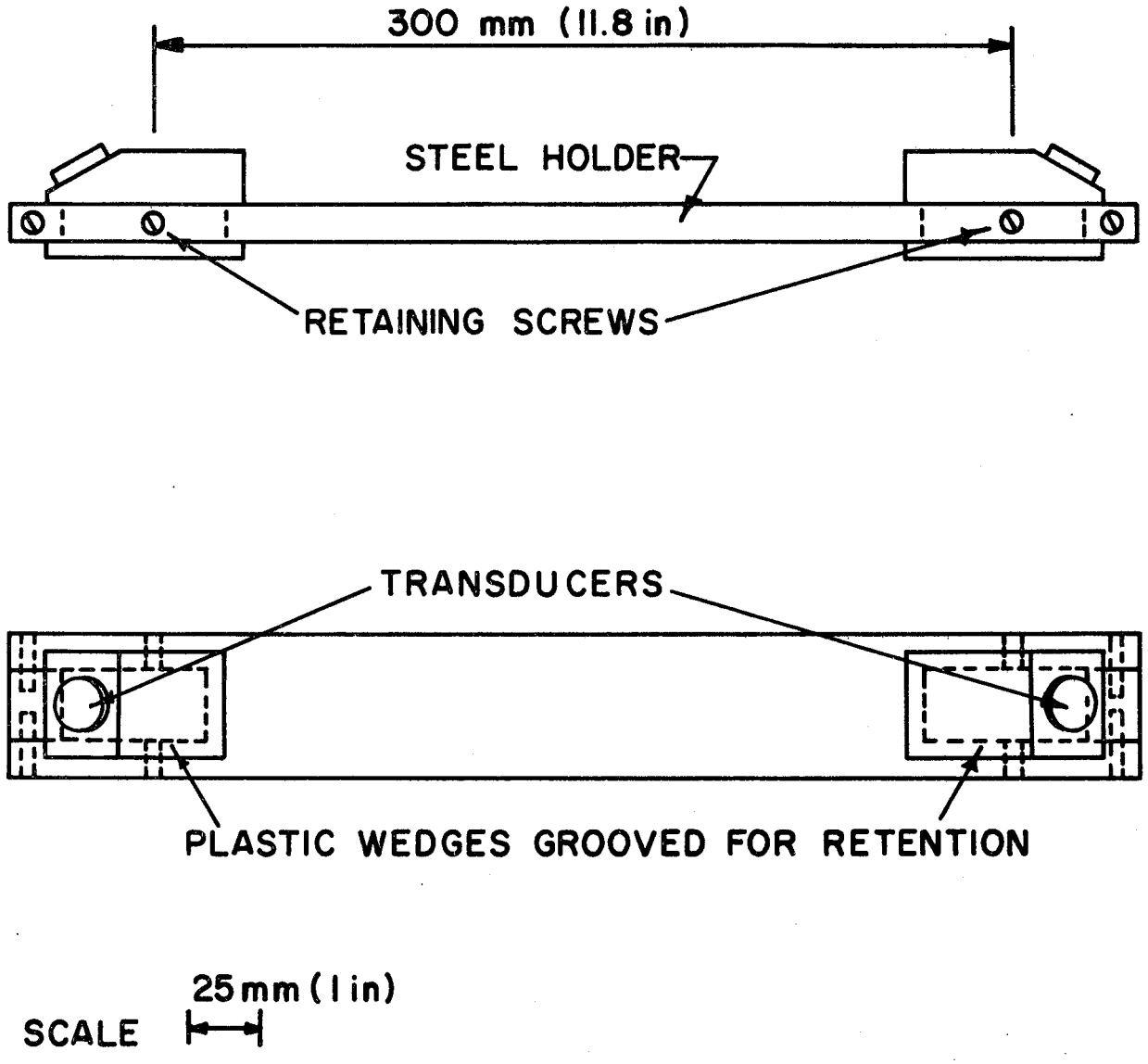

Figure 33 Proposed Probe Assembly for Stress Measurement.

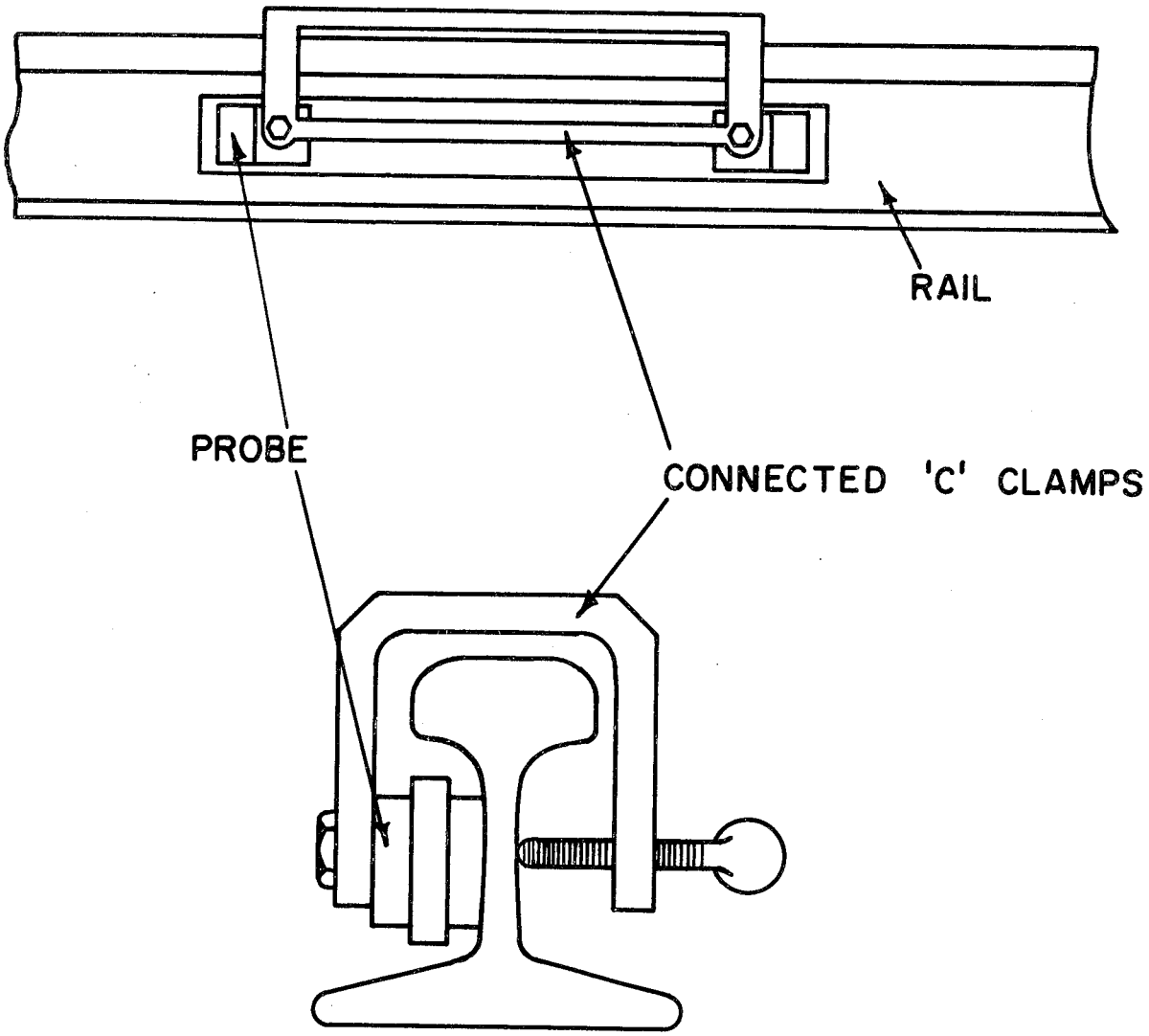

Figure 34 Method for Attaching Probe to Rail .

With the transducer frame controlling the travel path of 300mm, the nominal characteristics of the ultrasonic system can be specified. The P-wave described in an earlier section appears to be a logical initial choice of wave mode. This had an average velocity of 5937 m/s in the web which yields an expected nominal travel time of 50.53 μs for the 300 mm distance. The total travel time of the ultrasonic pulse must include the portion in each wedge. In this case, the travel time in each wedge is estimated to be 5.5 μs yielding a nominal overall travel time of 61.53 μs.

The velocity variation of P-waves in the web of control cooled rail was shown in Table VII to be +0.13% and -0.17%. In order to allow for a wider range of velocity variations, a range of $\pm$ 0.25% might be assumed because of material variablility. Table I shows the expected change in travel time per unit stress variations to be proportional to -2.40. Thus, at 82.737 MN/m^2 (12,000 psi) the time change due to stress would be 0.096%. In order to accomodate the full range of expected time changes, therefore, the proposed system should be able to read times on the order of 11 μs + 50.53 (1 $\pm$ 0.00346) or, 61.355 μs to 61.705 μs.

A general arrangement of the proposed system for measuring stress changes is shown in Figure 35. This system consists of a main unit having capabilities for pulsing, receiving, delaying and displaying the wave forms of interest. Additionally, an external time mark generator is provided for accuracy in measuring arrival times. Since the probes are at a fixed distance and, as just discussed, the only signal of interest should arrive between 61.355 μs and 61.705 μs, it would be convenient to insert a fixed 61 μs delay circuit as shown. The accurate variable delay circuit to be used in obtaining arrival times is shown also. For a pulse frequency of 2 MHz, a display of approximately 2 μs beyond the latest possible arrival must be specified in order to fully display the complete signal range.

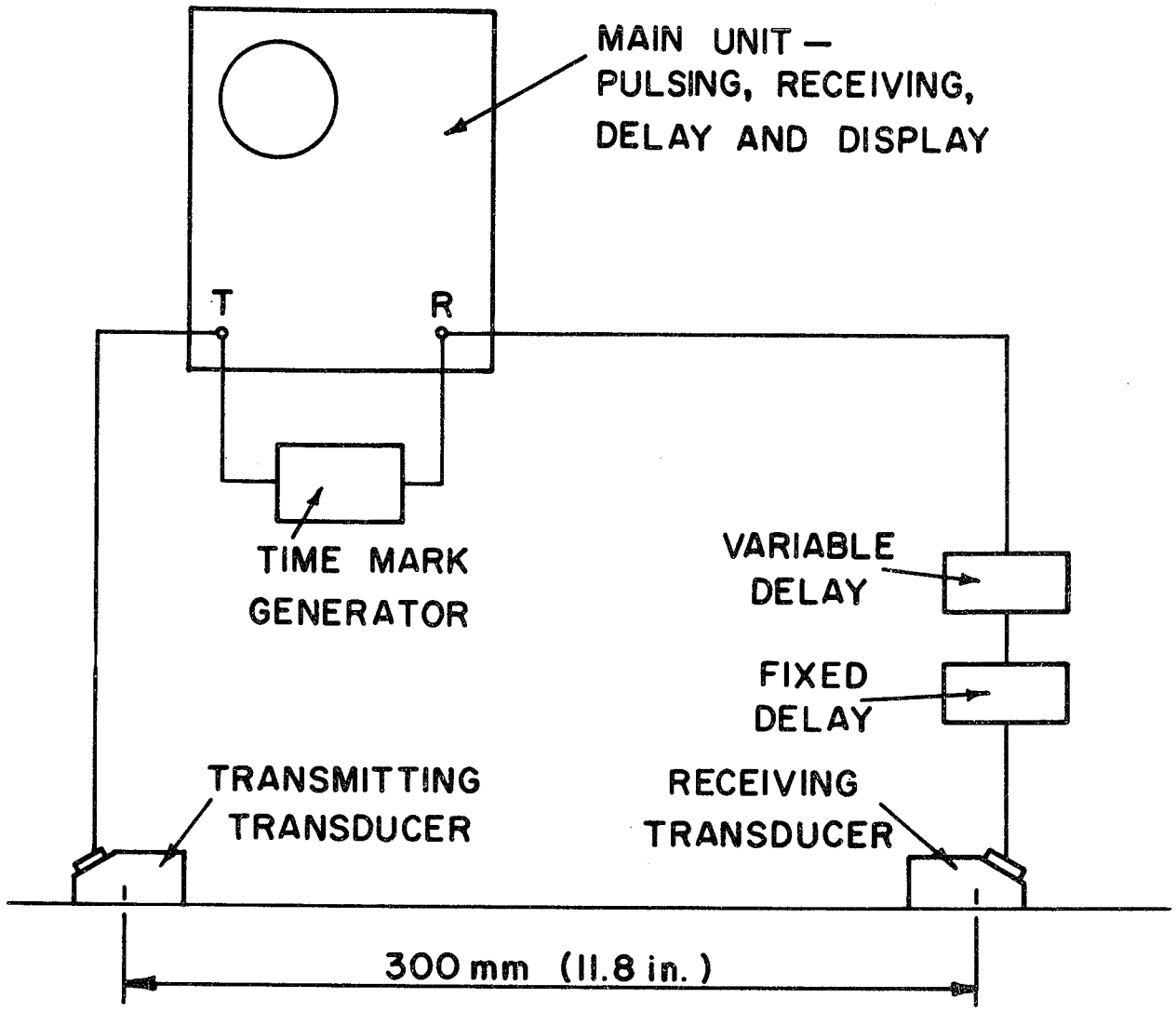

Figure 35 Schematic Diagram of Proposed Portable Stress Measuring System.

Although the foregoing equipment specifications are necessarily general, it is expected that they may be met in several ways. One possibility is to utilize a conventional ultrasonic flaw detection instrument as the main unit. The time mark generator would supply the required time accuracy. The sweep length required (equivalent to approximately 3 mm of steel (0.118in)) is smaller than commercially available but the possibility of slight modification of the unit exists. The advantage of having much of the required electronic functions performed in one small, battery powered unit are desirable. The time mark generator could be obtained in a battery powered configuration and the delay functions would be fairly small and would require no external power.

Other possible equipment combinations could be used to accomplish the desired result. These could include separate oscilloscope, pulser and receiving circuits, or possibly, modifications of existing circuits which are used for very accurate ultrasonic thickness measurements. All of these possibilities will be investigated.

Basis for Proposed Measuring System As is evident from other portions of this report, the speeds of various wave modes in a rail are dependent on initial material properties, temperature* as well as applied stress. Because the variactions in wave speed with initial properties and temperature are not negligible, a reference wave speed must be established for each individual rail if the acoustoelastic effect is to be feasible for measuring absolute stresses. Two possible means of determining this reference wave speed are discussed below.

Consider two wave modes which can be propagated and identified in a rail. Let C_1 and C_2 be the speeds of these waves both of which exhibit an

---

* See Appendix D

acoustoelastic effect. We may express the wave speeds as:

$$C_1 = C_1^o + \left(\frac{dC_1}{d\sigma}\right)\sigma \qquad (15a)$$

$$C_2 = C_2^o + \left(\frac{dC_2}{d\sigma}\right)\sigma \qquad (15b)$$

where C_1^o , C_2^o are the speeds of the two waves for zero longitudinal stress. It is assumed that C_1^o and C_2^o are proportional, that is:

$$C_1^o = KC_2^o \qquad (16)$$

where K is a constant independent of initial properties and temperature. In that case equations (15a, 15b and 16) may be solved for σ , thus:

$$\sigma = \frac{KC_2 - C_1}{K\left(\frac{dC_2}{d\sigma}\right) - \left(\frac{dC_1}{d\sigma}\right)} \qquad (17)$$

Having knowledge of K, $\left(\frac{dC_2}{d\sigma}\right)$, $\left(\frac{dC_1}{d\sigma}\right)$ and measuring C_1 , C_2 allows calculation of the absolute stress.

In utilizing this approach the ratio of velocities of the reference wave (C_1^o) to the inspection wave (C_2^o) along with the acoustoelastic constants $(dC_2/d\sigma)$, $(dC_1/d\sigma)$ must be determined for the rail material being inspected. It is expected that the reference wave will be one of the modes listed in Table V showing the smallest acoustoelastic effect. The inspection wave might be the P-wave. Both would be propagated in the same area of the rail, most likely the web.

The second means of establishing a reference velocity is somewhat less

desirable but still an operable option. That is to measure the reference wave speed on a particular rail when the rail is in an unstressed state. Presumably this would be accomplished when the rail is laid. Because of the changes in properties of the rail head in service this technique would limit stress measurement to the rail web.

Phase II of the research project will involve the practical application of the prototype apparatus under controlled, field condition. More specific information regarding apparatus configuration, procedure and performance will be available upon completion of that work.

CONCLUSIONS

The research reported herein was directed toward assessing the feasibility of using the acoustoelastic effect for measuring the state of longitudinal stress in railroad rails. The activities of this first phase have concentrated on determining the magnitude of the acoustoelastic effect for bulk and guided waves in both rail steel and in rails; and on studying the relevant wave propagation characteristics of full size rail.

The acoustoelastic effect for a large number of both bulk and guided wave modes was investigated. For this purpose specimens machined from the head and from the web of a full size (115 lb) rail and from the head of a smaller (12 lb) rail were used. A long length of 12 lb rail, instrumented with strain gages and loaded in a special purpose load frame with a hydraulic actuator, was used for additional acoustoelastic studies in both the head and the web of the rail.

Results of the acoustoelastic studies showed that a bulk longitudinal wave propagating parallel to the applied force exhibited the greatest acoustoelastic effect. Of the guided wave modes, the speed of those consisting predominately of longitudinal waves propagating nearly parallel to the applied load showed the greatest sensitivity to longitudinal stress. The guided wave modes showing the smallest acoustoelastic effect were Rayleigh waves and those consisting predominately of shear waves propagating at 45^{o} to the applied stress.

The fact that different guided wave modes have different sensitivities to applied stress suggests that a measuring system incorporating two wave types and measuring the relative difference in velocity in a particular rail may allow making absolute stress measurements. A more restricted although

potentially useful approach might be to take measurement data with a portable instrument at a specific location in a particular rail while in an unstressed condition. Data obtained after the rail was in operation could then be used to determine the relative stress change.

Wave propagation characteristics of full size rail were investigated for several conditions. In the rail head, both the rolling surface and the interior were studied. The web was also investigated. Both new and used rail were included. The characteristics along the length of two sections of 11.9 m (39 foot) new rail were also established.

These investigations showed the least variation in wave propagation velocities between the several samples to occur in the rail web. This is undoubtedly due to the more even cooling there and to the small residual stress level expected at the neutral axis. The least variation of all was at the web of control cooled rail. This indicates that the web is the most appropriate location for performing ultrasonic stress measurements despite the operational difficulties to be encountered there.

As a result of this work, it is concluded that a portable rail stress measurement unit based on the acoustoelastic effect is feasible in principle. There are of course many questions relating to the practical implementation of such a device that need to be addressed and will be studied during the second phase of this project. Considering the velocity variations found to occur from one new rail to another and between new and used rail, the development of a continuous, test car type measuring system seems very difficult at this time. Investigations into signal analysis could make the continuous technique more attractive. Also, the possibility of establishing a velocity profile of a particular track as a reference and noting changes at later times could be investigated. Some work in both of these areas is contemplated in Phase II.

APPENDIX A

RAIL PROPERTIES

The specifications for the steel, the cross-section and the manufacturing process for rail have continually evolved since the origin of railroads. Changes have been made in response to both failure patterns and to increased loading demands. Much useful information regarding rails is contained in references 2, 28, 29, 30 and 31. A summary relative to the present investigation will be presented here.

Material specifications for railway steels are governed by the American Railway Engineering Association (AREA). Table A-I shows the chemical requirements for the heavier rail associated with most main line North American railways. This steel has a relatively high carbon content in order to give good wear performance. This unfortunately sacrifices some fracture toughness, however. Other formulas containing higher contents of alloys such as silicon, manganese, aluminum, vanadium and others are either available or are being considered in order to gain a better combination of wear resistance and fracture toughness.

At the manufacturing plant, a large ingot of steel is poured as the beginning of the rail making process. Presently, rail steel is produced by both the open-hearth method and the more modern basic oxygen process. The ingot is sheared into blooms which are in turn rolled into rail. The rail to be rolled is designated by an alphabetic symbol, beginning with A, according to its order in the ingot. Normally two rails are rolled per bloom. The actual order of rolling may be inverse to the order of alphabetic designation.

CONSTITUENTS	NOMINAL WEIGHT IN POUNDS PER YARD	
	91/120	121 & over
Carbon (Percent)	0.67-0.80	0.69-0.82
Manganese (Percent)	0.70-1.00	0.70-1.00
Phosphorous, Max. (Percent)	0.04	0.04
Sulphur, Max. (Percent)	0.05	0.05
Silicon (Percent)	0.10-0.25	0.10-0.25

TABLE A-I Chemical Specifications for Railroad Rail Steel.

After the rolling process is complete, but while the steel is very near the forging temperature, the rail is cut to length. Standard finished length is 11.9 meters (39 feet). The cooling process begins after the rail is cut. The rails are held on "hot beds" until the temperature falls between 537.8°C to 385.6°C (1000°F to 725°F). At this time, the rails are moved to special cars which serve as control cooling bins. This cooling process requires a minimum of 10 hours for the rail to reach a maximum discharge temperature of 148.9°C (300°F).

The final process involves straightening, milling, hole drilling and inspection. Current U.S. practice is to "gag straighten" the rail until it meets specifications. This is a process where a drop hammer strikes a blow at a spot on the rail which is determined by the inspector to be arched. The rail is supported approximately 0.76 m (30 inches) to either side of the location to be struck. A rail may receive none or several such straightening blows. Specifications require that when the finished rail is resting on its base, it shall have a uniform sweep and the ends may be higher than the middle provided the middle ordinate does not exceed 31.75 mm (1¼ inches) in the 11.9 meter (39 foot) length. Straightening by any process would obviously affect the distribution of residual stress in the rail.

Some rails are produced for a specific purpose rather than for general service and may deviate from the previously described path. For example, the heads of some rails are fully heat treated for wear resistance on curves and in many cases the rail may be end-hardened to reduce the effect of wheel-batter. Heat treating the head affects the residual stress distribution throughout the rail as well as the mechanical properties of the head. End-hardening only affects a few inches of the rail head on each end.

	12-lb ASCE	115-lb AREA
Area (in^2)	1.18	11.26
Section Modulus Head (in^3)	0.58	18.53
Moment of Inertia (in^4)	0.55	64.34
Weight / length (lbs/yd)	12	115

TABLE A2 Properties of Two-Rail Sections Used in This Study.

The distribution of residual stress both along the rail length and through its cross-section are of vital interest to this study. These stresses are generated during the cooling process and, as previously mentioned, are subject to change as a results of subsequent heat-treatment and straightening.

The cooling process and the resultant stress pattern can best be understood by referring to Figure A-1 which shows typical rail cross-sections. When the rail emerges from the rolling operation and rests on the hot bed, the material temperature exceeds forging temperature and the rail is momentarily in stress equilibrium. The thin sections at the web and the base generally solidify before the head, however. Because the head is still hot enough to yield, material movement takes place to accomodate the shrinkage at the web and base. As the head cools, no plastic yielding is permitted in the solidified sections and shrinkage of the head generates residual stresses throughout the cross section. The areas which cool last, namely the middle portions of the head and also the base and web juncture, will have tensile residual stresses. Equilibrium requires compensating areas of compressive residual stress.

Residual stress data reported on heat treated rail shows values in the head to range from 206.84 MN/m^2 compression to 137.89 MN/m^2 tension (-30 ksi to 20 ksi, respectively). The web is shown to have values ranging from 0 near the fillets to 68.94 MN/m^2 (10 ksi) compression at the center. Heat treated rail is expected to have more favorable stress distributions than non-heat treated rail [32]. Although residual stress levels have been studied in non-heat treated rail, this data has not yet been reported in the literature [33].

Control cooled rail would be expected to have more uniform stress distribution than air cooled rail. The control cooling process became

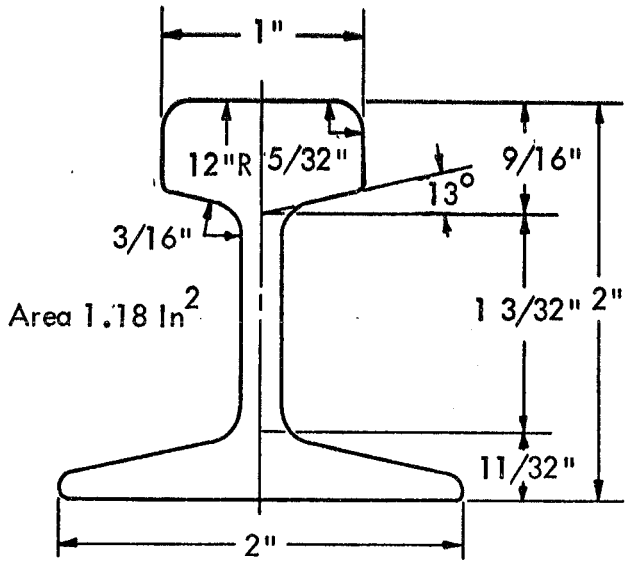

12-lb A.S.C.E.

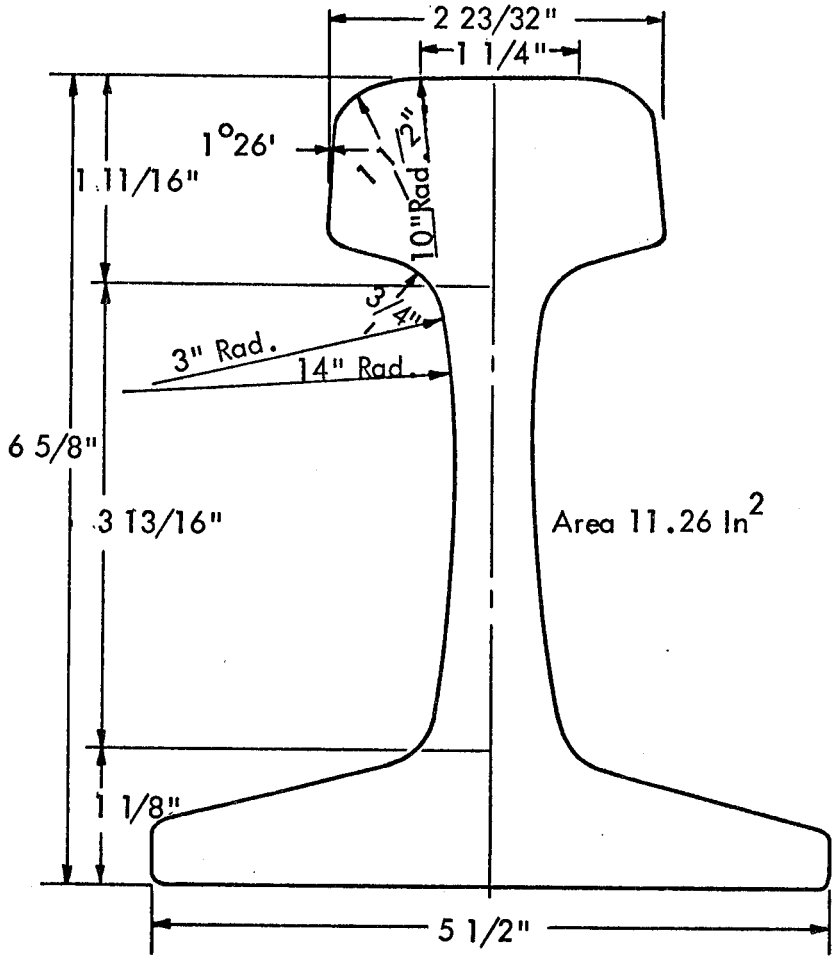

115-lb A.R.E.A.

Figure A1. Rail Sections

common practice in 1937 and became part of the AREA specifications in 1942.

APPENDIX B

METALLOGRAPHIC INVESTIGATIONS

by

Robert J. Block*

In connection with the interest in the early wave arrival discussed earlier and any relationship to impending rail shelling, metallographic investigations were made of a sample of new and used rail. The investigation was pursued in order to determine the extent to which plastic deformation of the rail head could be revealed. Figures B-1 through B-11 show the results of the initial metallographic survey. The rail heads were prepared using standard grinding, wet polishing and micro-etching techniques. A layer of flowed metal adjacent to the contact surfaces of the used rail could be observed even with the unaided eye. The gross effects observed in this manner were the result of plastic deformation affecting the etching characteristics of the metal.

Microscopic examination revealed flow patterns adjacent to the contact surfaces. In hypoeutectoid and decarburized steels these are emphasized by distortion of the light appearing proeutectoid phase. In eutectoid composition, distortion of the normally equiaxed pearlitic structure was used as an indicator. The depth to which the plastically deformed layer extended was determined from the polished section with a measuring metallurgical microscope or directly from the photomicrographs.

An overall view of the new rail (number 8) is shown in Figure B-1.

---

*Professor, Metallurgical Engineering, University of Oklahoma.

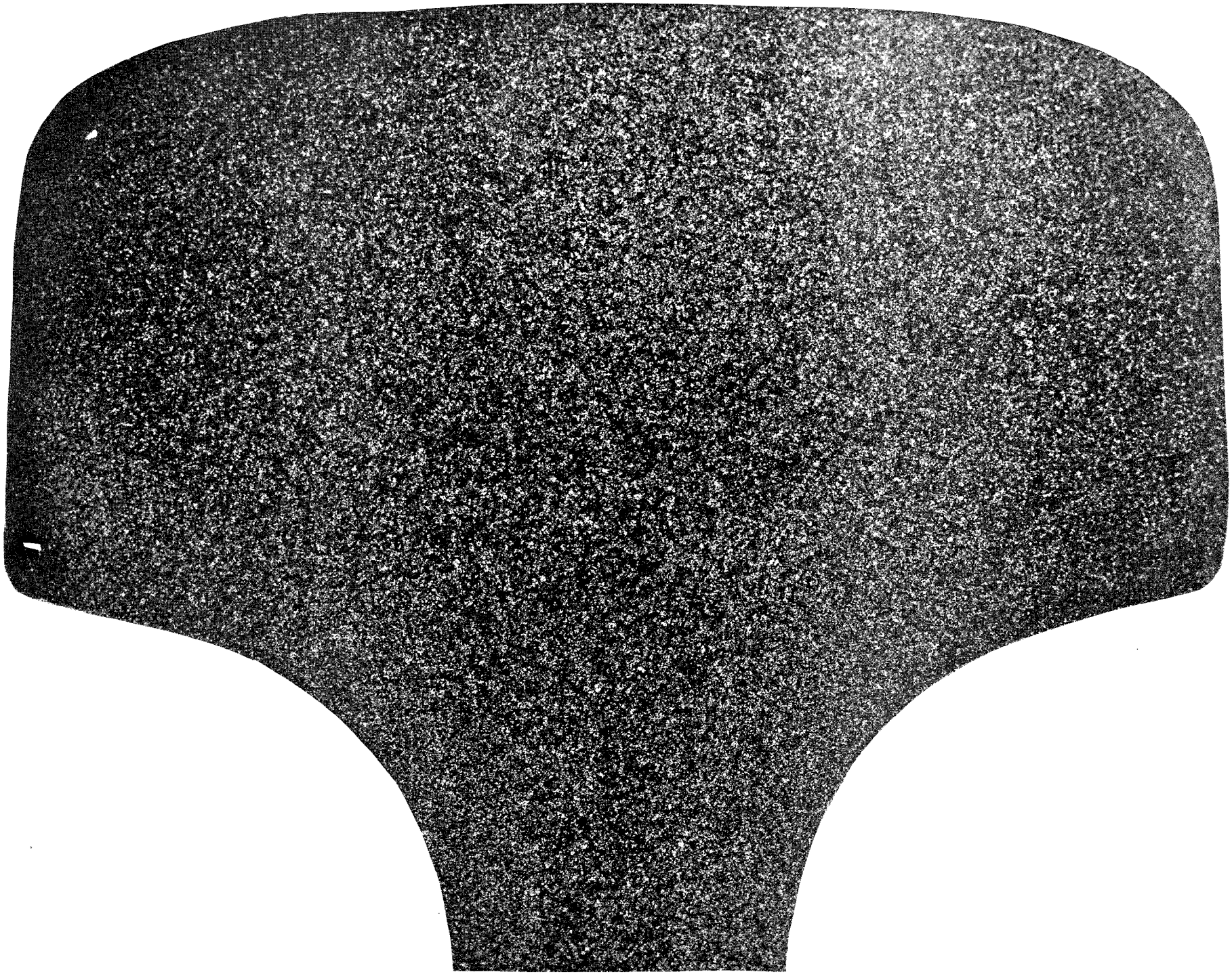

Figure B-1 Overall View of an Unused 115 lb AREA Rail Head (No. 8). (3.4X, Vilella's Etch)

The microstructure is somewhat coarser in the interior of the section than at the surface. This variation is probably a consequence of the deformation patterns and heat flow induced during hot rolling of the rail. No cold deformation is apparent in the cross section. Figure B-2 is the same cross section as shown in Figure B-1 with the locations of the areas examined microscopically and shown in Figures B-3 and B-4 indicated by the corresponding numbers.

The enlarged view of location 3 in rail 8 is shown in Figure B-3. The upper surface of the rail is shown at the top of the photomicrograph. Except for a decarburized layer adjacent to the external surface, a consequence of the manufacturing process, the structure is pearlitic. The pearlite nodules are generally equiaxed and do not show any evidence of plastic deformation in the metal. This is especially apparent in the rear surface region. Here loss of carbon has induced the formation of light etching ferrite along the prior austenitic grain boundaries. The ferrite serves to outline the pearlite and emphasize its equiaxed structure.

The typical structure in the interior of the rail head (location 4) is shown in Figure B-4. The high magnification confirms the structure to be almost entirely pearlitic. Only a few small areas of free ferrite were noted. The microstructure shows a mixture of fine and coarse pearlite characteristic of a normalized steel of close to 0.80% carbon content. A few small nonmetallic inclusions are shown in the micrograph.

The cross section of used rail number 7 is shown in Figure B-5. The profile of the section shows one corner (presumably the gauge corner) severly deformed and upset. The opposite (field) corner also has been

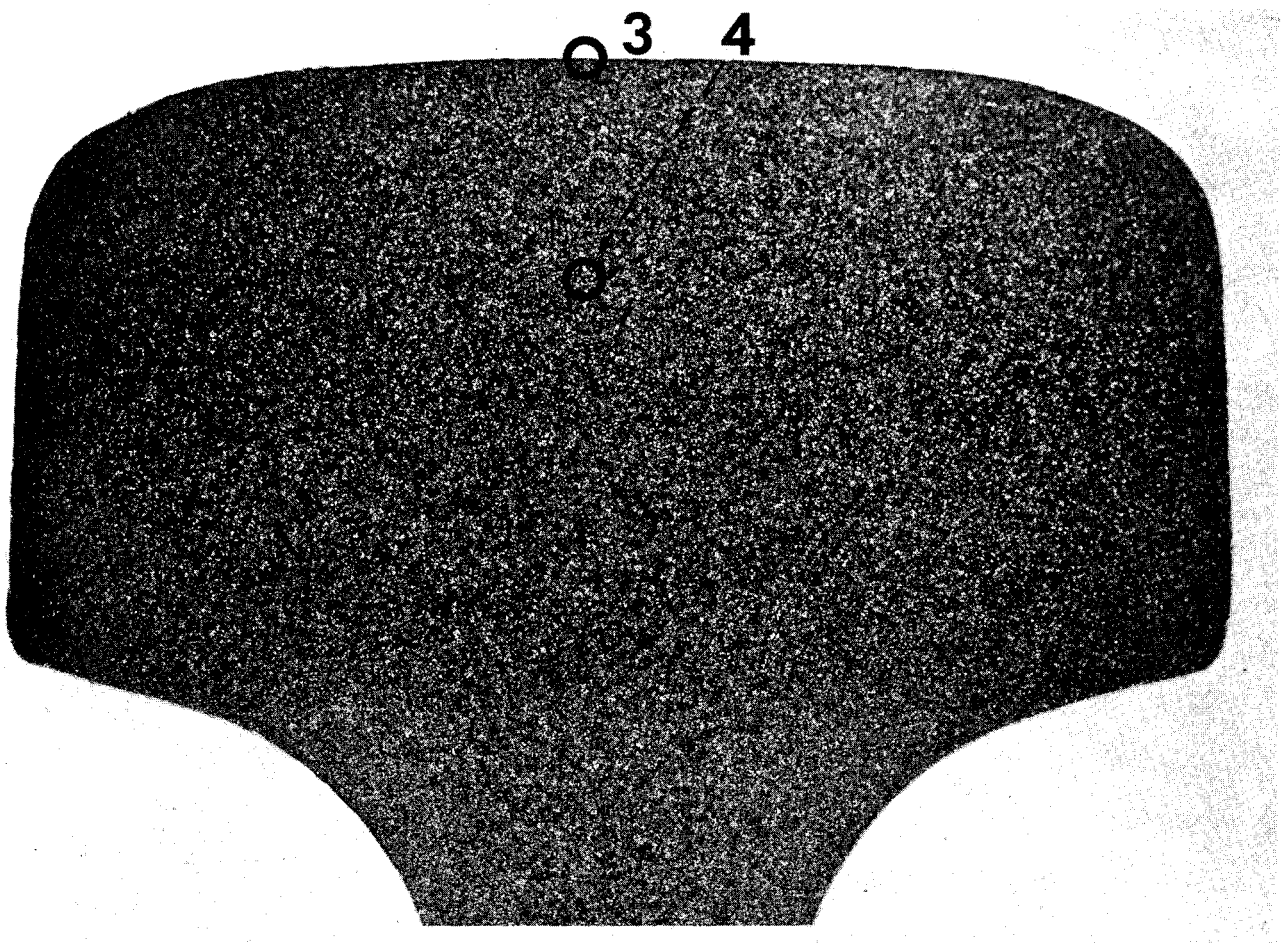

Figure B-2 Same Cross Section as Shown in Figure B-1. Microphotographs of Locations 3 and 4 Are Shown in Figures B-3 and B-4, Respectively.

Figure B-3 Section Through the Top of Rail 8 as indicated in Figure B-2. (100X, Vilella's Etch)

Figure B-4 Typical Structure in The Interior of Rail Head 8. (100X, Vilella's Etch)

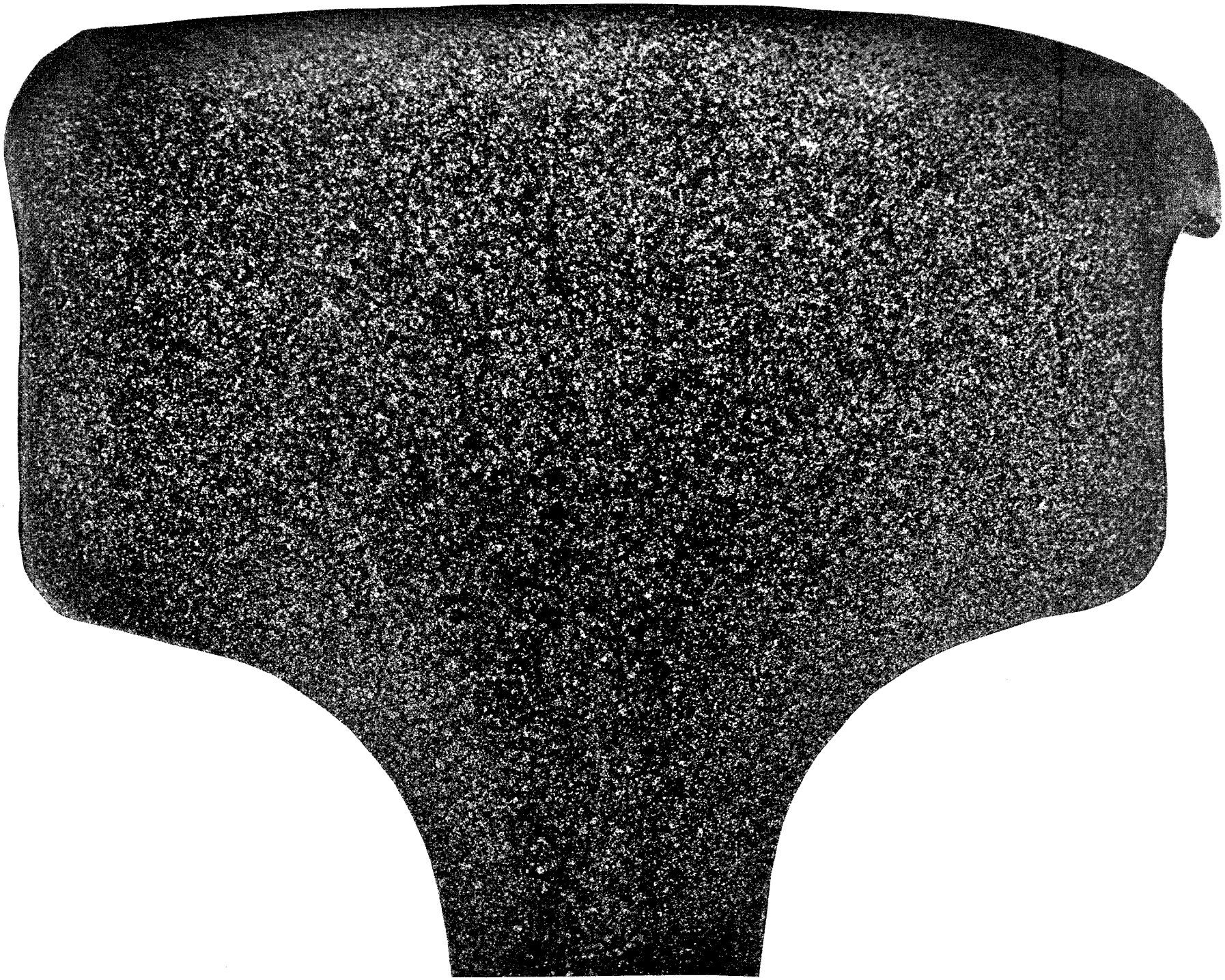

Figure B-5 Overall View of a Used 119 lb AREA Rail Head (No. 7). (3.3X, Vilella's Etch)

deformed as evidenced by the contour of the side of the rail head. Evidence of plastic deformation extending beneath the surface is shown as a generally flowed pattern of the etched structure. Consistent with the contour of the rail head, the severly flowed layer is thickest at the corners and relatively shallow beneath the center. Figure B-6 shows the cross-section of rail 7 with the locations of areas shown in the following micrographs indicated. Figure B-7 shows the section through the top of the used rail. Evidence of deformation appears as a distortion of the normally equiaxed pearlite nodules. The distortion extends to a depth of approximately 1.0 mm (.04 inches) beneath the surface. In this and subsequent micrographs the flow pattern in the metal is not generally parallel to the external surface of the rail. Flow of the metal is shown to be the result of a combination of compression and shear forces acting on the surface. The undeformed coarse structure in the core of the rail head is shown in Figure B-8. The microstructure is entirely pearlite and has a normalized structure. A composite micrograph of the plastic deformation near the field corner of the rail head is shown in Figure B-9. The visibly disturbed layer beneath the surface gradually disappears at a depth of about 5.1 mm (0.20 inches). Figure B-10 shows the deformed structure at the surface near the gauge corner. The deformed structure at location 11 is shown in Figure B-11. Distortion of the structure is most severe at the top of the micrograph and gradually diminishes with increasing depth beneath the rail surface. The area shown extends into the coarse structure at the core of the rail. Measurements indicate that preceptable plastic deformation extends to a depth of approximately 6.6 m (.26 inches) in this area. And, Figure B-12 shows a section through the side beneath the gauge corner. The structure shows a shallow layer of

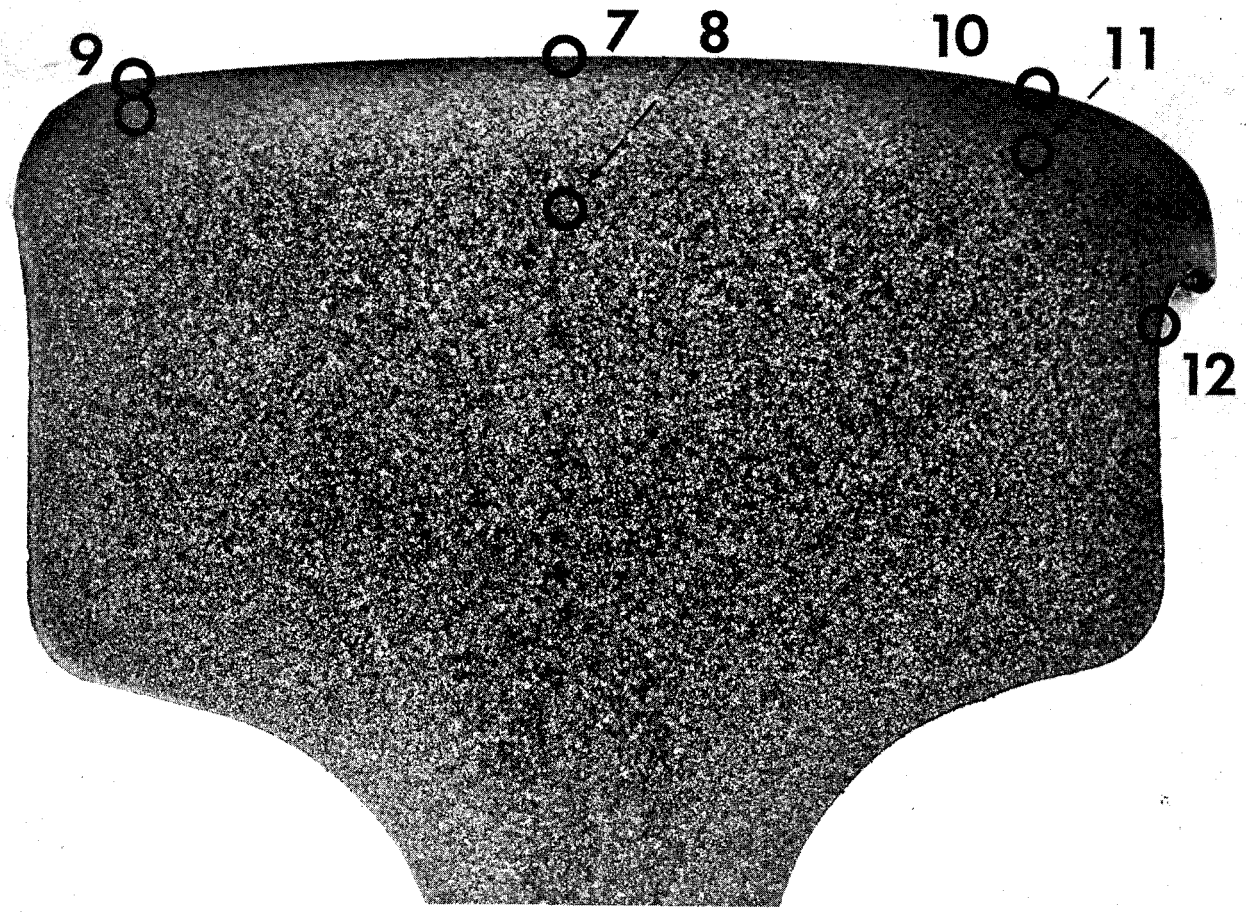

Figure B-6 Same Cross Section as Shown in Figure B-5. Microphotographs of Locations 7-12 Are Shown in Figure B-7 - B-12, Respectively.

Figure B-7 Section Through The Top of The Used Rail Head 7. (100X, Nital Etch)

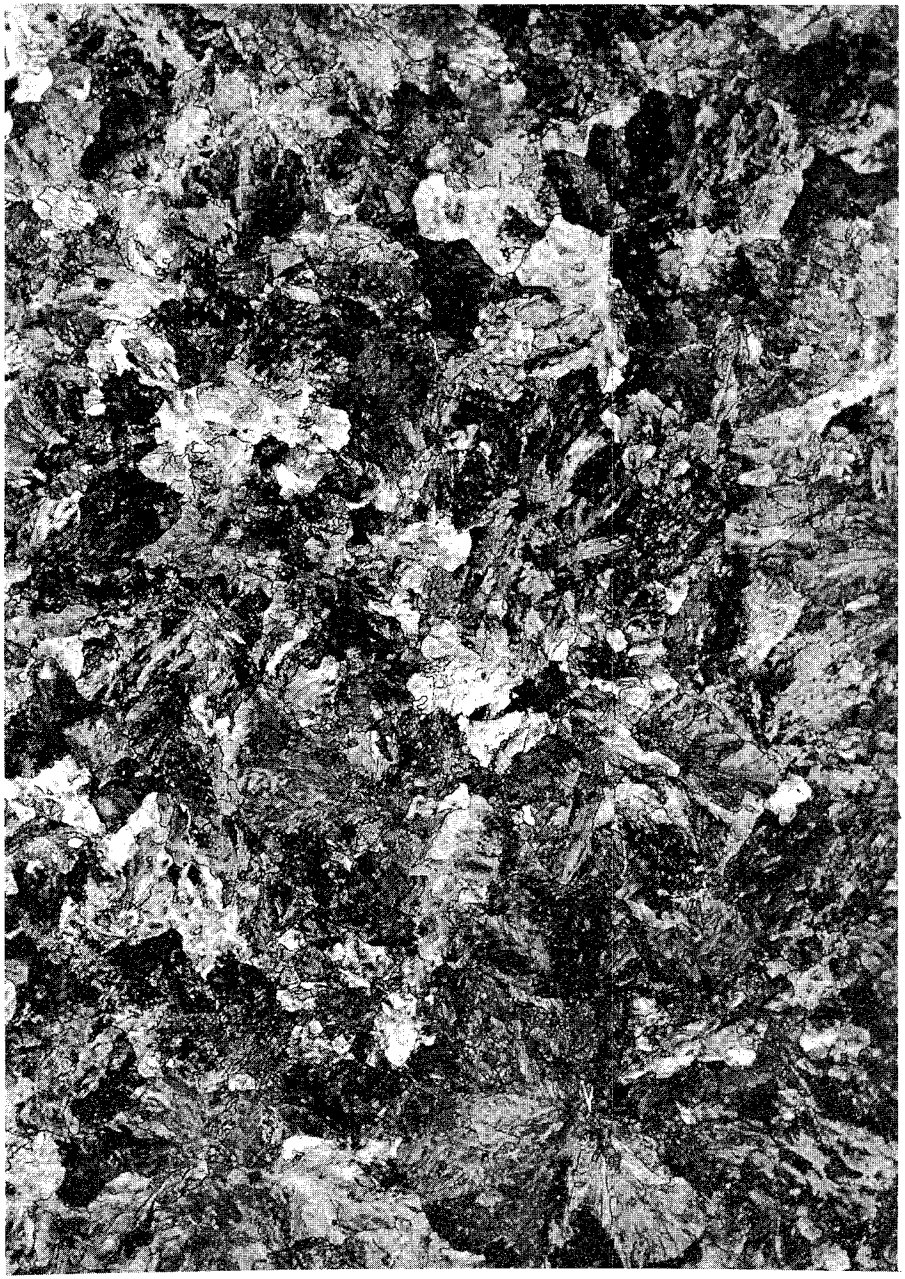

Figure B-8 Undeformed Coarse Structure in The Core of Rail Head 7. (100X, Nital Etch)

Figure B-9 Composite Micrograph Showing Plastic Deformation Near the Field Corner of Rail Head 7. (50X, Nital Etch)

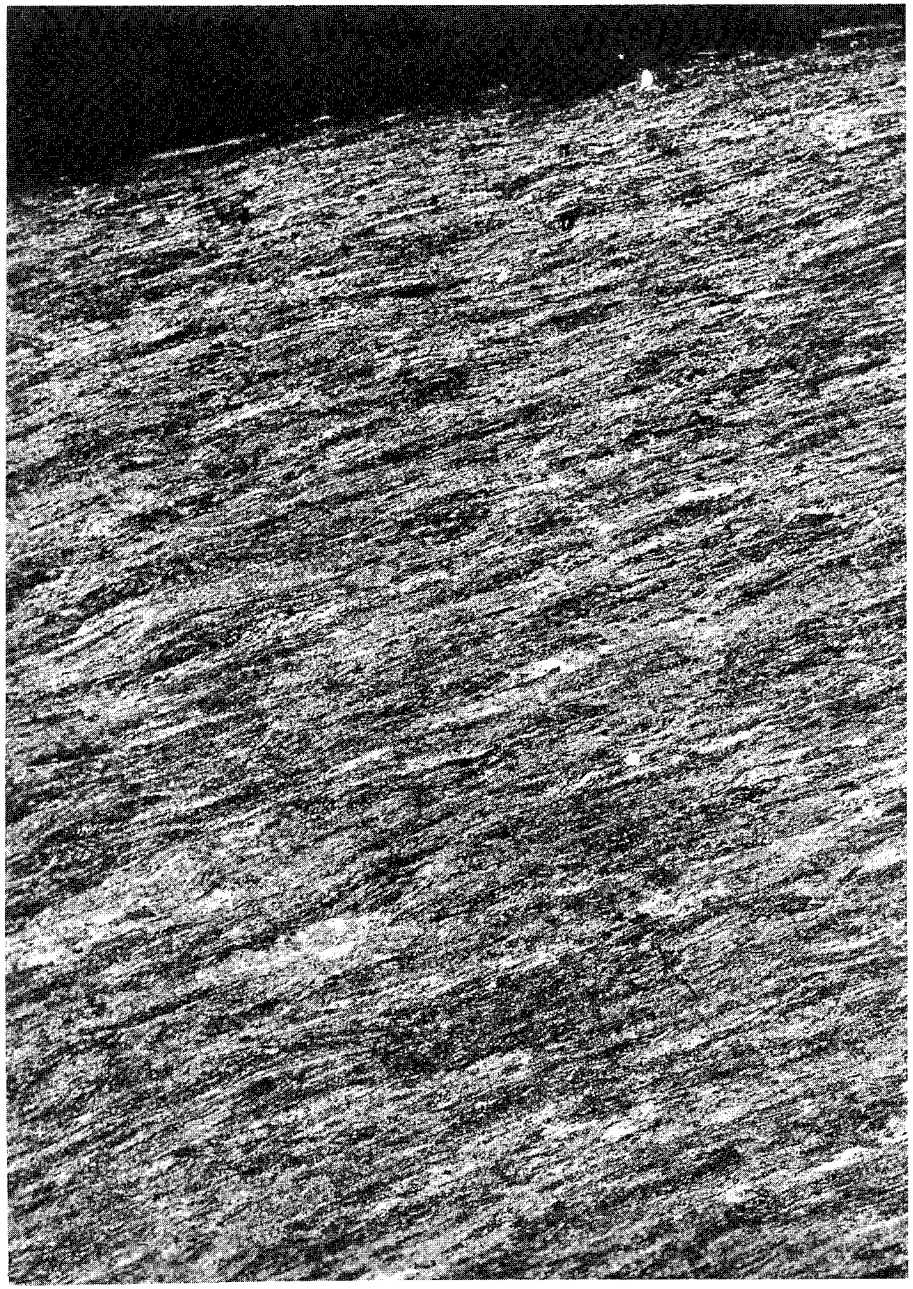

Figure B-10 Deformed Structure at The Surface Near The Corner of Rail Head 7.
(100X, Nital Etch)

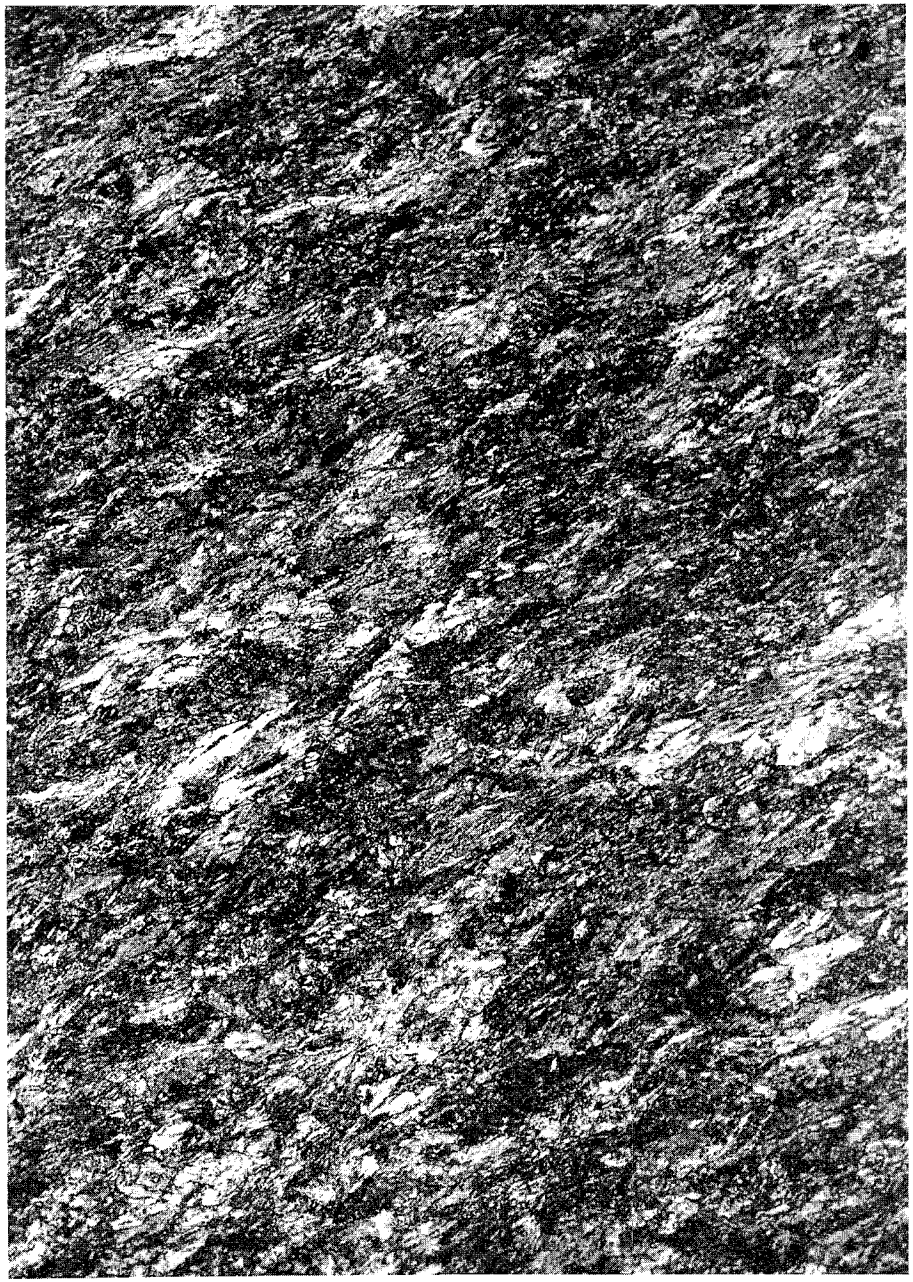

Figure B-11 Deformed Structure Beneath The Surface Near The Gauge Corner of Rail Head 7.
(100X, Nital Etch)

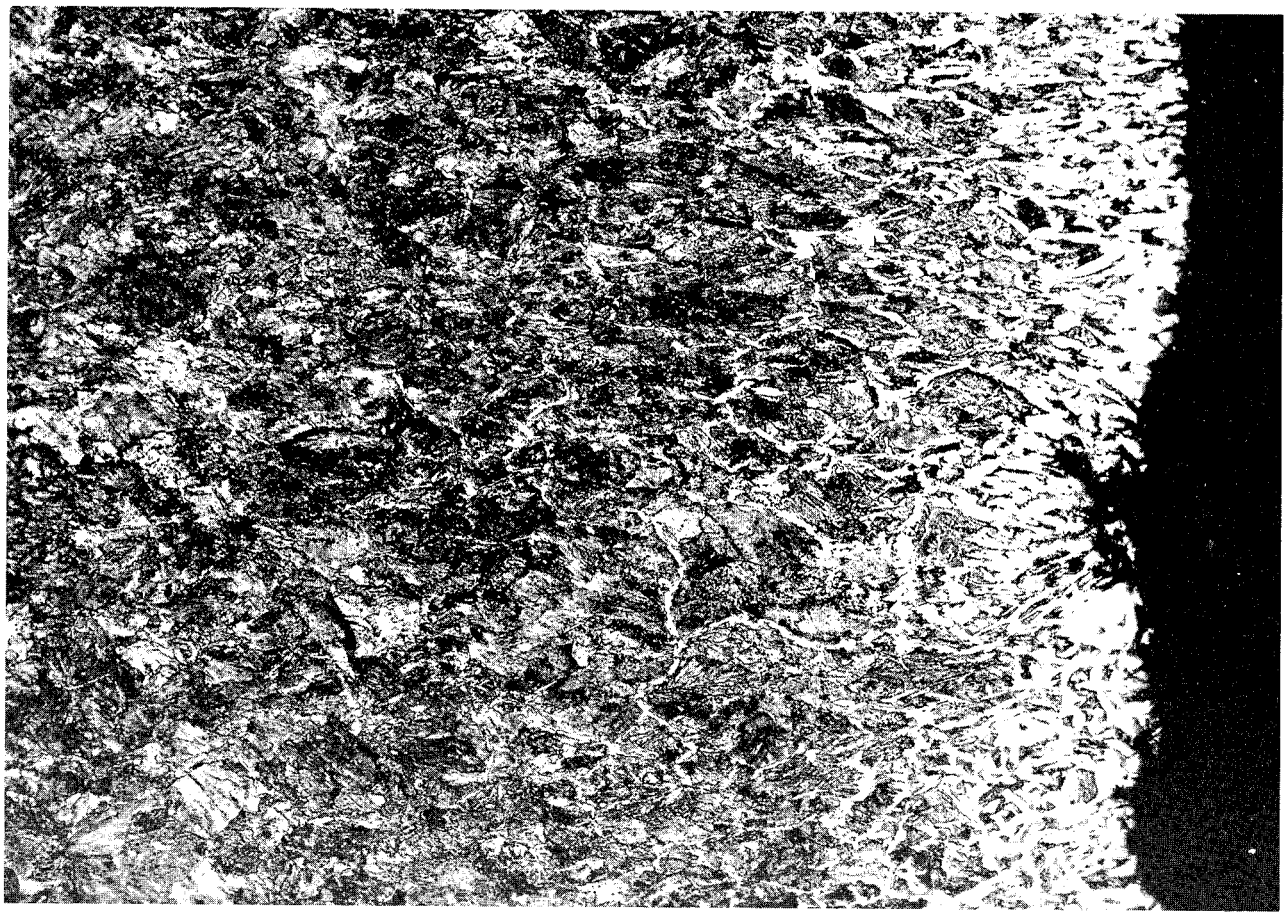

Figure B-12 Deformed Structure At The Surface Beneath The Gauge Corner of Rail Head 7.

compression extending inward from the decarburized surface. Although these micrographs show a good definition of the plastically worked zone in the used rail, the investigation of any correlation with the appearance of the early wave arrival discussed in the text of this report has not been completed. This investigation should be completed during the next phase of the program.

APPENDIX C

PHYSICAL PROPERTIES OF THE COLD WORKED ZONE

At one time during this investigation the wave arrivals on the top of the rail just prior to the Rayleigh waves were erroneously identified as Stoneley waves. This observation was based on the existence of the worked layer in the railhead and the fact that the velocity of these waves was very near to shear wave velocity as discussed by Ewing, Jardetsky and Press [34]. A more in-depth investigation of the criteria for the existence of Stoneley waves as set forth by Scholte [34,35], showed that for the material properties of the rail head and the worked layer, a real solution of the equation for Stoneley waves was not possible. Scholte's presentation was for a homogeneous isotropic material and no effort was made to account for the anistropy of the rail head. It was later determined that these early arrivals were merely shear waves travelling near the surface.

The material properties of the worked and underlying layers of rail numbers 7 and 11 were established in the course of the Stoneley wave investigation and the results are reported here as a matter of record. These properties are listed in Table C-I. Layer 1 is the upper layer and layer 2 is the bulk layer in the rail. For each rail, a section approximately 6.36 mm (1/4 in.) thick was removed from the top of the rail (layer 1). This and the section from the underlying layer (layer 2) were machined to form blocks with parallel sides. Densities were determined by accurately weighing each sample first in air to obtain the mass and then in water to obtain the volume. The velocities were obtained by observing the travel times of a very short pulse across the thickness of each piece. The densities are shown to be very close for layer 1 and layer 2 in each rail.

	RAIL 7		RAIL 11	
	LAYER 1	LAYER 2	LAYER 1	LAYER 2
DENSITY ρ (g/m^3)	$7.735(10)^6$	$7.799(10)^6$	$7.839(10)^6$	$7.812(10)^6$
DIL. WAVE VEL. α (m/s)	5942	5870	6009	5901
SHEAR WAVE VEL β	3237	3209	3241	3234
α/β	1.836	1.829	1.854	1.825

TABLE C-I Physical Properties of Used Rail.

In rail 7 the upper layer is less dense while the opposite is true for rail 11. The differences are small, however. It should be noted that the densities thus obtained represent the average density in each layer and do not account for any variations such as might occur near the outer extremities. The velocities shown for layer 2 are close to those obtained by end to end measurements. Any significant variations in the velocities can most likely be explained by the differences in the direction of beam propagation and particle motion in the two cases.

APPENDIX D

TEMPERATURE INDUCED CHANGES IN WAVE SPEED

A consideration which must be made is the wave speed changes induced by temperature variations alone, that is, independent of the temperature induced stress changes. The direct temperature induced wave speed change is not negligible [36]. For steel, the change is given approximately by

$$\frac{dc}{cdT} = -1.8 \times 10^{-4} \text{ per } ^{o}C$$

where c is the dilatational wave speed

T is temperature

for the temperature range $20^{o}C$ - $100^{o}C$. Thus a $10^{o}C$ ($18^{o}F$) temperature change will produce a 0.18% change in wave speed which is approximately the same magnitude as the change expected from a longitudinal stress of 25×10^{3} psi.

There are two possible means of accounting for the direct temperature induced wave speed changes. First the use of one guided wave mode (whose wave speed is independent of stress) as a reference will allow determination of a reference wave speed. Assuming Poisson's ratio is independent of temperature, this reference wave speed will be proportional to the zero stress wave for a guided wave mode whose speed is not independent of stress. Hence the speed of the stress sensitive mode can be corrected for the direct temperature induced change. Actual rail temperature measurement could also permit a direct correction to be made in the observed velocity.

REFERENCES

1. Coombs, D.H., ed., British Railway Track, London, Permanent Way Institution, 1971.

2. Hay, W.W., Railroad Engineering, New York, John Wiley, 1953.

3. Kerr, A.D., "A Model Study for Vertical Track Buckling," Report No. DOT-FRA-OHSGT, October 1971.

4. Kerr, A.D., "On the Stability of the Railroad Track in the Vertical Plane," DOT Report Contract No. DOT-FR-20064, November 1972.

5. National Transportation Safety Board, Railroad Accident Report, Penn Central Company, Train Second 115 (Silver Star) Derailment at Glenn Dale, Maryland, June 28, 1969, Report No. NTSB-RAR-70-1, June, 1970.

6. Pasley, R.L., "Barkhausen Effect -- An Indication of Stress," Materials Evaluation, Vol. 28, No. 7, July 1970, pp. 157-161.

7. Klug, H.P., and L.E. Alexander, X-Ray Diffraction Procedures, New York, Wiley, 1954.

8. American Railway Engineering Association, "Report on Pennsylvania Railroad M. of W. Test No. 591, Determination of Plastic Flow in Rail Head," Appendix 8-b, Report of Committee 4 - Rail, Report on Assignment 8, Chicago: Proceedings of the Fifty-Seventh Annual Meeting of the Railway Engineering Association, Vol. 59, 1959, pp. 962-975.

9. King, R.R., J.A. Birdwell, D.E. Bray, W.N. Clotfelter and E.R. Risch, "Improved Methods for Nondestructively Measuring Residual Stresses in Railway Wheels," Proceedings of the Ninth Symposium on Nondestructive Evaluation, San Antonio, April 1973.

10. Truell, R., "Internal Stress and Ultrasonic Measurements," Internal Stresses and Fatigue in Metals, Proceedings of the Symposium on Internal Stresses and Fatigue in Metals, Detroit and Warren, Mich., 1958, G.M. Rassweiler and W.I. Grube, Eds. New York, Elsevier, 1959.

11. Smith, R.T., "Stress-Induced Anisotropy in Solids -- The Acousto-Elastic Effects" Ultrasonics, July-Sept 1963, pp. 135-147.

12. Hughes, D.S. and Kelly, J.L., "Second-Order Elastic Deformation of Solids," Physical Review, Vol. 92, No. 5, December 1953, pp. 1145-1149.

13. Toupin, R.A. and Bernstein, B.,"Sound Waves in Deformed Perfectly Elastic Materials.Acoustoelastic Effect," Jour. Acous. Soc. Amer., Vol. 33, No. 2, 1961, pp. 216-225.

14. Kammer, E.W. and I. Vigness, "The Use of Ultrasonic Waves for Stress Determinations," NRL Project F03-52, AD-438 449, April 1964.

15. McKannan, C.C., "Ultrasonic Measurement of Stress in Aluminum," Nondestructuve Testing: Trends and Techniques, Proceedings of the Second Technology Status and Trends Symposium, NASA Marshall Space Flight Center, NASA SP-5082, October 1966.

16. Alers, G.A., "The Measurement of Very Small Sound Velocity Changes and Their Use in the Study of Solids," Physical Acoustics, Principles and Methods, V. IV, pt A, W.P. Mason, ed., New York, Academic Press, 1966, pp. 277-297

17. Breazeale, M.A., "Ultrasonic Studies of the Nonlinear Properties of Solids," International Journal of Nondestructive Testing, Vol. 4, 1972, pp. 149-166.

18. Noronha, P.J., J.R. Chapman, and J.J. Wert, "Residual Stress Measurement and Analysis Using Ultrasonic Techniques," Journal of Testing and Evaluation, Vol. 1, No. 3, May 1973, pp. 209-214.

19. Noronha, P.J. and Wert, J.J., "An Ultrasonic Technique for the Measurement of Residual Stresses," Jour. Testing and Evaluation, Vol. 3, no. 2, March 1975, pp. 147-152.

20. Becker, F.L., "Ultrasonic Determination of Residual Stress," Battelle-Pacific Northwest Laboratories, Richland, Washington, January 1973.

21. Hsu, N.N., "Acoustical Birefringence and the Use of Ultrasonic Waves for Experimental Stress Analysis, "Experimental Mechanics, Vol. 14, No. 5, May 1974, pp. 169-176.

22. Clotfelter, W.M. and Risch, E.R., "Ultrasonic Measurement of Stress in Railroad Wheels and in Long Lengths of Welded Rail," NASA Technical Memorandum, NASA TM X-64863, July 1974.

23. Martin, B.G., "Rayleigh-wave Velocity, Stress and Preferred Grain Orientation in Aluminum," Non-Destructive Testing, Vol. 7, No. 4, August 1974, pp. 199-203.

24. Martin, B.G., "The Measurement of Surface and Near-Surface Stress in Aluminum Alloys Using Ultrasonic Rayleigh Waves", Materials Evaluation, Vol. 32, No. 11, November 1974, pp. 229-234.

25. Schreiber, E., Anderson, O.L. and Soga, H., Elastic Constants and Their Measurement, New York, McGraw-Hill Book Company, 1973.

26. Garland, G.D., Introduction to Geophysics, Philadelphia, W.B. Saunders Company, 1971.

27. Tittman, B.R. and Thompson, R.B., "Measurement of Physical Property Gradients with Elastic Surface Wave Disperson," Preprint #SC-PP-73-36,

Rockwell International, Science Center, Thousand Oaks, California 91360, May 1973.

28. Steel Products Manual, Railway Track Materials, New York, American Iron and Steel Institute, November 1961.

29. Rail Defect Manual, Danbury, Connecticut, Sperry Rail Service, 1964.

30. The Making, Shaping and Treating of Steel, Pittsburgh, Pennsylvania, United States Steel Corporation, 1971.

31. Proceedings of the Rail Steel Conference, London, Iron and Steel Institute, 23 November 1972.

32. Railroad Facts, Technical Report No. 3, United States Steel Corporation, 1968.

33. Gross, J.H. United States Steel Corporation, Private Communication, letter dated September 19, 1974.

34. Ewing, W., Jardetzky, W. and Press, F., Elastic Waves in Layered Media, New York, McGraw-Hill, 1957.

35. Scholte, J.G., "The Range of Existence of Rayleigh and Stoneley Waves," Monthly Notices of the Royal Astronomical Society, Geophysics Supplement, V. 5, No. 5, 1947, pp. 120-126.

36. Forsythe, W.E., Smithsonian Physical Tables 9th ed. Smithsonian Institution, 1954, p. 306.